HIGH TEMPERATURE EQUILIBRIA AND CONDENSATION

SOLAR WIND INTERACTION WITH SOLIDS

HARRY CHESTER LORD, III

1967

UNIVERSITY OF CALIFORNIA

San Diego

Part I. High Temperature Equilibria and Condensation.

Part II. Solar Wind Interaction with Solids.

A dissertation submitted in partial satisfaction of the

requirements for the degree Doctor of Philosophy

in Chemistry

by

Harry Chester Lord, III

Committee in charge:

Professor James R. Arnold, Chairman
Professor Harold C. Urey
Professor Hans E. Suess
Professor Edward D. Goldberg
Professor Russell W. Raitt

1967

The dissertation of Harry Chester Lord, III

is approved, and it is acceptable in quality

and form for publication on microfilm:

_____

_____

_____

_____

_____
                              Committee Chairman

University of California, San Diego

1967

TABLE OF CONTENTS

TABLES (cont.)

FIGURES

FIGURES (cont.)

ACKNOWLEDGMENTS

VITA

May 28, 1939 – Born – Utica, New York

1961 – B.S., Tufts University

1961-1964 – N.D.E.A. Fellow, D..artment of Chemistry,
University of California, San Diego

1964-1966 – Research Assistant, Department of Chemistry,
University of California, San Diego

1966-1967 – Teaching Assistant, Department of Chemistry,
University of California, San Diego

PUBLICATIONS

"Molecular Equilibria and Condensation in a Solar Nebula and Cool
Stellar Atmospheres." Icarus 4, 279-288, July, 1965.

FIELDS OF STUDY

Major Field: Chemistry

Studies in the Application of Physical Chemistry to the
Origin and Evolution of the Solar System.
Professor James R. Arnold

ABSTRACT OF THE DISSERTATION

Part I. High Temperature Equilibria and Condensation.

Part II. Solar Wind Interaction with Solids.

by

Harry Chester Lord, III

Doctor of Philosophy in Chemistry

University of California, San Diego, 1967

Professor James R. Arnold, Chairman

Part I. High Temperature Equilibria and Condensation.

An expanded presentation is given of the work by Lord (1965).
This is a study of the molecular equilibria present in a gas cloud with
cosmic elemental abundances, temperatures of 2000° K or 1700° K, and
total pressures of approximately 1 atm. and 5×10^{-4} atm. with special
consideration of the formation of a condensed phase. From some 150

species considered, Al_2O_3, HfO_2, W, ZrO_2, and $MgAl_2O_4$ are found to be condensed at 2000° K at a total pressure of 1 atm. Decreasing the temperature or increasing the pressure condenses more species, which in general are of complex structure.

It is shown that in the atmospheres of cool stars polyatomic molecules and possibly condensed species play an important role. The calculated equilibria should be useful for spectral studies, and the order and type of condensates should prove helpful in cosmochemical problems.

Using the technique of flash heating to produce the vapor phase, condensation in simple systems is studied. Vaporization of iron has given a supersaturated vapor which condensed as small spherules ($\leqslant$ 1000 Å diameter). One wants to study the condensation from the O-Si-Mg-Fe-Al system and in particular look for those species which are predicted in the above work to be the primary condensates. However, principally because of the spectral distribution of the lamp, these refractory materials are not vaporized. Melting is observed but no new phases are detected.

Part II. Solar Wind Interaction with Solids.

The solar wind is thought to be a principal source of primordial rare gases in meteorites and may also be effective in the identification of cosmic dust. To simulate the effects of the solar wind, olivine has been irradiated with 2 keV protons, and olivine, dunite, enstatite, and fayalite have been irradiated with 1.8 keV He ions. Both the hydrogen and helium are quantitatively retained at the lowest integrated fluxes

used ($\sim 5 \times 10^{16}$ ions/cm^2). Decreased retention with increasing integrated flux (saturation effects) is observed.

X-ray diffraction analysis, electron probe microanalysis, microscopic analysis, and studies of the characteristic X-rays produced by low energy protons, have been performed on the bombarded surfaces. Only the last technique detected elemental composition changes, and most likely these are only a result of the irradiation instrumentation. Samples of Pesyanoe, Norton County, and Plainview meteorites and a biotite sample have been analyzed for H$_2$ and He. Gas release curves and diffusion constants are derived and compared with the experimental studies described above.

Part I: High Temperature Molecular Equilibria and Condensation.

Theoretical investigation

Introduction: It is generally agreed that condensation from a solar nebula led to processes that formed the solid bodies we now observe in the solar system. During the sun's contraction toward the main sequence, if the Hayashi effect of convective heat transfer is applicable, there must have been a high temperature, moderate pressure stage (Hayashi, 1961). Equally as important, with convective heat transfer, the contraction would occur quite rapidly, probably within 10^6 to 10^7 years. However, meteorites show a record of comparitively short-lived ($T_{\frac{1}{2}}=10^7$ years) radioactive species being incorporated in them during their formation as Xe^{129} from I^{129}. This would suggest that the meteoritic parent bodies, and presumably the inner planets, condensed prior to or during this contraction phase (Faulkner et al., 1963).

As this hot nebula cooled, eventually condensation would occur, and if the molecular equilibria in the gas cloud were known, both the type of condensing species and the order of condensation could be determined, assuming a specific set of relative elemental abundances. This in turn would predict the composition of the primordial condensates. However, today we observe element fractionations among volatiles, silicates, and iron in the various solid bodies of the solar system as compared to the observed elemental abundances of the sun. As Urey (1953) has pointed out, though, we can assume that the fractionations occurred after the major condensation, as certain volatile elements as

Cd, Zn, and Hg are present in the earth with abundances similar to those expected.

The conditions being studied here are found in other places also. Many M, S, and C class stars are known to have temperatures in the reversing layer below 2500° K, and in a limited number of cases even lower than 1700° K (Merrill, 1960). Recently a whole new class of stars, the I. R. stars, have been discovered (Neugebauer et al., 1965). One particular object in Cygnus is brighter than Orionis at 10.2μ, while in the visible it can not even be detected with the 200 inch telescope. Fitting the observed flux densities to a black body curve, an effective temperature of 700° K is obtained (Johnson et al., 1965). Detailed spectroscopic work is now being carried out to help fit these objects into the general spectral classification. Preliminary investigations suggest that at least two (NML Cygnus, and NML Taurus) show more resemblance to the carbon rather than M-type stars (McCammon et al., 1967).

With a given set of elemental abundances, the composition of the atmosphere can be predicted. This then determines the major species of each of the elements, which is of particular importance in spectroscopic studies, especially at low temperatures where much blending of spectral lines occurs. The presence of a condensed phase certainly would enhance the opacity, and important parameter for theories of stellar evolution. Finally, a condensed phase may be directly related to the variability observed in the advanced spectral types of red stars.

History: Russell (1934) and Wildt (1933, 1934) performed the first serious studies of molecules in stars. Since then better

thermodynamic data has been obtained, as well as a better set of elemental abundances. Bouigue (1957), Stanger (1960), and especially de Jager and Nevin (1957) have also considered the problem. In the latter case six temperatures (2500° to 6400° K) and six pressures (log $P_H=1$ to 6) were used, but only compounds of H, C, N, and O were considered. Kamijo (1963), including several metals and metal oxides in the calculations, has found that solids will be present in the circumstellar envelope of M-type long period variable stars. Tsuji (1964a, 1964b) has carried out a detailed study of gaseous molecules in late-type carbon stars, and is extending his work to oxygen-rich giant stars and also those containing equal amounts of carbon and oxygen. Calculations of the molecular abundances in the outer atmosphere of K and M stars for a wide range of optical depths have been made by Vardya (1966).

The application of thermodynamics to the early history of the solar system was initiated with work by Latimer (1950) and Urey (1951, 1952). Wood (1963) has made some simple calculations for condensation from a gaseous nebula. However, he considered only a few species, mainly iron, and magnesium silicates. Gaustad (1963) has carried out a thorough investigation of opacity sources in both gaseous nebulae and stars, and he too has been concerned with condensation of a few major species.

Shimazu (1967) has presented another attack on this problem. He has given a detailed geophysical discussion of the early evolution of the Earth. At the same time he has attempted a thermodynamic study of the H-O-C-N-S-Si-Mg-Fe system wherein the equilibrium partial

pressures of some species in this system are determined. The calculations are for temperatures of 300° C, 1000° C, and 2000° C, pressures of 10^2 atm., 1 atm., and 10^{-2} atm., and decreasing hydrogen abundances, maintaining all other abundances constant throughout. Unfortunately the exactness of the calculations and usefulness for studies of condensation and subsequent planet formation are limited by the paucity of species considered. The more detailed compositional analysis by Lord (1965) and this paper becomes especially important at the higher temperatures where the first mineral species are being formed by condensation. Because of the likely slow kinetics for the transformation, these high temperature species may well be representative of the solids accreting to form the planets.

On the other hand, the effects of a gradual fractionation, losing hydrogen (and also He, if required), are well displayed in this work. Again some of the changes are over-emphasized, as for instance the rapid removal of CH_4 from the system as H decreases. This certainly is a real effect, but is partially offset at high temperatures by the less rapid decrease in the species CH_X, X=1 to 3. Finally, it should be mentioned that the minimum accepted abundance for any species was 10^{-8} of the (H_2) at the solar ratio of the elements. This is very restrictive, and coupled with the limited species considered might be expected to cause anomalous results. In at least one readily observed case, this is true. He reports that in his calculations "the solid phase of C and S cannot be found", but yet when one considers for example the equilibrium $C_{(s)} + CO_{2(g)} = 2\ CO_{(g)}$ at a temperature of 300° C, a pressure of 1 atmosphere, and a hydrogen depletion giving H/O=3.0/2.8,

one finds that the derived $(CO)^2/(CO_2)=10^{-7}$. Here, graphite would be present (Suess, 1962; Dayhoff et al., 1964). Further calculations of the C-H-O system with special interest paid to the wealth of species formed with high relative amounts of C has been performed by Eck et al. (1966) and Lippincott (1967).

A derivation of the condensation history for most of the major elements as well as those trace elements whose abundances have been carefully studied in meteorites has been performed by Larimer (1967). The interest is not in the primordial condensates, but rather the stable solid species which are then later incorporated into the planets and the meteorites. Two basic histories, slow and rapid cooling, predict considerably different results. Rapid cooling freezes in the condensed elements, while the slow cooling results are similar to those derived by Lord (1965).

A discussion is given of the presence of FeS in this system which indicates a lack of understanding of the results of the present work. "For example, Lord (1965) finds significant condensation of FeS at 1700° and 2000° K, although FeS is not stable in an atmosphere of cosmic composition until the temperature drops to 680° K." Table V (Table 6 of this paper) lists a series of species giving the P_{H_2} required for their condensation, or thus actually indicating whether any of these species need be considered as competing in the molecular equilibria. It is readily obvious that at 2000° all of these molecules can be safely disregarded, and at 1700° only CaS and ZrS_2 need be considered.

In this work, I have considered a fairly complete set of compounds of H, C, N, and O, including many polyatomic molecules. Also,

Table 1. Relative abundances of the elements.(a)

H	1.0	Ca	1.6×10^{-6}
He	1.6×10^{-1}	Ni	9.0×10^{-7}
O	8.9×10^{-4}	Mn	1.4×10^{-7}
Ne	5.0×10^{-4}	Ti	7.9×10^{-8}
C	4.0×10^{-4}	V	6.6×10^{-9}
N	1.2×10^{-4}	Kr	1.6×10^{-9}
Si	3.3×10^{-5}	B	7.6×10^{-10}
Mg	2.5×10^{-5}	Zr	3.2×10^{-10}
S	2.3×10^{-5}	Xe	1.0×10^{-10}
Ar	7.6×10^{-6}	Sn	3.7×10^{-11}
Fe	3.9×10^{-6}	W	3.9×10^{-12}
Na	2.0×10^{-6}	Hf	2.5×10^{-12}
Al	1.7×10^{-6}	Th	1.0×10^{-12}

(a) from Goldberg et al. (1960)

the more important compounds of all the other relatively predominant elements have been considered. Finally, elements expected to form non-volatile compounds were considered, as one of the major tasks in this work was to investigate the formation of condensed species.

Method of calculation: The elemental abundances used here were the set compiled by Goldberg et al. (1960) for our sun (see Table 1), where $H/O = 1.1 \times 10^3$, $O/C = 2.2$, $O/N = 7.4$, $O/Si = 27$. Pressures were picked so as to be in general agreement with postulated conditions in our evolving solar system (Cameron, 1962). They also conform to the best estimates for total pressures in the reversing layer of M5 dwarfs and giants, $P_{H_2} = 0.5$ atm., and 2.25×10^{-4} atm. respectively (Allen, 1963). The specific values were determined by the adopted relative H abundances, 1 and 5×10^{-4}. All other elements then have abundances with negative exponents. The temperatures 2000° K and 1700° K were chosen, so that the calculations were done in the range where condensation should occur. The most complete set of thermodynamic data is the Joint Army-Navy-Air Force (JANAF) Thermochemical Tables, and these were used where possible. The other calculations used are described further on.

Consider the simple reaction

$$X_{(g)} + Y_{(g)} = XY_{(g)}$$
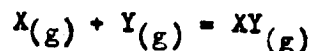
where the equilibrium constant is the ratio of the partial pressures of the products to the partial pressures of the reactants

$$K_p = \frac{P_{XY}}{P_X P_Y}$$

Then by determination of the equilibrium constant, and the knowledge of any two partial pressures, the third may be determined. However, from thermodynamics, we have

$$\Delta F^\circ = -RT \ln K_p$$

where ΔF° is the standard free energy change for the reaction at temperature T. Since K_p is a constant depending only upon temperature, we see that a decrease in total pressure (as going from a dwarf to a giant star) at any temperature results in driving the reaction back toward the reactants, that is, increasing the relative importance of the monatomic species.

Theoretically the calculations are made by summing the partial pressures of all the X-containing molecules and setting this equal to the total relative abundance of X. However, in practice it turns out that for all elements there are only a few molecules whose partial pressures are greater than 1% of the total elemental abundance. Thus only those molecules need be considered in the division of the total elemental abundance. By necessity, the first equilibrium to be considered is the H, H_2 equilibrium, and under our conditions the "total" H abundance is as H_2. At 2000° K, and H abundance of 1, we have

$$2H = H_2$$

$$K_p = \frac{P_{H_2}}{(P_H)^2} = 10^{5.6}$$

or $$P_{H_2} = 4 \times 10^5 (P_H)^2$$

then $$P_{H_2} = \tfrac{1}{2}(\text{H abundance}) = 0.5 \text{ atm.}$$

and $$P_H = 1.1 \times 10^{-3} \text{ atm.}$$

The next most abundant elements, O and C, are now considered. (It is quickly discovered that N is present as N_2, with the next most abundant species, NH_3, being 10^{-3} less). For simplification H_2O and CO are assumed to be the major O species. This assumption is checked when

the other species are calculated, and in only one case (Si) was the $\frac{P_{XO}}{P_O}$ found to be at least 1% of the $\frac{P_{H_2O}}{P_O}$. This then requires that the total O elemental abundance must be divided three ways. In Table 2 are listed the various major compounds of the more abundant elements.

Table 2. Assumed division of major elemental abundances.

$$H \text{ abundance} = 2P_{H_2}$$

$$O \text{ abundance} = P_{H_2O} + P_{CO} + P_{SiO}$$

$$C \text{ abundance} = P_{CO}$$

$$N \text{ abundance} = 2P_{N_2}$$

$$S \text{ abundance} = P_{H_2S} + P_{HS} + P_S + P_{SiS}$$

The calculations are continued in this manner, and are corrected whenever another major species is discovered. In only one case did the calculations become particularly involved, and that was in the S family where SiS is found to be important, altering the Si and S pressures and thus the SiO pressure. The calculations are repeated until a self-consistent set of data is obtained. It should be mentioned that the correctness of the derived molecular partial pressures depends upon the assumption that all the major species have been considered, and this assumption is questionable in certain cases, as Ni, Mn, V, Hf, and Th, where the data were abailable for only a few compounds.

Many elements important to our study are not tabulated in the JANAF tables, and thus the standard free energy change for the reaction under consideration must be derived. In many cases tabulated free energy functions (fef) from Lewis and Randall (1961), Brewer (personal

communication), Searcy (personal communication), or Freeman (1962) were used, and where these were not available, both the required ΔH^o and ΔS^o were calculated. The fef $-\left(\frac{F_T^o - H_{298}^o}{T}\right)$, which at 298° K is just equal to $-S_{298}^o$, is often determined from spectroscopic data for gaseous species. Then one needs only the standard enthalpy of the reaction at 298° K, which if not available is calculated from some known ΔH, as D_o^o (the dissociation energy of the gaseous molecules to the gaseous atoms at 0° K), or from the heat of vaporization. An alternate method of calculation, not using fef's, is derived in an analogous manner.

$$\Delta F^o = \Delta H^o - T\Delta S^o$$

$$\Delta H^o = -D_o^o + (H^o - H_o^o)_{XY} - (H^o - H_o^o)_X - (H^o - H_o^o)_Y$$

$$\Delta S^o = S_{XY}^o - S_X^o - S_Y^o$$

and $(H^o - H_o^o)$ and S^o can be calculated from C_p. For a diatomic gaseous molecule

$$C_P = C_{tr} + C_{rot} + C_{vib} = R\left(\frac{5}{2} + \frac{2}{2} + u^2 \frac{e^u}{(e^u - 1)^2}\right)$$

and $u = \frac{h}{kT} = \frac{hc\omega_o}{kT} = 1.4387 \frac{\omega_o}{T}$

where ω_o = vibration frequency (cm^{-1})

In Table 3 are listed the calculated ΔF_{2000}^o's for simple compounds which are not included in the JANAF Tables. As a check on the methods, the values for ZrO using the JANAF Tables and method B, and also the values for ZrO_2 using both the JANAF Tables and method C are listed here. The agreement is very good.

In this table, for the reaction $X_{(g)} + \frac{1}{2}Y_{2(g)} = XY_{(g)}$, method A uses ΔH calculated from C_p and ΔS calculated from statistical mechanics. Method B uses fef and ΔH_{298}^o from D_o^o. For the reaction $X_{(g)} + Y_{2(g)} = XY_{2(g)}$

Table 3. Calculated free energy values.

species	F^0_{3000}(kcal)	Method	D^0_e(kcal)	ω_e
CaO	– 30.2	B(g)	104(b)	
CaS	– 4.0	A		450(e)
FeO	– 31.1	B(g)	110(a)	
FeO	– 17.1	JANAF		
HfO_2	–174	C		
MnO	– 23.3	B(g)	101(a)	
NiO	– 20.7	B(g)	101(d)	
SnO	– 48.5	B(g)	130(a)	
SnS	+ 4.1	A		488(a)
ThO_2	–191	C		
VO	– 66.8	B(g)	147(c)	
VO_2	–114	C		
ZrO_2	–158.3	C		
ZrO_2	–158.2	JANAF		
ZrO	– 98	B(s)	180(c)	
ZrO	– 96.2	JANAF		

References: a) Herzberg (1950)

b) Herzberg (1957)

c) Inghram et al. (1957)

d) estimated from values for MnO, FeO, CuO

e) estimated from ω for CaO, using data from SiO/SiS, PbO/PbS, GeO/GeS, and SnO/SnS from (a)

f) fef's from Brewer and Chandrasekharaiah (1960)

g) fef's from Brewer (personal communication)

method C, involving fef and ΔH^o_{298} (Brewer and Rosenblatt, 1961), is used.

The calculation made for FeO is subject to considerable error as the heat of formation, ΔH^o_{298}, is not well known. My earlier calculations used $\Delta H^o_{298}=-51.6$ kcal, which is calculated from $D^o_o=110$ kcal (Herzberg, 1950). Subsequent investigations indicate that this D^o_o is an upper limit (see JANAF Table FeO(v) Data Sheet.) The value chosen for use in the JANAF Tables given $\Delta H^o_{298}=-60\pm5$ kcals. This then results in decreasing the P_{FeO} at 2000° K and $P_{H_2}=0.5$ atm. by a factor of 35.

All the above described calculations are first made for gaseous reactants and products. Then from studying the reaction between the same gaseous reactants going to products in the condensed state, the vapor pressure can be determined.

$$X(g)+Y(g)=XY(g) \qquad \Delta F_1$$

and $\qquad X(g)+Y(g)=XY(g) \qquad \Delta F_2$

$$\log P_{vap}=-\frac{(\Delta F_1-\Delta F_2)}{2.303 \ RT}$$

If the calculated partial pressure in the gas cloud of the species considered is greater than the vapor pressure, the species will be present in the condensed phase (assuming that there is no kinetic hold-up).

Results: The species whose partial pressures have been calculated are listed in Table 7 by element, and arranged in order of decreasing partial pressures for 2000° K and $P_{H_2}=0.5$ atm. Thus the first species listed for each element is the most stable form of that element under the assumed conditions. Table 8 lists the calculated

partial pressures for these species under the three conditions considered, along with the vapor pressure of those species which are likely to condense.

From some 120 atoms and molecules considered, only four (Al_2O_3, HfO_2, W, ZrO_2) were found to be condensed at 2000° K and P_{H_2}=0.5 atm. and at 2000° K and P_{H_2}=2.25x10^{-4} atm. nothing was found to condense. However, at 1700° K and 0.5 atm. P_{H_2} there was a wealth of material condensed, including Al_2O_3, TiO, TiO_2, VO, CaO, MgO, CaS, W, ZrO , HfO_2, with Fe, Ni, and SiO_2 almost condensed. The calculations have not been extensively carried out for 1700° K and 2.25x10^{-4} atm. P_{H_2}, but the molecular equilibria should be similar to those at 2000° and 0.5 atm. P_{H_2}. All of the materials found here to be condensed at 1700° K or above go directly to the solid state. Thus the possibility of liquids acting as glue to bind the various grains together seems to be unimportant.

Upon surveying the list of condensed compounds, one immediately notices that no mention is made of the complex refractories, the silicates. This is due to bias in the data available, as the thermodynamics of the molecules in the vapor phase are not known. Wood (1963) has considered a few of these molecules, and the method he used will be used here. As he has not worked out the detailed molecular equilibria, he sets up an equilibrium going to the solid silicate starting from the most abundant gaseous species of each of the elements involved. He then uses the total elemental abundance as the partial pressure of that species. In most cases this leads to errors in the partial pressure of less than a factor of two. In the present calculation this is not

necessary as the inter-relationships between species have already been calculated.

The equilibrium constant, then, can be written in terms of the partial pressures derived here. Consider

$$2 \ Mg(g) + SiO(g) + 3H_2O(g) = Mg_2SiO_4(s) + 3H_2(g)$$

then $\quad K_p = \dfrac{P_{H_2}^3}{P_{Mg}^2 P_{SiO} P_{H_2O}^3} = \dfrac{P_{H_2}^6}{P_{Mg}^2 \ P_{SiO} \ P_{H_2O}^3} \cdot \dfrac{1}{P_{H_2}^3} = B \ \dfrac{1}{P_{H_2}^3}$

where P = partial pressures of the species

$\quad\quad\quad B$ = constant for a given T and total P

Data from Kelley (1962) was used to calculate the ΔF^o for the reactions. The H_2 pressure (which is approximately equal to the total pressure) required at this temperature for the species to be present in the condensed phase is given by

$$P_{H_2} = \left[\frac{B}{10^{- \frac{\Delta F^o}{2.303 RT}}} \right]^{1/3}$$

Of course in this calculation and all prior ones, it is assumed that the activity of the condensed species is unity. By comparing the required P_{H_2} with that taken for the gas cloud, it is found that at 2000° and P_{H_2}=0.5 atm., $MgAl_2O_4$ is just being condensed, while $CaTiO_3$ is close. Table 4 shows the results of the calculations for 2000° K and 1700° K. It is difficult to predict how the condensation of one species quantitatively affects a related one; however, it should be remembered that not all of the possible condensates will be present in the condensed phase. This table is a list of some which could be present.

From the table one can easily see what would be the first species of each of the major elements to condense. However, in many

Table 4.   Required P_{H_2} for condensation.

Species	P_{H_2} at 2000° K	P_{H_2} at 1700° K
$MgAl_2O_4$*	5.3×10^{-1} atm.	7.7×10^{-3}
$CaTiO_3$	8.7×10^{-1}	1.9×10^{-3}
$Ca_3Ti_2O_7$	1.4	4.1×10^{-3}
$CaTiSiO_5$	3.8	6.7×10^{-2}
Ca_2SiO_4	3.9	3.6×10^{-2}
Al_2SiO_5	4.1	1.4×10^{-2}
$CaAl_2Si_2O_8$	4.5	8.6×10^{-3}
$CaSiO_3$	8.4	6.3×10^{-2}
$MgTi_2O_5$	1.8×10^1	1.5×10^{-2}
Mg_2TiO_4	2.1×10^1	4.8×10^{-2}
$CaMgSi_2O_6$**	4.1×10^1	1.9×10^{-1}
$NaAlSi_3O_8$	8.8×10^1	1.8×10^1
Mg_2SiO_4	5.6×10^2	2.3
$MgSiO_3$	1.1×10^3	4.3
$FeTiO_3$	3.1×10^3	1.0×10^1
$MnSiO_3$	5.3×10^4	3.2×10^2
$FeSiO_3$	6.6×10^4	1.5×10^3
Na_2SiO_3	1.5×10^5	3.9×10^3
Fe_2SiO_4	3.8×10^5	3.0×10^3
$Na_2Si_2O_5$	1.9×10^8	3.0×10^4

*only this species is condensed at 2000° K

**this compound and those above it in the list are condensed at 1700° K

cases this first condensate would be of low concentration due to the
lower abundance of another element in the compound. For example the
first Ca species to condense is $CaTiO_3$, but the Ti abundance is only
1/20 of Ca. Secondly, a later condensate may be more stable at lower
temperature, and thus the primary condensate will revert to this, if it
possibly can. Table 5 lists both the first condensates and the major
reservoir for the more abundant elements. Beside each element is listed
its elemental abundance relative to Si.

Table 5. Major condensates of more abundant elements.

Element $(\frac{X}{Si})$	First Condensate	Major Reservoir
Si	$CaTiSiO_5$	$MgSiO_3$
Mg $(\frac{5}{7})$	$MgAl_2O_4$	$MgSiO_3$
Fe $(\frac{1}{10})$	Fe	$(Mg,Fe) SiO_3$ (?)
Al $(\frac{1}{20})$	$MgAl_2O_4$	$MgAl_2O_4$
Ca $(\frac{1}{20})$	$CaTiO_3$	$CaMgSi_2O_6$
Ti $(\frac{1}{400})$	$CaTiO_3$	$CaTiSiO_5$

A similar type of calculation has been made for some other
compounds which also have not been studied in the vapor phase at these
high temperatures. The results are shown in Table 6. It is especially
interesting to note that iron sulfide would not be condensed under any
of the conditions assumed here; however, the required P_{H_2} drops rapidly
with decreasing temperature. This species is very widespread in
meteorites. Also notice that the titanium compounds would not be con-
densed, and thus these compounds would not remove titanium from the

Table 6. P_{H_2} required for condensation.

	1700° K	2000° K
FeS	4.4×10^2	2.3×10^4
CaS*	3.8×10^{-2}	1.8×10^1
TiS	7.0	1.2×10^3
Ti_2S_3	2.0	2.0×10^3
TiS_2	6.8×10^4	6.4×10^7
ZrS_2*	2.8×10^{-1}	3.6
MnS_2	7.0×10^{11}	4.5×10^{11}
SnS_2	8.4×10^{15}	1.8×10^{17}
TiN	4.4×10^5	2.5×10^6
TiC	1.4×10^1	3.3×10^3
SiC	1.6×10^6	1.6×10^7
ZrC	8.2×10^2	1.2×10^5

*Only the two species starred would be condensed at 1700° K under our conditions. No species would be condensed at 2000° K.

already observed stable titanium condensed species.

    Discussion: A comparison of the results listed in Table 8 at the end of the paper show that the predominant hydrogen species is H_2 in all cases, but at the lower pressure H increases in importance to 10% of the H_2 pressure. At the same time all the hydrides decrease in relative importance, except those of oxygen. The very abundant molecule, H_2O, for so long undetected, has recently been observed in the spectra of cool stars (Woolf et al., 1964; Boyce and Sinton, 1965; and Spinrad and Newburn, 1965). In the carbon hydride series at $P_{H_2}=0.5$ atm. the order of partial pressures decreases CH_4, CH_3, CH_2, to CH, but at $P_{H_2}=2.25x10^{-4}$ atm., the order decreases CH_2, CH_3, CH_4, to CH.

    Also note that not only is carbon not condensed, it is not close to condensing at any of the conditions studied here. Recent work has predicted that graphite grains should condense in the atmospheres of cool carbon stars (Tsuji, 1964a, 1964b), and in order to make the results more general, it is also suggested that M giant stars may condense out these graphite particles (Donn et al., 1966; Wickramasinghe et al., 1966). Graphite has been suggested even under conditions where thermodynamics would not predict it, as it was thought that only graphite could reproduce the observed ratio of interstellar polarization to extinction (Cayrel and Schatzman, 1954).

    Recently it has been shown, however, that dielectric cylinders with an index of refraction=1.33 (dirty ice), when randomly oriented, can in fact reproduce the observed conditions (Greenberg and Shah, 1966). Furthermore Greenberg (1966) has shown that for graphite flakes with $r \leqslant 0.05\mu$ in the form of oblate spheroids, the wavelength dependence of

the polarization is proportional to the wavelength dependence of the
extinction rather than the observed approximate constancy through the
visual region. A search for absorption in the infra-red by interstellar
ice grains during a flight of Stratoscope II led to the conclusion that
those grains could explain no more than twenty-five percent of the
interstellar reddening (Danielson et al., 1965). Taken together, these
arguments suggest that the condensates discussed in this paper should be
considered carefully as a possible explanation for these interstellar
grains.

In looking at the complex condensates, it is striking to note
the preponderance of Ti in the various primary condensates. Also it
was shown that Ti would not prefer to condense as a sulfide, nitride, or
carbide. These condensates would be an important scavenger of Ti from
the gas phase, but the low relative abundance of Ti compared to that of
Si, Mg, Al, or Ca will restrict them to being a small fraction of the
total condensed phase. Similarly, condensation of Al_2O_3 and $MgAl_2O_4$
should effectively remove Al from the gas phase. The presence of both
Al and Ti as constituents in most rocks indicates a later lower temper-
ature re-equilibration.

In the calculations presented here we have made some limited
assumptions as to the dependence of the partial pressures on species
other than those involved in the equilibria considered. That is, the
sum of the pressures of the X species must equal the X abundance. How-
ever, due to the lack of data, it is impossible to calculate the effect
of condensation of a species as $MgTi_2O_5$ on the partial pressures of
related species, as MgO or TiO. There certainly will be a slight

lowering of the pressures, as material is being removed from the system. Thus the calculated partial pressures should be exact for the case where no condensation occurs in any related species, and should be an upper limit for the case where condensation does occur.

The sensitivity of these calculations is directly dependent upon the algebraic form of the equation of equilibrium considered. Using the equations on page 7 and 14 , a large error of 10 kcal in ΔF^{o} would result in only a change of 2.2 in the ratio of partial pressures. Minor temperature and pressure changes have little effect on the results, and in fact the order of condensation is seen to be essentially the same at 2000° K and 1700° K.

Finally we must consider the effect of a change in the relative elemental abundances. Drastic changes in the H/O or C/O ratios would make these calculations inapplicable, but otherwise the major species predicted here would retain their importance.

Table 7. Compounds considered, listed by element, in order of
decreasing abundance (excluding complex compounds).

__Element__

H H_2, H, H_2O, H_2S, HS, AlH, MgH, OH, NH_3, NaH, NaOH, HCN, CH_4,
    CHO, $AlHO_2$, HBO_2, NH_2, CH_3, NH, AlOH, MgOH, SiH_4, $Fe(OH)_2$,
    C_2H_2, SiH, HCNO, CH_2, BH_2, H_2WO_4, ZrH, CH, C_2H_4, BH.

O H_2O, CO, SiO, OH, CO_2, Al_2O, TiO, VO, NaOH, CHO, $AlHO_2$, TiO_2,
    SO, AlO, CaO, HBO_2, O, VO_2, ZrO_2, SiO_2, AlOH, MgO, ZrO, FeO,
    NiO, NO, MgOH, BO, MnO, $Fe(OH)_2$, WO, HfO_2, SO_2, SnO, HCNO, ThO_2,
    BO_2, NaO, O_2, WO_2, H_2WO_4, WO_3, B_2O_2, B_2O_3, NO_2.

C   CO, CO_2, CS, HCN, CH_4, CHO, CH_3, C_2H_2, HCNO, CS_2, CH_2, CN,
    C_2H_4, C, C_2, C_2N_2, C_3.

N N_2, NH_3, HCN, NH_2, NH, NO, N, HCNO, AlN, CN, SiN, NO_2, C_2N_2.

Si SiO, SiS, Si, SiO_2, SiH_4, SiH, SiN, Si_2.

Mg Mg, MgH, MgS, MgO, MgOH.

S H_2S, SiS, HS, S, CS, S_2, SO, MgS, CaS, AlS, SO_2, CS_2, SnS, BS.

Fe Fe, FeO, $Fe(OH)_2$.

Na Na, NaH, NaOH, NaO, Na_2.

Al Al, AlH, Al_2O, $AlHO_2$, AlO, AlOH, AlS, AlN.

Ca Ca, CaO, CaS.

Ni Ni, NiO.

Mn Mn, MnO.

Ti TiO, TiO_2, Ti.

V   VO, V, VO_2.

B HBO_2, BO, BO_2, BH_2, BS, BH, B, B_2O_2, B_2O_3.

Zr ZrO_2, ZrO, ZrH, Zr.

Table 7. Compounds considered (cont.)

Sn   Sn, SnO, SnS.

W   WO, WO_2, H_2WO_4, W, WO_3.

Hf HfO_2.

Th ThO_2.

Table 8. Partial pressures.[a]

xy	2000° K $P_{H_2} = 0.5$ atm. P_{xy}	P_{vap}	$P_{H_2} = 2.25 \times 10^{-4}$ P_{xy}	1700° K $P_{H_2} = 0.5$ atm. P_{xy}	P_{vap}
H_2	5.0×10^{-1}		2.25×10^{-4}	5×10^{-1}	
He	1.6×10^{-1}		8.0×10^{-5}	1.6×10^{-1}	
H	1.1×10^{-3}		2.6×10^{-5}	1.0×10^{-4}	
Ne	5.0×10^{-4}		2.5×10^{-7}	5.0×10^{-4}	
H_2O	4.9×10^{-4}		2.4×10^{-7}	4.9×10^{-4}	
CO	3.9×10^{-4}		2.1×10^{-7}	4.1×10^{-4}	
N_2	6.0×10^{-5}		3.0×10^{-8}	6.0×10^{-5}	
Mg	2.5×10^{-5}	4.8×10^{1}	1.3×10^{-8}	2.5×10^{-5}	1.3×10^{-1}
SiO	1.8×10^{-5}	$6.6 \times 10^{-2}(SiO_2)$	1.7×10^{-8}	1.8×10^{-5}	$1.3 \times 10^{-4}(SiO_2)$
H_2S	1.2×10^{-5}		2.9×10^{-10}	8.2×10^{-6}	
SiS	8.7×10^{-6}		4.5×10^{-10}	1.5×10^{-5}	
Ar	7.6×10^{-6}		3.8×10^{-9}	7.6×10^{-6}	
Fe	3.9×10^{-6}	$2.2 \times 10^{-4}(1)$	2.0×10^{-9}	3.9×10^{-6}	6.0×10^{-6}
HS	2.5×10^{-6}		3.6×10^{-9}	3.6×10^{-7}	
Na	2.0×10^{-6}		1.0×10^{-9}	1.9×10^{-6}	
Ca	1.6×10^{-6}	1.8	8.0×10^{-10}	1.6×10^{-6}	
Al	1.4×10^{-6}	$8.0 \times 10^{-3}(1)$	8.5×10^{-10}	1.2×10^{-6}	5.1×10^{-4}
Ni	9.0×10^{-7}	$2.0 \times 10^{-4}(1)$	4.5×10^{-10}	9.0×10^{-7}	3.3×10^{-6}
AlH	2.6×10^{-7}		3.2×10^{-12}	4.1×10^{-7}	
MgH	2.2×10^{-7}		2.9×10^{-12}	2.1×10^{-7}	
S	1.6×10^{-7}		8.5×10^{-9}	3.8×10^{-9}	
Mn	1.4×10^{-7}	1.8×10^{-1}	6.8×10^{-11}	1.4×10^{-7}	1.2×10^{-2}

Table 8. Partial pressures (cont.)

xy	P_H2 = 0.5 atm. P_{xy}	P_{vap}	P_H2 = 2.25x10^-4 P_{xy}	P_H2 = 0.5 atm. P_{xy}	P_{vap}
		2000° K		1700° K	
OH	1.2×10^{-7}		2.5×10^{-9}	5.2×10^{-8}	
CO_2	9.0×10^{-8}		4.7×10^{-11}	1.2×10^{-7}	
Al_2O**≠	8.3×10^{-8}	5.4×10^{-8} (Al_2O_3)	2.8×10^{-14}	6.5×10^{-10}	1.8×10^{-12} (Al_2O_3)
NH_3	5.0×10^{-8}		1.2×10^{-14}	8.2×10^{-8}	
TiO**	7.1×10^{-8}	1.6×10^{-6}	3.5×10^{-11}	6.1×10^{-8}	4.5×10^{-9}
NaH	1.1×10^{-8}		1.2×10^{-13}	8.2×10^{-9}	
CS	7.4×10^{-9}		2.1×10^{-15}	6.9×10^{-9}	
NaOH	6.0×10^{-9}		6.3×10^{-14}	1.5×10^{-7}	
HCN	5.8×10^{-9}		1.4×10^{-16}	1.8×10^{-9}	
VO**	5.4×10^{-9}	8.5×10^{-7}	2.7×10^{-12}	5.4×10^{-9}	4.5×10^{-9}
CH_4	5.2×10^{-9}		7.1×10^{-19}	1.5×10^{-8}	
TiO_2**	4.8×10^{-9}	1.2×10^{-7}	2.4×10^{-12}	1.8×10^{-8}	1.9×10^{-10}
CHO	4.7×10^{-9}		6.6×10^{-14}	1.5×10^{-9}	
$AlHO_2$	4.7×10^{-9}		5.6×10^{-14}	7.9×10^{-8}	
CH_2O	4.5×10^{-9}		1.5×10^{-12}	8.2×10^{-9}	
MgS	3.9×10^{-9}	8.5×10^{-4}	1.3×10^{-10}	2.7×10^{-9}	5.5×10^{-6}
Ti	3.7×10^{-9}	1.3×10^{-5}	1.9×10^{-12}	5.4×10^{-10}	9.2×10^{-8}
S_2	2.4×10^{-9}		4.7×10^{-12}	1.1×10^{-10}	
Kr	1.6×10^{-9}		8.1×10^{-13}	1.6×10^{-9}	
SO	1.5×10^{-9}		5.0×10^{-11}	3.1×10^{-11}	
AlO	1.3×10^{-9}	1.6×10^{-9} (Al_2O_3)	7.4×10^{-13}	9.3×10^{-10}	3.2×10^{-13} (Al_2O_3)
CaO	1.0×10^{-9}	3.2×10^{-8}	4.2×10^{-14}	3.9×10^{-10}	2.8×10^{-10}

25

Table 8. Partial pressures (cont.)

| | 2000° K | | | 1700° K | |
| | P_{H_2} = 0.5 atm. | | P_{H_2} = 2.25x10^{-4} | P_{H_2} = 0.5 atm. | |
xy	P_{xy}	P_{vap}	P_{xy}	P_{xy}	P_{vap}
V	9.8×10^{-10}	2.3×10^{-6}	5.0×10^{-13}	2.6×10^{-10}	1.1×10^{-8}
BHO$_2$	7.7×10^{-10}		1.8×10^{-13}	7.9×10^{-10}	
NH$_2$	7.4×10^{-10}		7.4×10^{-14}	1.1×10^{-10}	
Si	7.3×10^{-10}	2.6×10^{-5}	6.0×10^{-13}	6.7×10^{-11}	9.6×10^{-6}
CH$_3$	5.5×10^{-10}		3.5×10^{-18}	1.9×10^{-10}	
CaS**	2.6×10^{-10}	1.3×10^{-8}	4.7×10^{-15}	1.4×10^{-10}	4.4×10^{-11}
VO$_2$	2.3×10^{-10}	2.8×10^{-4}	1.1×10^{-13}	1.1×10^{-9}	2.2×10^{-6}
O	2.2×10^{-10}		2.1×10^{-10}	8.2×10^{-13}	
ZrO$_2$**≠	2.2×10^{-10}	6.9×10^{-11}	1.1×10^{-13}	2.6×10^{-10}	2.5×10^{-14}
SiO$_2$	1.8×10^{-10}	2.7×10^{-6}	1.6×10^{-13}	1.9×10^{-10}	1.5×10^{-9}
NH	1.5×10^{-10}		7.1×10^{-14}	3.7×10^{-12}	
Xe	1.2×10^{-10}		5.8×10^{-14}	1.2×10^{-10}	
AlOH	1.0×10^{-10}		1.3×10^{-15}	2.1×10^{-10}	
MgO**	9.7×10^{-11}	1.0×10^{-7}	5.3×10^{-14}	1.5×10^{-10}	1.5×10^{-10}
ZrO	9.3×10^{-11}		5.1×10^{-14}	6.0×10^{-11}	
FeO	8.6×10^{-11}	7.1×10^{-4}	4.2×10^{-14}	3.5×10^{-11}	5.1×10^{-6}
AlS	6.3×10^{-11}		2.0×10^{-15}	3.9×10^{-11}	
NiO	5.2×10^{-11}	2.6×10^{-4}	2.5×10^{-14}	7.7×10^{-12}	3.1×10^{-6}
NO	4.8×10^{-11}		1.0×10^{-13}	1.1×10^{-12}	
MgOH	3.9×10^{-11}		4.1×10^{-16}	2.2×10^{-10}	
Sn	3.8×10^{-11}	1.3×10^{-3}	1.9×10^{-14}	3.7×10^{-11}	1.6×10^{-4}
BO	2.3×10^{-11}		2.2×10^{-13}	9.0×10^{-13}	

Table 8. Partial pressures (cont.)

xy	2000° K $P_{H_2} = 0.5$ atm. P_{xy}	P_{vap}	$P_{H_2} = 2.25 \times 10^{-4}$ P_{xy}	1700° K $P_{H_2} = 0.5$ atm. P_{xy}	P_{vap}
MnO	1.4×10^{-11}	7.1×10^{-5}	6.9×10^{-15}	3.0×10^{-12}	1.6×10^{-7}
N	8.0×10^{-12}		1.7×10^{-13}	2.3×10^{-11}	
SiH$_4$	7.4×10^{-12}		1.4×10^{-21}	2.3×10^{-11}	
Fe(OH)$_2$	4.6×10^{-12}		1.1×10^{-18}	5.5×10^{-11}	
WO	3.8×10^{-12}		2.0×10^{-15}	2.0×10^{-13}	
HfO$_2$**≠	3.3×10^{-12}	1.4×10^{-12}	1.6×10^{-15}	3.3×10^{-12}	3.8×10^{-15}
SO$_2$	2.5×10^{-12}		7.8×10^{-14}	8.4×10^{-14}	
SnO	2.1×10^{-12}	2.0×10^{3}	1.0×10^{-15}	3.0×10^{-12}	1.3×10^{1}
C$_2$H$_2$	1.7×10^{-12}		3.9×10^{-22}	1.5×10^{-13}	
SiH	1.5×10^{-12}		2.9×10^{-17}	4.0×10^{-14}	
HCNO	1.2×10^{-12}		3.9×10^{-20}	1.1×10^{-12}	
ThO$_2$**	1.0×10^{-12}	6.3×10^{-11}	5.0×10^{-16}	1.0×10^{-12}	2.5×10^{-14}
CS$_2$	8.1×10^{-13}		5.3×10^{-19}	8.0×10^{-13}	
BH$_3$	5.9×10^{-13}		5.6×10^{-20}	9.3×10^{-17}	
BO$_2$	4.4×10^{-13}		4.5×10^{-15}	3.7×10^{-14}	
NaO	3.6×10^{-13}		1.7×10^{-16}	3.6×10^{-14}	
AlN	2.5×10^{-13}		3.2×10^{-18}	5.1×10^{-14}	
CH$_2$	1.2×10^{-13}		4.1×10^{-17}	1.9×10^{-15}	
BH$_2$	1.2×10^{-13}		5.4×10^{-19}	9.8×10^{-16}	
O$_2$	9.6×10^{-14}		9.1×10^{-14}	3.6×10^{-16}	
CN	9.3×10^{-14}		9.2×10^{-18}	2.6×10^{-15}	
WO$_2$	8.9×10^{-14}	1.3×10^{-7}	4.5×10^{-17}	1.4×10^{-14}	1.2×10^{-10}

Table 8. Partial pressures (cont.)

xy	2000° K $P_{H_2} = 0.5$ atm P_{xy}	P_{vap}	$P_{H_2} = 2.25 \times 10^{-4}$ P_{xy}	1700° K $P_{H_2} = 0.5$ atm P_{xy}	P_{vap}
H_2WO_4	7.9×10^{-14}		1.9×10^{-20}	3.7×10^{-12}	
Na_2	2.9×10^{-14}		7.2×10^{-21}	5.4×10^{-21}	
ZrH	1.9×10^{-14}		2.7×10^{-19}	5.7×10^{-16}	
$W**\!\!/$	1.9×10^{-14}	4.6×10^{-15}	9.9×10^{-18}	1.4×10^{-16}	3.6×10^{-19}
Zr	1.5×10^{-14}	2.4×10^{-9}	8.0×10^{-18}	1.2×10^{-16}	3.3×10^{-12}
WO_3	8.0×10^{-15}	5.5×10^{-5}	3.9×10^{-18}	4.5×10^{-15}	2.2×10^{-7}
CH	8.0×10^{-15}		1.2×10^{-19}	1.5×10^{-17}	
C_2H_4	5.6×10^{-15}		6.6×10^{-22}	5.3×10^{-15}	
BS	2.8×10^{-15}		1.0×10^{-18}	2.0×10^{-17}	
BH	1.6×10^{-15}		3.4×10^{-19}	9.1×10^{-18}	
B	1.3×10^{-15}		1.3×10^{-17}	2.1×10^{-18}	
C	1.1×10^{-15}	3.9×10^{-11}	6.2×10^{-19}	6.3×10^{-18}	1.7×10^{-14}
SnS	7.1×10^{-16}	6.2×10^{-3}	1.5×10^{-20}		
SiN	8.3×10^{-17}		1.4×10^{-20}	2.5×10^{-17}	
Si_2	5.3×10^{-17}		3.5×10^{-23}	1.8×10^{-16}	
B_2O_2	5.2×10^{-17}		4.8×10^{-21}	1.9×10^{-17}	
B_2O_3	3.8×10^{-17}		1.7×10^{-21}	9.2×10^{-17}	
NO_2	5.3×10^{-20}		1.1×10^{-22}	1.3×10^{-22}	
C_2	2.5×10^{-21}		8.1×10^{-26}	5.3×10^{-23}	
C_2N_2	3.6×10^{-23}		3.5×10^{-31}	1.3×10^{-19}	
C_3	1.1×10^{-24}		2.0×10^{-34}	4.3×10^{-25}	

a-Those species condensed at 2000° K are denoted by a $\neq$, and those condensed at 1700° K are marked with **.

Experimental Investigation

Introduction: The theoretical calculations presented in the previous section suggest experiments which would help to analyze the kinetic effects involved. In particular, condensation from a vapor phase whose chemical composition is carefully controlled gives products which can be analyzed for their chemical and mineralogical composition.

One needs both an intense and rapid heat source. Nelson (1962) described one such source using a flash discharge lamp where in pulses of a few milliseconds radiant energies of many tens of joules/cm^2 are obtained. The usual lamp is the standard quartz helix filled with Xe used to excite ruby lasers. The crystal is replaced with a sample and a reflector placed around the lamp. With a finely divided sample, so that the surface area to volume ratio is large, temperatures large enough to vaporize the sample are produced. In this way such refractory materials as C or W have been vaporized.

Instrumentation: An apparatus was designed based on this technique, and is shown in fig. 1. The operating characteristics of these circuits are described by Warner (1956), Marshak and Shchoukin (1961), Buck et al. (1963), and Lincoln (1964). Initially, a Kemlite reverse helix YRH-50-16 (special) lamp was used. This had a hold-off voltage of 20 kV, and could be operationally fired at 15 kV. The lamp is mounted horizontally and held in place with a fixed base at one end. Around this is placed a reflector—generally a silvered pyrex sleeve. The sleeve is supported at both ends in a plexiglas mount. This tube broke the first time it was fired (at 5.5 kV). Although not confirmed, apparently the lamp vibrates while discharging. The unmounted end

Fig. 1. 9000 Joule flash apparatus

strikes the reflector, snapping off several coils of the lamp, and shattering the reflector. In all cases the greatest amount of damage to the tube was at the unrestrained end. After breaking three lamps of similar design, a Kemlite HH-103-6 lamp was tested. This lamp is a nine-turn helix, mounted vertically, with no supports except the electrical connections. Thus movement in the system is allowed. The lamp is constructed of 12 mm o.d. quartz and the helix has an i.d. of 38 mm. The hold-off voltage is only 5 kV and therefore a General Electric Gl-7703 Ignitron was installed in the circuit. The maximum operational voltage for the tube is 20 kV and maximum energy is 20 kjoules. A G.E. Ft-625 lamp was loaned to us by Dr. Nelson and was used too. It is very similar in all characteristics except operating voltage. It has a hold-off voltage of 5.5 kV and an operating voltage of 4 kV. However the maximum energy is 25 kjoule.

The system was further modified by adding a third 60 μf, 10 kV Sangamo capacitor, plus a (630 μh or 330 μh) choke. These lengthen the pulse to about 1 msec and thus decrease the shock to the system. However, they do cause ringing which if severe enough could rupture the capacitors. Lincoln (1964) has shown that when the resistance of the choke is negligible compared to that of the lamp, the total energy output of the lamp is not seriously affected.

At this point it is useful to discuss the various physical parameters of the apparatus. Table 9 gives the basic data. The resistance of the flashlamp can be calculated using the equation of Edgerton et al. (1963), where:

$$R_{tube} = \frac{4 \gamma L}{D^2}$$

$$= 2.0 \text{ ohms, for the Kemlite HH-103-6}$$

lamp. γ is a constant depending upon the current density, L equals the arc length in centimeters, and D is the bore diameter in centimeters. This figure agrees with values found by Lincoln (1964) for the G.E. FT-625 lamp.

Table 9. Flash apparatus data.

C = x . 60 μf, where x = 2 or 3

V = 10 kV max   (lower limit depends upon lamp)

$E_{max} = \frac{1}{2} C_{max} V^2_{max}$ = 9 kjoules

Because heavy Cu bus bar is used, the resistance of the electrical connections in the apparatus is small. Similarly, the resistance of the ignitron is infinite until pulsed and then is essentially zero. The chokes were designed to have a resistance of less than 0.1 ohms, and are installed in series with the lamp. Then the current is 5000 amps and the pulse length without a choke is 0.36 msec.

The capacitors and the ignitron each have an inductance of 0.04 μh. The lamp has a fairly large inductance, on the order of 60 μh. Without a choke, $\frac{R^2}{4L^2} > \frac{1}{LC}$, and thus the system is overdamped. However, with a choke, when L = 700 μh, the system is underdamped and has a ringing frequency of 3.9×10^2 cycles/sec. The life expectancy of the capacitors is a function of the ringing frequency, and this low value should allow extended life times.

The radiant output of the lamp was studied following the work of Kuebler and Nelson (1961). A 3.50x30.00 mm graphite cylinder, weighing 0.4644 gm with a hole 0.60 mm x 10.0 mm deep taped into the center of one end, was obtained by turning down on a lathe a larger C
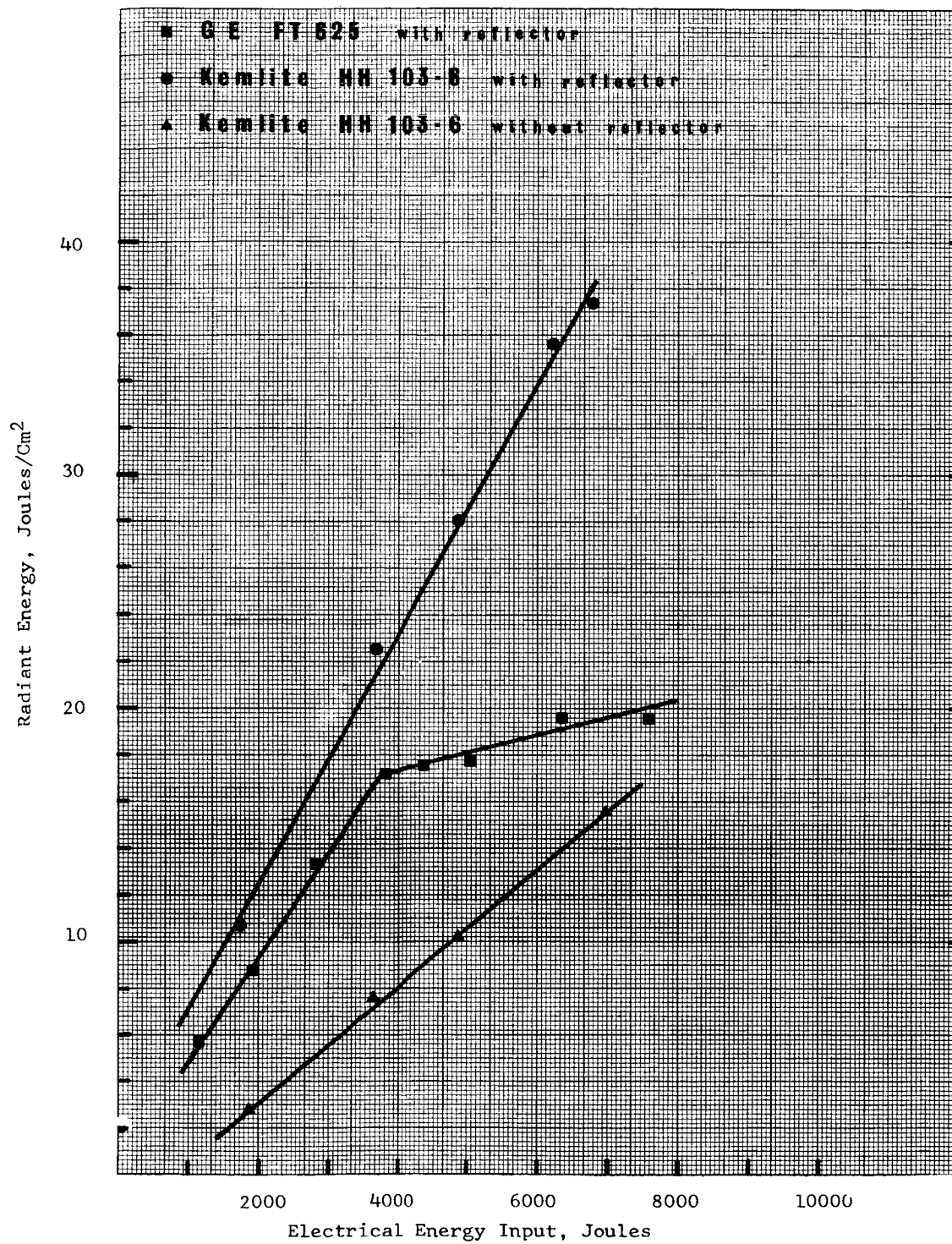
Fig. 2. Relationship of observed radiant energy
to the input electrical energy.

Manual). With increasing voltages, the peak in the infra-red becomes less important, while the second peak moves toward lower wavelengths. This may be an explanation for the observed radiant energy output of the FT-625 lamp. Possibly at high voltages most of the radiation is being generated primarily in the U. V. and is absorbed by the quartz tube.

Consider the heating (and subsequent cooling) of particles using this apparatus. The radiant energy absorbed by the particle must be equal to the energy used in heating the particle plus energy lost by conduction and radiation after flashing (Lundberg et al., 1957). This neglects small energy sinks, such as phase changes, and also assumes for simplicity that the conduction and radiation occur at some temperature corresponding to T max. Then one derives:

$$\alpha_1 4\pi r^2 F = \frac{4}{3}\pi r^3 \rho_1 C_{P_1}(T-T_0) + 4\pi r K_2 \Delta t (T-T_0) + \alpha_1 \sigma 4\pi r^2 \Delta t (T^4-T_0^4)$$

where $(T-T_0)$ is the particle temperature rise, κ_1 is the emissivity, F the radiant flux (cal/cm^2), ρ_1 the particle density, C_{P_1} the particle's specific heat, r the radius for the assumed spherical partical, K_2 is the thermal conductivity of the matrix of the particles, t is the pulse length, and σ is the Stephan-Boltzmann constant. For the purposes of this calculation it will be assumed that the absorption coefficient is unity, whereas in reality it varies with wavelength, and for this system would be a very difficult number to deduce. This point will be discussed later.

Consider the cases for r = 0.5μ, and 5μ for both silicates and metal, with a pulse length of 0.4 msec. and 1 msec.

let $A = \dfrac{\rho_1 C_{P_1} r}{3}$, $B = \dfrac{K_2 \Delta t}{r}$, $C = \alpha_1 \sigma \Delta t$

then $T - T_0 = \dfrac{\alpha_1 F}{A + B + C(T^2 + T_0^2)(T + T_0)}$

or $T + \left(\dfrac{C}{A + B}\right) T^4 = \dfrac{\alpha_1 F}{A + B} + T_0 + \left(\dfrac{C}{A + B}\right) T_0^4$

Then for iron, $\rho_1 = 7.86$ gm/cc, $C_p = 0.2$ cal/gm . deg, $\alpha_1 = 0.10$, and for air $K_2 = 5.7 \times 10^{-5}$ cal/cm.sec.deg, giving $\alpha_1 F = 1$ cal/cm^2, and $T_0 = 298°$ K. Similarly for stones, use $\rho = \frac{1}{2}\rho_{iron}$, C_p same, and $\alpha = 0.06$ (very dependent on smoothness of the surface), so that $A_{stone} = \frac{1}{2} A_{iron}$, $B_{stone} = B_{iron}$, and $C_{stone} = 6 C_{iron}$.

The results of the calculations are shown in Table 10. It is readily seen that two very different sets of conditions are required in the case of the two materials, to achieve maximum heating. Low emissivity material requires a relatively long pulse but small particle radius, while material with a higher emissivity requires a relatively short pulse on larger grains for maximum heating. As is seen, there is a play-off between A (particle heating) and B (conduction loss) in the region of the conditions chosen. Also we see that the radiation losses (C) increase with increasing pulse length. However, most important, this data suggests that by judiciously picking the experimental conditions, this apparatus should be able to heat any samples of interest to or above their boiling points.

For evaporation of the particles the heating pulse-length must be longer than the time required for the evaporation. When the pressure is kept low, so that vapor diffusion is not a controlling step, the evaporation rate is dependent upon the surface area, and is easily calculated using the Langmuir equation:

Rate of evaporation $= KP\theta$, where K is a factor derived from

Table 10. Conditions for maximum sample heating.

Iron

r(cm)	t(sec)	A $\left(\frac{cal}{cm^2 \cdot deg}\right)$ particle heating	B $\left(\frac{cal}{cm^2 \cdot deg}\right)$ conduction	C $\left(\frac{cal}{deg^4}\right)$ radiation	$\frac{C}{A+B}$ (deg^{-3})	$\frac{\alpha_1 F}{A+B}$ (deg)	T (deg)
5×10^{-5}	4×10^{-4}	2.5×10^{-5}	4.6×10^{-4}	5.6×10^{-17}	1.2×10^{-13}	2.06×10^3	2.36×10^3
	1×10^{-3}	2.5×10^{-5}	1.1×10^{-5}	1.4×10^{-16}	3.9×10^{-12}	2.7×10^4	9.2×10^3
5×10^{-4}	4×10^{-4}	2.5×10^{-4}	4.6×10^{-5}	5.6×10^{-17}	1.9×10^{-13}	3.4×10^3	3.7×10^3
	1×10^{-3}	2.5×10^{-4}	1.1×10^{-4}	1.4×10^{-16}	3.9×10^{-13}	2.7×10^3	3.0×10^3

Stone

r(cm)	t(sec)	A	B	C	$\frac{C}{A+B}$	$\frac{\alpha_1 F}{A+B}$	T (deg)
5×10^{-5}	4×10^{-4}	1.3×10^{-5}	4.6×10^{-4}	3.4×10^{-16}	7.2×10^{-11}	1.3×10^4	3.5×10^3
	1×10^{-3}	1.3×10^{-5}	1.1×10^{-5}	8.4×10^{-16}	3.4×10^{-11}	2.5×10^5	9.1×10^3
5×10^{-4}	4×10^{-4}	1.3×10^{-4}	4.6×10^{-5}	3.4×10^{-16}	1.9×10^{-12}	3.4×10^4	1.2×10^4
	1×10^{-3}	1.3×10^{-4}	1.1×10^{-4}	8.4×10^{-16}	3.4×10^{-12}	2.5×10^4	7.8×10^3

kinetic theory

$$K = \frac{N}{(2\pi RMT)^{\frac{1}{2}}}$$

P = sample vapor pressure

θ = fraction of unoccupied sites on the sample

N = Avogadro's number

For iron, $K = 2\times10^{20}$ atoms/(gr. joule)$^{\frac{1}{2}}$ and at the standard boiling point (2800° C), the vapor pressure of iron is one atmosphere. This gives a rate of evaporation of 6×10^{22} atoms/cm^2 sec., assuming $\theta = 1$. If we chose 10μ as the particle diameter, $t = 2.4\times10^{-4}$ sec., which is just inside the capabilities of the apparatus without the choke. It is believed that in fact, under these conditions, iron powder was vaporized. This will be discussed in more detail later.

If a total of 100 mg. of Fe, with particle diameters less than 10μ, is so arranged that each particle is side-by-side and thus visible to the light pulse, they will be vaporized. This requires, from ΔH of vaporization = $\int C_p dT$ = 197.1 kcal/mole (where C_p data for the solid is from Kubachewski and Evans (1958), and for the liquid is from Stull and Sinke (1956), only 350 cal. However, over this area, the radiant energy of the pulse is 380 cal, or just enough for the vaporization. Going to smaller particles (as 1μ diameter) requires that the sample be uniformly spread over a larger area and thus a larger fraction of the energy from the lamp is unused in the vaporization.

A volume of about 100 cc at a rough vacuum of 100μ contains about 3.6×10^{17} molecules of air. During the vaporization of 100 mg of iron there will be 1.1×10^{21} Fe$_{(g)}$ atoms present, giving a momentary P_{Fe} = 310 mm. These atoms will have a root mean square velocity of

$1.1x10^5$ cm/sec, and since the i.d. of the sample container is on the order of 4 cm, there is time for several traversals of the container in a time of 0.1 msec. This supports the argument that thermal and chemical equilibration is achieved inside the container in the times of the light pulse. Since the energy of vaporization is only a fraction of the energy supplied, it is very possible that the particles are superheated before vaporization occurs. This phenomenon has been suggested to explain results observed in flash heating experiments with W by Nelson and Kuebler (1963), and with Cd by Saltsburg (1965).

Another physical property of the gas phase of particular interest is the degree of ionization. Using the Saha equation, this can be easily calculated (Aller, 1963):

$$\frac{N_i P_e}{N_0} = \frac{(2\pi M)^{2/3}(kT)^{5/2}}{h^3} \cdot \frac{2U_1(T)}{U_0(T)} e^{-I_x/kT}$$

where N_x is the number of atoms per cm^3 in the Xth state of ionization, I_x is the ionization potential for the Xth state of ionization, $U_X(T)$ is the partition function, and P_E is the electron pressure. However, substituting $P_e = N_e kT$ and expanding, we get

$$\log \frac{N_1 N_e}{N_0} = \frac{5040\ I_1}{T} + 1.5 \log T - 0.48 + \log 2\ U_1(T)/U_0(T)$$

Assuming that only the singly ionized iron is formed, and that $N_E = N_1$, we find that

$$\frac{N_1^2}{N_0} = 1.3x10^{-8}$$

and thus in the vapor containing $1.1x10^{21}$ Fe atoms at $3000°$ C there will be only $3.8x10^6$ Fe^+ ions, indicating a very weakly ionized gas phase. This number is certainly only a lower limit, though, as the

presence of trace quantities of atoms with a very low ionization potential may produce impurity ions swamping out those of the dominant atomic species. An abundance of Na at 10^{-4} of Fe, gives 6.6×10^6 Na$^+$ ions, which is almost twice the number of Fe$^+$ ions. The presence of these ions are very important as possible sites for nucleation, especially in more sophisticated experiments where the vapor is contained in such a way as to prevent interaction with the vessel walls and other surfaces.

Results: The preliminary flash experiments were carried out at 2 cal/cm^2, using powders. These were suspended on the inside of the normal pyrex test tube by slurrying the powder in acetone, and then horizontally rotating the test tube until all the acetone had evaporated. The tube was left open. Repeatedly, dark powders, as Fe_3O_4, Fe_2O_3, or Fe showed agglomeration apparently due to in situ melting of the powders. The lighter powders, as MgO, SiO_2, or Al_2O_3 showed no change. The next set of samples was prepared as above but the tubes were evacuated to about 100μ pressure and sealed. The results were more striking, as the dark iron and iron oxides formed a metallic mirror on the inside of the walls. Again the light powders showed no effect. When these tubes were inspected under the microscope it was seen that the iron has reacted with the glass walls of the tube causing the glass to craze and in places to flake off. It was impossible to remove samples from the wall of the tube, and thus this material was not analyzed.

The pyrex dish was replaced with a quartz boat to reduce interaction between sample and support. The boat was simply a piece of quartz tubing sliced along its long axis, with end plates added and

covered with a quartz slide.
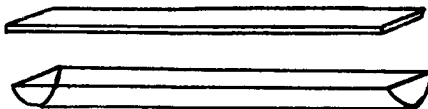
The sample was loaded on the bottom curved surface using a dispersant such as acetone. Then any sample on the glass slide arrived during the flash. This slide is easily inspected with a microscope, and powder in the boat is used for X-ray analysis. With this technique, the following samples were flashed as fine powders at about 6 cal/cm^2, Fe_3O_4, Fe_2O_3, Fe, 1:1 Fe + Fe_2O_3, 1:1 MgO + Fe_2O_3, 1:2 Fe_2O_3 + Al_2O_3 and 1:1 Mg + Fe_2O_3. These samples were analyzed by X-ray powder diffraction techniques using Fe Kα X-rays (λ = 1.9360 $\overset{o}{A}$), and in no case were any new phases detected. Furthermore, in many cases it was difficult to collect the material for the analysis suggesting that the melted (and possibly reacted) material was at least partially bonded to the quartz, and that the loose powder may have been shielded and thus not substantially heated.

Further experiments were designed so as to minimize the wall interactions. In these experiments the vertical flash lamps were used. First the sample was led into a gas stream, usually N_2, which was controlled with baffles, etc., to keep it away from the walls. Both injections from above and below the lamp were attempted, but three major problems must be solved before successful operation:

(a) prevention of electrostatic attraction of the dust for the walls,

(b) simultaneous pulsing with the passage of the primary

dust band, and

(c) absolute separation of the flashed and unflashed sample. The last problem is the most difficult and eventually caused the termination of this mode of operation.

Next as a solution to the problem of separating the heated from the non-heated sample, it was decided to return to having the sample sit at a fixed position. Then after flashing, all material collected from sites where there was originally no sample must have been transported there during the flash. Furthermore, to remove the problem of the interaction of the substrate with the sample, it is proposed that substrate and sample be chemically identical. However, to fulfill the physical reqirements for maximum heating, the cross-sectional area must be large as compared to the volume. These requirements can be satisfied with fibers. They would provide us with:

(a) known and reproducible geometry

(b) easily calculated volume vaporized

(c) simplified handling and mounting

(d) simplified separation of the unvaporized sample.

Unfortunately unless the composition desired can be obtained commercially, considerable time and expense must be invested in preparing these fibers. Both Owens-Corning Fiberglas Corp. in Los Angeles and Western Fibrous Glass in Los Angeles were contacted about this problem. Due to the proprietary nature of their work they were unable to supply chemical compositions of the glass fibers that they have available. The expense of special batches made this route not feasible.

Simultaneously experiments were performed to find a lining

material for the quartz container that would simplify the recovery of the heated sample but would not seriously reduce the radiant energy density. Various plastics, particularly fluorocarbons, were obtained in 0.5 mil, 1 mil, and 2.5 mil thicknesses and flashed inside an evacuated quartz column. Polyethylene, mylar, and Aclar (Allied Chemical trademarked name for polytrifluorochloroethylene) all proved to be unacceptable, with some local charring, tearing, and shriveling. DuPont's FEP (a copolymer of tetrafluoroethylene and hexafluoropropylene) is transparent, and thus possibly more desirable than the TFE (tetrafluoroethylene) which is translucent. After heating, the FEP developed small bubbles ($< 100 \mu$) in the film, while the TFE was unaffected. When a pyrex fiber was flashed inside each of these films the same amount of heating was seen. Thus for all the future fiber experiments a single layer of 1 mil TFE teflon was used as a lining immediately inside the quartz container.

The glass fibers (9μ diameter) were hung from a slotted teflon disc (1 mm thick) which snugly fitted into the quartz container just above the TFE liner. This disc had two large holes in it for pressure equilibration on each side, and the fibers were held by friction with the edges of the slit. A teflon cup is placed at the bottom of the liner to intercept falling particles. When flashed at 8 cal/cm^2 the fibers melt (at least) completely, and only glass spherules are detected. These tend to be about 100μ in diameter, show bubbles inside them, and appear opalescent under the microscope with reflected light. The spherules are collected by placing the teflon liner and cup in a beaker of water in an Acoustica ultrasonic bath for five minutes. This water

is passed through a Millipore filter with pore size of 0.45μ. The teflon liner and the quartz container are inspected carefully for material still adhering. In this way it was found in the above experiment that only about 5% of the original mass could be accounted for, suggesting that significant vaporization had occurred.

Next, 5 quartz fibers were flashed in the same manner, with no detectable effects. Then these quartz fibers were used as support for powders. However it now became difficult to collect much sample. In successive experiments, Fe, Fe_3O_4, Fe_2O_3, and dunite were flashed and the sample collected on Millipore filters. Probably some fifty experiments would be required to build up enough flashed powder for X-ray analysis. Thus these samples were merely inspected under a microscope. It was found that contamination becomes important at these levels. Contaminants most easily picked out are bright red or yellow flakes with lengths of 50 to 100μ. Also organic fibers, both clear and colored, are seen. When the iron and iron oxides are flashed, hundreds of small (30μ down to the resolving limit at 100x, $\sim 2\mu$) metallic appearing spherules are seen. With the dunite similar results are seen with a large number of clear spherules in the same size range. Apparently the dunite was melted.

Finally the sample was slurried directly onto the teflon liner. In this way several hundred mg of sample could be irradiated simultaneously. Using Fe_3O_4 powder ($\leqslant 43\mu$) and flashing in one atmosphere pressure of N_2 at 10 cal/cm^2 the following results were observed on the teflon liner: (a) the entire length of liner was covered with "whiskers", each of which had an apparent size of about 0.5 x 1 mm.

In any particular area (a few square mm) all the whiskers are aligned, but no gross pattern is seen between each adjacent area, and also (b) there was a general brown coloration uniformly distributed over the liner, as if a layer of Fe were plated out. The teflon liner was cut into several pieces which were set aside. In Fig. 3 are shown a picture of these whiskers taken at 250x and a picture of the same sample taken at 8000x. These "whiskers" are aligned spherules, ranging in size from typically 100 $\overset{o}{A}$ to 1000 $\overset{o}{A}$ in diameter. Realizing this, the particles were tested and found to be magnetic. This suggests that momentary magnetic fields associated with the flash lamp aligned the condensing material on the teflon liner. However they must have been cool, as the liner was carefully inspected, and no holes, scorching, or other evidence was detected to suggest that the liner had been heated significantly.

Chemical analyses of two of the larger single spherules were attempted by X-ray diffraction using a Chesley camera (Chesley, 1947). Fe $K\alpha$ X-rays at 20 kV and 15 ma were used for a period of 11.3 hours for sample #1 and 22.7 hours for #2. The film was then placed in an enlarger in a dark room and the spots were traced on a white piece of paper. The film to sample distance, a, was recently calibrated and found to be 1.13 cm. Then the d spacings were obtained knowing that

$$r/a = \tan 2\theta.$$

The results are ambiguous, and are listed in Table 11. The sample is certainly not Fe and since it is magnetic, the next best bet consistent with the X-ray analysis is Fe_3O_4. If that is true one would postulate that 100% vaporization and mixing in the gas phase did not occur, since
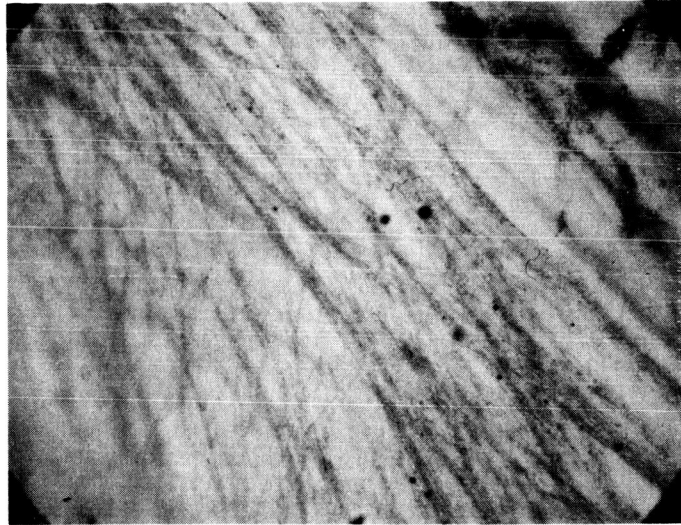
250x
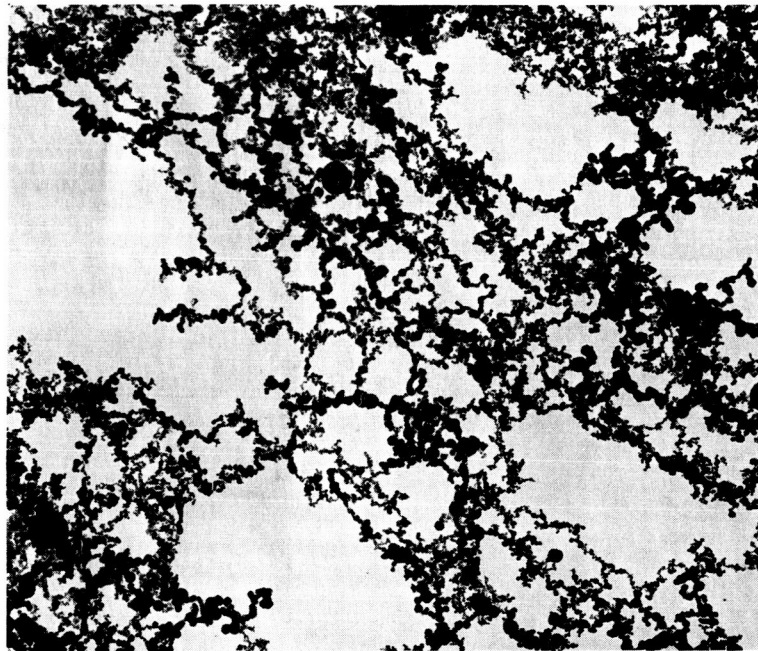
8000x

Fig. 3. Condensation "whiskers".

Table 11. Results from Chesley Camera X-ray analysis.

			ASTM cards (3 strongest lines)			
Fe_3O_4 #1	Fe_3O_4 #1		Fe	Fe_3O_4	Fe_4N	FeN
	7.62		2.03	2.97	2.19	2.34
d = 3.42	3.51		1.43	2.53	1.90	2.19
2.87	2.78 , 2.74		1.17	1.48	1.14	2.06
2.29	2.37 , 2.33					

Fe_3N, Fe_2N have no lines in common

under those conditions N should be incorporated into the condensing species.

In similar experiments, sieved dunite powder ($\leq 43\mu$) was flashed. No abnormal crystal growth was observed and no very fine particles were detected. On the other hand the powder did melt as the sample was primarily in the form of spherules ranging from a few microns in diameter up to about 30 microns. Also considerable variation in coloring was observed from clear to pale green to pale brown to dark spheres. The latter were definitely magnetic. Several of the dark spherules were examined with the Chesley Camera. Their pattern was very complex and difficult to interpret because of the extreme spottiness of the circles. Several grains of the original dunite powder were analyzed in this manner and the resulting film showed no detectable patterns, but rather an apparently random orientation of spots. This suggests that the flashed material is at least more crystalline than the sample powder.

Because of the failure to (a) generate a homogeneous vapor phase, (b) be able to control its chemical composition and (c) also control the subsequent condensation so as not to introduce influencing surfaces or species, this project was abandoned at this point. For future work on this type of problem it appears that one wants a different type of energy source, in particular one that can operate over a large distance (so that the containing volume is large) and yet be focused on a small area so that the sample is the substrate. Finally, the energy should be primarily in the IR, since the absorption coefficient for most silicates is a maximum near $\lambda = 10\mu$.

References

Allen C. W. (1903) <u>Astrophysical Quantities</u>. Athlone Press, London.

Aller L. H. (1963) <u>Astrophysics: The Atmospheres of the Sun and Stars</u>, 2nd edition. Ronald Press, New York.

Bouigue, R. (1957) Remarques comparatives sur les etoiles de types S et C. <u>Liege Mem</u>. <u>18</u>, 346-351.

Boyce P. and Sinton W. (1965) Infrared spectroscopy with an interferometer. <u>Sky and Telescope</u> <u>29</u>, 78-80.

Brewer L. (1953) The thermodynamic properties of the oxides and their vaporization processes. <u>Chem</u>. <u>Rev</u>. <u>52</u>, 1-75.

Brewer L. and Chandrasekharaiah M. S. (1960) Free energy functions for gaseous monoxides. <u>UCRL-8713</u> (rev.).

Brewer L. and Rosenblatt G. M. (1961) Dissociation energies of gaseous metal dioxides. <u>Chem</u>. <u>Rev</u>. <u>61</u>, 257-263.

Buck A., Erickson R., and Barnes F. (1963) Design and operation of Xe flashtubes. <u>J</u>. <u>Appl</u>. <u>Phys</u>. <u>34</u>, 2115-2116.

Cameron A. G. W. (1962) The formation of the sun and planets. <u>Icarus</u> <u>1</u>, 13-69.

Cayrel R. and Schatzman E. (1954) Sur la polarisation interstellaire par des particules de graphite. <u>Ann</u>. <u>d'ap</u>. <u>17</u>, 555-574.

Chesley F. G. (1947) X-ray diffraction camera for microtechniques. <u>Rev</u>. <u>Sci</u>. <u>Instr</u>. <u>18</u>, 422-424.

Danielson R. E., Woolf N. J., and Gaustad J. E. (1965) A search for interstellar ice absorption in the infrared spectrum of Mu Cephei. <u>Astrophys</u>. <u>J</u>. <u>141</u>, 116-125.

Dayhoff M. O., Lippincott E. R., and Eck R. V. (1964) Thermodynamic equilibria in prebiological atmospheres. <u>Science</u> <u>146</u>, 1461-1464.

De Jager C. and Nevin L. (1957) Les constantes de dissociation des molecules diatomiques d'interet astrophysique. <u>Liege Mem</u>. 18, 357-391.

Donn B., Wickramasinghe N. C., Hudson J. P., and Stecher T. P. (1966) On the formation of graphite grains in cool stars. Preprint.

Eck, R. V., Lippincott E. R., Dayhoff M. O., and Pratt M. O. (1966) Thermodynamic equilibrium and the inorganic origin of organic compounds. <u>Science</u> <u>153</u>, 628-633.

References (cont.)

Edgerton H. E., Goncz J. H., and Jameson P. W. (1963) Xenon flash lamp limits of operation. E. G. & G. Report.

Faulkner J., Griffiths K., and Hoyle F. (1963) On the Hayashi effect in the early phases of gravitational contraction of the sun. Roy. Ast. Soc., Mon. Not. 120, 1-10.

Freeman R. D. (1962) Thermodynamic properties of binary sulfides. Oklahoma State University Research Foundation Report #60.

Gaustad J. E. (1963) The opacity of diffuse cosmic matter and the early stages of star formation. Astrophys. J. 138, 1050-1073.

General Electric flashtube data manual, 9-50. General Electric Photo Lamp Dept., Nela Park, Cleveland, Ohio.

Goldberg L., Muller El, and Aller L. H. (1960) The abundances of the elements in the solar atmosphere. Astrophys. J. Suppl. 5.

Greenberg J. M. (1966) Wavelength dependence of polarization by small graphite flakes. Astrophys. J. 145, 57-62.

Greenberg J. M. and Shah G. (1966) A unified model of interstellar extinction and polarization I. Astrophys. J. 145, 63-74.

Hayashi C. (1961) Stellar evolution in early phases of gravitational contraction. Publ. Astr. Soc. Japan. 13, 450-452.

Herzberg G. (1950) Molecular Spectra and Molecular Structure, I: Spectra of Diatomic Molecules, second edition. D. Van Nostrand Co., Inc.

Herzberg G. (1957) Recent laboratory investigations on molecules of astronomical interest. Mem. Soc. R. Sci. Liege, 18, 397-418.

Inghram M. G., Chupka W. A., and Berkowitz J. (1957) Dissociation energies from thermodynamic equilibria studied with a mass spectrometer. Mem. Soc. R. Sci. Liege 18, 513-535.

JANAF thermochemical tables (1960) and later, compiled by Dow Chemical Co. Thermal Laboratory, Midland Mich.

Johnson H. L., Low F. J., and Steinmetz D. (1965) Infrared observations of the Neugebauer-Martz-Leighton "Infrared Star" in Cygnus. Astrophys. J. 142, 808-810.

Kamijo F. (1963) A theoretical study on the long period variable stars III, formation of solid or liquid particles in the circumstellar envelope. Publ. Ast. Soc. Japan. 15, 440-448.

References (cont.)

Kelley K. K. (1949) High temperature heat contents and entropies of inorganic substances. U. S. Bureau of Mines 476

Kelley K. K. (1962) Heats and free energies of formation of anhydrous silicates. U. S. Bureau of Mines. R. I. 5901.

Kubachewski O. and Evans E. (1958) Metallurgical Thermochemistry, third edition. Pergamon Press, London.

Kuebler N. A. and Nelson L. S. (1961) Radiant energies and irradiances of capacitor discharge lamps. J. Op. Soc. Am. 51, 1411-1416.

Larimer J. (1967) Chemical fractionations in meteorites, I. condensation of the elements. Preprint.

Larimer J. W. and Anders E. (1967) Chemical fractionations in meteorites, II. abundance patterns and their interpretations. Preprint.

Latimer W. M. (1950) Astrochemical problems on the formation of the earth. Science 112, 101-104.

Lewis G. N. and Randall M. (1961) Thermodynamics, second edition (revised by Pitzer K. S. and Brewer L.). McGraw-Hill, New York.

Lincoln K. A. (1964) Thermal radiation characteristics of xenon flash-tubes. Appl. Optics 3, 405-412.

Lippincott E. R., Eck R. V., Dayhoff M. O., and Sagan C. (1967) Thermodynamic equilibria in planetary atmospheres. Preprint.

Lord H. C. (1965) Molecular equilibria and condensation in a solar nebula and cool stellar atmospheres. Icarus 4, 279-288.

Lundberg J. L., Nelson L. S., and Hellman N. Y. (1957) Carbon formation by the flash illumination of polymers. Proc. third Conf. on Carbon, Buffalo, New York. 411-418.

Marshak I. S. and Shchoukin L. I. (1961) Physical and technical parameters of flashtubes. J. Soc. Mot. Pict. & TV. Engr. 70, 169-176.

McCammon D., Munch G., and Neugebauer G. (1967) Infrared spectra of low-temperature stars. Astrophys. J. 147, 575-586.

Merrill P. W. (1960) "Spectra of long-period variables." Chapt. 13, Stellar Atmospheres edited by J. L. Greenstein. Univ. of Chicago Press, Chicago.

References (cont.)

Nelson L. S. (1962) Intense rapid heating with flash discharge lamps. Science 136, 296-303.

Nelson L. S. and Kuebler N. A. (1963) Vaporization of tungsten studied by flash heating and kinetic spectroscopy. I. near-ultraviolet region. J. Chem. Phys. 39, 1055-1061.

Neugebauer G., Martz D. E., and Leighton R. B. (1965) Observations of extremely cool stars. Astrophys. J. 142, 399-401.

Russell H. N. (1934) Molecules in the sun and stars. Astrophys. J. 80, 317-342.

Saltsburg H. (1965) Flash evaporation. J. Chem. Phys. 42, 1303-1309.

Shimazu Y. (1967) Thermodynamic aspects of formation processes of the terrestrial planets and meteorites. Icarus 6, 143-174.

Spinrad H. and Newburn R. L. Jr. (1965) A low dispersion spectroscopic search for water vapor in cool stars. Astrophys. J. 141, 965-975.

Stanger P. (1960) Ohio State University thesis, unpublished.

Stull and Sinke (1956) Thermodynamic Properties of the Elements. Amer. Chem. Soc., Adv. in Chem., Series 18.

Suess H. E. (1962) Thermodynamic data on the formation of solid carbon and organic compounds in primitive planetary atmospheres. J. Geophys. Res. 67, 2029-2034.

Tsuji T. (1964a) Abundance of molecules in stellar atmospheres. Proc. Jap. Acad. Sci. 40, 99-104.

Tsuji T. (1964b) Molecular abundance in stellar atmospheres. Tokyo Ast. Obs. Annals, second series 9, #1, 1-110.

Urey H. C. (1951) The origin and development of the earth and other terrestrial planets. Geochim. et Cosmochim. Acta 1, 209-277.

Urey H. C. (1952) The origin and development of the earth and other terrestrial planets. A correction. Geochim. et Cosmochim. Acta 2, 263-268.

Urey H. C. (1953) On the concentration of certain elements at the earth's surface. Proc. Roy. Soc. 219A, 281-292.

Urey H. C. (1966) Chemical evidence relative to the origin of the solar system. Mon. Nat. R. Astr. Soc. 131, 199-223.

References (cont.)

Vardya M. S. (1966) March of molecular abundances in the outer layers of K and M stars. Joint Inst. Lab Astrophysics. Report #75.

Warner D. F. (1956) The application of large capacitors for use in energy storage banks. IRE Trans. Comp. Parts, 81-88.

Wickramasinghe N. C., Hudson J. P., and Stecher T. P. (1966) On the formation of graphite grains in cool stars. Preprint.

Wildt R. (1933) Kondensation in Sternatmospharen. Zeit f. Astrophysik 6, 345-354.

Wildt R. (1934) Uber die stellare Dissoziation des Wasserstoffmolekuls. Zeit f. Astrophysik 9, 176-184.

Wood J. A. (1963) On the origin of chondrules and chondrites. Icarus 2, 152-180.

Woolf N. J., Schwarzchild M., and Rose W. K. (1964) Infrared spectra of red-giant stars. Astrophys. J. 140, 833-852.

Solar Wind Interaction With Solids

Introduction

Meteorite research has grown very rapidly in the recent past, partly because of the possibility of using this information to help solve the more general problems of the origin and evolution of the solar system. Another source of material for these studies are the fine dust grains raining on the earth--the so-called "cosmic dust". Many origins have been postulated for this material, including comets, meteorite ablation products, rubble from collision of asteroids, secondary ejecta from meteorite impacts on the moon, etc. However, there exists the very difficult problem of recognizing a sample when it has been collected. Chemical or mineralogical identification is arbitrary, and this bias could eliminate much true cosmic dust. A property exhibited only by extraterrestrial dust is needed. One possibility is the occurrence of gases, primarily H_2 and He, injected by the solar wind as these grains spiraled toward the sun.

An experimental study of the retention of low energy ($\sim$2 keV) hydrogen and helium ions in several silicate materials is described here. Both the hydrogen and helium ions are retained quantitatively at the lowest integrated fluxes used ($\sim$5x10^{16} ions/cm^2), and above this, saturation of the gas in the silicates apparently occurs. Furthermore, X-ray diffraction studies, electron probe microanalysis, and microscopic examinations of the bombarded surfaces were performed.

Solar Wind

Parker (1964) describes the solar wind as "simply the expanding corona of the sun." This solar corona is the very tenuous outer atmosphere, containing some 10^9 atoms/cc, whose kinetic energy corresponds to a temperature of about 10^6 °C. The lighter atoms are thus completely ionized. However equal numbers of electrons travel with the ions, so that the plasma is neutral. The existence of the solar wind had been postulated for some time, and was used to explain certain observations, like the aurora borealis (possibly an interaction of the solar wind ions with the terrestrial upper atmosphere), and more importantly, that cometary tails nearly always point away from the sun, independent of the direction of travel of the comet (Biermann and Lüst, 1963).

However, only with the advent of space probes has experimental data about the solar wind been obtained. Lunik II (Gringauz et al., 1960) and Explorer X (Bonetti et al., 1963) made preliminary measurements of fluxes. Mariner II (Neugebauer and Snyder, 1962, 1966) was equipped with a ten channel electrostatic spectrometer which was set to point toward the sun. The current for each channel, corresponding to an energy range per unit charge varying from 230 volts for channel number one to 8224 volts for the tenth channel, was transmitted by the spacecraft. In general the spectra showed two peaks, or at least an anomalous shoulder to the main peak. The two channels most populated were at 1664 V and 2476 V, corresponding to velocities of 560 and 690 km/sec. for protons. However the double peaks are interpreted as being due to the presence of both protons and helium nuclei which have equal thermal velocities. The resulting flux appears to be about 2×10^8 particles/cm^2

/sec near the earth's orbit, or an average density of about 5 particles /cm^3 (Neugebauer and Snyder, 1966).

More recent observations with higher resolution apparatus have shown that there exists considerable anisotropy in both the ion temperature and the direction of plasma flow (Wolfe et al., 1966; Hundhausen et al., 1966). All other measured parameters are seen to vary with time, also. Mariner II results indicate that the plasma density and proton velocity are inversely related and values ranging from 300 to 800 km/sec are seen for the velocity. The proton to alpha ratio is not directly related to the bulk velocity, nor any other detected parameter.

Pioneer VI results (Wolfe et al., 1966), assuming some constant velocity for all ions in the solar wind over some small unit V and t, suggest that a third ionic species is present, most easily described as having m/q=4, giving He$^+$. The derived composition for a particular spectrum observed by Pioneer VI is given in Table 12. However, the

Table 12. Typical solar wind composition.

H$^+$	91.3%
He^{2+}	8.6%
He$^+$	0.1%

percent He^{2+} and He$^+$ was observed to vary widely, and at times was essentially zero. The solar wind ions are deflected by magnetic fields, but are expected to strike all other bodies in their path. The solar wind density decreases as 1/r and thus at some distance from the sun the streaming pressure becomes too small to push back the interplanetary medium. At this point it is thought that a shock front forms as the

The lifetimes of particles in orbits near the earth are easily calculated. Radiation pressure is effective in ejecting very small particles ($r \leqslant 0.1\mu$) from the solar system (Öpik, 1956). The Poynting-Robertson effect (Robertson, 1937) is primarily responsible for governing the lifetimes of the larger dust grains. Consider a particle in some orbit about the sun. It is continuously receiving radiation from the sun, which is then re-emitted isotropically. The incoming radiation has negligible angular momentum, but the outgoing radiation has the same angular momentum per unit mass as the particle. Thus with time the particle's momentum is reduced, causing the particles to spiral into the sun. The residence time (lifetime of the dust in the inner part of the Solar System) allowed by this Poynting-Robertson drag is given by:

$$t = 7.0 \times 10^6 \ r\rho qa \ \text{(years)} \quad \text{where } q = \text{initial perihelion (A.U.)}$$

$$a = \text{semi-major axis (A.U.)}$$

and for a circular orbit:

$$r = 1, \rho = 3.5 \ \text{gm/cm}^3, \ a = 1 \ \text{A.U.}, \ t = 2.45 \times 10^3 \ \text{yrs.};$$

$$a = 3 \ \text{A.U.}, \ t = 2.2 \times 10^4 \ \text{yrs.}$$

$$r = 100, \rho = 3.5 \ \text{gm/cm}^3, \ a = 1 \ \text{A.U.}, \ t = 2.45 \times 10^5 \ \text{yrs.}$$

$$a = 3 \ \text{A.U.}, \ t = 2.2 \times 10^6 \ \text{yrs.}$$

Öpik (1951) and Whipple (1950) have shown that particularly for those particles which intersect the earth with grazing orbits and low relative velocities a large fraction, increasing with decreasing particle size, are able to survive entry into the earth's atmosphere.

As we will see below, irradiations with more than approximately 10^{16} protons/cm^2 result in a rapidly decreasing retention coefficient (saturation). Since the solar wind flux is on the order of 6×10^{15}

supersonic solar wind mixes with the subsonic interstellar medium (Dessler, 1967). No measurements have yet been made beyond the orbit of Mars.

Cosmic Dust

There is considerable evidence for the presence of dust, at least in the inner part of the solar system. The zodiacal light, a faint glow observed on dark nights along the ecliptic, with intensity increasing toward the sun, has been carefully studied and explained by diffraction of light from small particles distributed around the sun (Ingham, 1963). The mass density is not known accurately, and values range from 5×10^{-21} gm/cm^3 by Van der Hulst (1947) to 10^{-24} gm/cm^3 by Ingham (1961). To account for the same sky brightness the Ingham distribution places most of the mass in much smaller particles ($< 1\mu$) than Van der Hulst (100-350μ). Furthermore, the type II comet tails which tend to be undistinctive in appearance show a reflected solar spectrum. This suggests that they too are dust, and by photometric and polarimetric measurements the sizes are calculated to be about 0.5μ (Belton et al., 1963).

By following meteors before they vaporize, Watson (1937) derived a distribution law for the smaller particles near the earth, of the form $N(r)dr = Cr^{-t}dr$ (r in cm). He proposed that the constant t was about 5. Later work has tended to revise this downward, but any value greater than 3 indicates that due to the large total surface area, the very fine dust is the major source for the scattering of light. For the latest work on this distribution, see Parkin and Tilles (1967).

protons/cm^2/year, the space lifetimes are indeed long as compared to saturation bombardment times. These considerations strongly suggest that the injected gas would serve as a tag for extraterrestrial dust (Merrihue, 1964; Tilles, 1965, 1966).

Low Energy Bombardment

What happens to a 2 keV proton when it strikes a solid object? The ion is slowed down by successive collisions with the lattice atoms, imparting some ΔE to each, until finally the ion comes to rest or finds itself back outside the lattice. The important features here are the range (penetration depth) of these bombarding 2 keV ions, the sticking coefficient for these ions, and finally the number of lattice atoms ejected for each incoming 2 keV ion (the sputtering ratio).

This range of energies, around 2 keV, has not been well studied. However, the group at Chalk River has carried out some experiments, primarily using an electromagnetic isotope selector (Davies et al., 1963; Brown and Davies, 1963; and Kornelson, 1964), which are useful in this discussion. Small integrated fluxes ($<10^{10}$ ions/cm^2) of radioactive atoms were used to bombard target foils. Sticking coefficients, S, were first measured, by comparing to 5 keV ions in Al targets where S was assumed to be 1, and later experimentally determined to be so. In general for the materials tried, Al, W, Be, Ni, Zr, Ta, the sticking coefficient for Ar, Kr, and Xe was equal to 1 by about 5 keV (50 keV for W), and at 2 keV, was about 0.4 to 0.7 (Brown and Davies, 1963). It is important to note that this is the case where the integrated flux is small, so that the bombarding atoms do not become a major fraction of the surface

atoms, and also sputtering is limited. Total beam current for any irradiation was about $10\mu a/cm^2$.

Range studies were performed consisting of (a) "saturation", (b) "postsaturation", and (c) "presaturation" experiments, wherein both a stable and radioactive ion are used. Irradiation (a) is with both ions at the same time, while (b) is a short bombardment with the radioactive ion and then a saturation bombardment with the stable species. Experiment (c) is a saturation bombardment with the stable ion and then a short bombardment with the radioactive species. These bombardments were then compared to the results of a single irradiation range determination (Davies et al., 1963). In the "saturation" case, it was found that the median depth occurred at only about half the depth observed in the typical range determination, and that the peak was considerably broadened. In the "postsaturation" experiment the depth is found to have been increased by a factor of 1.4 (at 10% activity level). (This is for the radioactive atoms--thus they have been knocked into the lattice). Finally in the "presaturation" case, one finds a narrow distribution, with the depth of penetration significantly lowered. The experiments also showed that the penetration depth is not defined by a Gaussian as might be expected, but rather the deeper end falls off exponentially. Robinson and Oen (1963) have suggested that this is due to channeling effects, where, in preferred directions (as $\langle 110 \rangle$ in Al) there are tunnels allowing greater penetration before coming to rest. Davies et al. (1963) conclude "that the mechanism of saturation is a complex equilibrium between sputtering, scattering, knock-on, and perhaps crystal lattice effects."

Kornelson (1964) investigated the sticking coefficients, for example, of Ar in a W target, with ion energies varying from 100 eV to 4 keV, and integrated fluxes ranging from 10^{11} to $> 10^{16}$ ions/cm^2, and for 2 keV finds S=0.8 until the W has been bombarded with 10^{15} ions/cm^2. At that point saturation apparently is setting in, asymptotically approaching $2x10^{15}$ ions/cm^2, which is just 10^{-4} cc/cm^2. He also has looked into the desorption spectra--amount of gas vs. temperature, for various ion energies--and finds in general, for Ne, Ar, Kr, Xe, in W that there is a double peak; one of the maxima is at 1000°K, and the other above 2000°K. As the mass of the ion increases, the higher temperature peak becomes more important. No explanation has been given for this.

Bühler et al. (1966) have studied the trapping of low energy ions (0.46 to 7 keV) of He, Ne, and Ar in Al, as a measure of the trapping of solar wind ions by solids. For integrated fluxes less than $2x10^{14}$ Ar^+/cm^2 saturation effects were not detected. Furthermore for 2 keV ions, $S_{He} \approx 0.6$, $S_{Ne} \approx 0.5$, and $S_{Ar} \approx 0.9$. Lal (personal communication) has also studied the trapping efficiencies of low energy (2.5, 5, 10, 20 keV) ions in a variety of thin films. Comparing H^3 and He results, it is seen that for all materials studied (Al, Mg, Mo, Pt, Au, and mylar) the hydrogen trapping efficiency is lower. The absolute values are similar to earlier studies.

Next we want to compare these results with the theoretical derivations of the range as treated by considering the stopping process. The total stopping cross-section is the sum of the terms from the electronic (inelastic) collisions and the nuclear (elastic) collisions. Bohr (1948) considered the low-energy nuclear collisions and proposed

that they could be best calculated by considering an exponentially screened coulombic field. However this tends to underestimate the significance of atoms at large r's, and Lindhard and Scharff (1961), and Lindhard et al. (1963) corrected for this by replacing the Bohr potential by a Thomas-Fermi potential. They were able to derive a curve (assuming electronic contribution can be neglected) which agrees well with the Davies et al. (1963) range results. Ormrod et al. (1965) report that for their studies of low energy (10<E<70 keV), low mass (13≤Z≤19) projectiles in C and also in Al, the atomic cross-sections are best explained by the electronic component being the dominant factor.

Wehner et al. (1963a, 1963b) bombarded known density foils with a known current density and then calculated the sputtering yield by determining length of time to sputter a hole through the foil. By comparing the sputtering results for a variety of rocks by Hg^+, they conclude that the volume sputtering rates for silicates is of the same order of magnitude as for Fe, which is a metal of moderate sputtering rate.

Heymann and Fluitt (1962) have bombarded some meteorite targets with 20 keV Ar^+ from an isotope separator. They find that rates of erosion are 1.5 times greater for the metal, Canyon Diablo (in mg/coul) than the two stones studied, Arapahoe and Richardton. They then calculated erosion rates for the important elements lighter than Ar. They assumed that the ratios of the sputtering coefficients on the iron meteorite would be the same as the ratios on Cu, which has been studied by Almen and Bruce (1961). From this they find that only H and He are

important in solar wind sputtering as long as the heavies (ie. C, N, O, and heavier) are in Aller abundance ratios to H, or less. Table 13 lists their results.

Table 13. Sputtering by the solar wind.

	Rates of erosion (volume sputtering)	% erosion
H^+	0.02 mg/coul	63
He^+	0.08	34
C^+	0.2	
N^+	0.5	
O^+	0.5	3
Ne^+	0.9	
Ar^+	2.0	

The solar wind is best explained as being a constant velocity phenomenon. Then we find that higher mass elements will have lower relative abundance, but higher energies than protons:

if for H^+ E=2 keV

then for He^+ E=8 keV

and for Ar^+ E=80 keV

Grønlund and Moore (1960) have shown that the sputtering yields are constant, within a factor of two, at low energies (2 to 12 keV), for each mass from H^+ to D_3^+. Almen and Bruce (1961) have found for higher mass incident ions (Ne to Xe) that once a threshold energy is reached, usually ⩽10 keV, the sputtering yield remains fairly constant up to the limits of their study at about 70 keV.

However, Davies et al. (1963) find that the mean range for Ar

ions in Al increases linearly with energy, and up to about 60 keV the relationship is of the form

$$R = 1/3 \; E \quad \mu g/cm^2 \; keV.$$

Thus if heavier ions are present in the solar wind it seems reasonable to expect that bombarded samples should be enriched in these. For any given pressure, temperature, and compositional conditions the diffusion coefficients are smaller for the higher mass elements. Thus diffusion losses will in general decrease as the mass of the rare gas atom increases, further enriching the sample.

Rare Gas Studies

Beyond the macro-differences observed among meteorites (as stones vs. irons), many variations in elemental and isotopic abundances are detected. Because of the simplicity of the sampling procedure, the rare-gas contents in meteorites are as well known as any other major element or group, except possibly iron.

The primary contributions to the meteoritic rare-gas contents as given by Signer and Suess (1963) are from

(a) radioactive decay (U, Th, K) - radiogenic

(b) cosmic-ray induced spallation - cosmogenic

(c) terrestrial contamination

(d) the gas not explained by the above, supposed to be gas incorporated before and during the dust accumulation forming the meteorites - primordial.

The last type, primordial, is of the most interest here, and was detected first by Gerling and Levskii (1956) investigating Staroe

Pesyanoe. They found enormously large amounts of He, Ne, and Ar, with the He being about 10^3 higher per gram than that from sources a - c. The isotopic ratio observed is a further indication that none of these processes are relevant.

In Table 14 are listed typical meteoritic primordial gas abundances, as well as solar abundances, typical abundances in chondrites, and terrestrial abundances. The first group, including Pesyanoe, Kapoeta, Pantar, Breitsheid, Tabor, Fayetteville, Pultusk, Khor Temiki, and St. Mesmin are all physically distinctive in that they show a salt and pepper appearance. This light-dark structure has been looked at by many workers, and it is found that the primordial fraction of rare gases is present only in the dark phase (Signer and Suess, 1963; Manuel and Kuroda, 1964). The one exception known to this is a sample from the dark phase of Pantar II (a separate fragment of the Pantar fall), which contains essentially no primordial gases (Signer and Suess, 1963). However the two phases are identical in the chemical composition of the major elements (Fredriksson and Keil, 1963), while there are differences in the trace element abundances. Müller and Zähringer (1966) have shown that for Kapoeta, Pesyanoe, and Fayetteville the primary consistent chemical difference between the light and dark phase is the carbon content which tends to be 2 to 3 times higher in the dark phase. Also they mention the interesting discovery by Ramdohr of a layer lattice mineral in Kapoeta of the approximate composition FeCS, suggesting a location for this excess carbon. Furthermore, Marti (1967) has found a strong correlation of concentration of trapped Xe^{132} with the %C in ordinary and disequilibrium chondrites, carbonaceous chondrites, and Novo Urei.

Table 14. Rare gas abundances.

	Primordial gas abundances for gas-rich meteorites (10^{-8} cc/gm)					Total rare gas for typical chondrite	Terrestrial Atmosphere	Sun
	Pesyanoe	Kapoeta	Breitscheid	Fayetteville	Khor Temiki			
He^3	1.3×10^2	3.9×10^1	6.0	4.2×10^2	n.d.	3.3×10^1	7×10^{-4}	
He^4	7.3×10^5	1.3×10^5	1.7×10^4	1.4×10^6	2.0×10^5	1.5×10^3	5.2×10^2	
Ne^{20}	1.9×10^3	1.9×10^3	2.0×10^2	5.3×10^3	5.2×10^2	9.1	1.7×10^2	
Ne^{21}	n.d.*	5.2	2×10^{-1}	n.d.	n.d.	9.5	4.7	
Ne^{22}	1.6×10^2	1.5×10^2	1.5×10^1	4.4×10^2	n.d.	1.1×10^1	1.6×10^2	
Ar^{36}	1.7×10^2	7.8×10^1	9.5	2.9×10^2	1.3×10^1	1.4	3.2×10^3	
Ar^{38}	3.6×10^1	1.5×10^1	2.0	n.d.	n.d.	1.2	5.9×10^2	
Ar^{40}	n.d.	n.d.	n.d.	n.d.	n.d.	5.4×10^3	9.3×10^5	
$\frac{He^3}{Ne^{21}}$		7.5	3.0×10^1			3.5	1.5×10^{-4}	
$\frac{He^4}{Ne^{20}}$	3.9×10^2	6.9×10^1	8.0×10^1	2.9×10^2	3.8×10^2	1.7×10^2	3.2×10^{-1}	350
$\frac{Ne^{20}}{Ne^{22}}$	1.2×10^1	1.3×10^1	1.3×10^1	1.3×10^1		8.7×10^{-1}	1.0×10^1	9.4
$\frac{Ne^{20}}{Ar^{36}}$	1.1×10^1	2.5×10^1	2.1×10^1	1.9×10^1		6.5	5.2×10^{-1}	72
$\frac{Ar^{36}}{Ar^{38}}$	4.7	5.2	4.8			1.2	5.4	5.3
type	aubrite	howardite	bronzite chondrite	bronzite chondrite	aubrite			
ref.	1	2	2	3	4	5	5	6

*not detected

1) Gerling and Levskii, 1956

2) Signer and Suess, 1963

3) Heymann and Mazor, 1966

4) Eberhardt et al., 1966

5) Eberhardt, 1964

6) Aller, 1963

Frederiksson et al. (1964) performed shock experiments on meteoritic material (Bjurböle) in an Ar atmosphere, and showed that the sample retained large amounts of Ar, and that the shocking darkened the sample. (This point will be referred to later, but it should be mentioned here that the associated darkening need not be explained as a physical result of the shocking.) Recent work has shown that vacuum systems working at high temperatures (as when the shock front passes) invariably are contaminated with carbon containing material unless very stringent precautions are taken (Nash, 1967). Suess et al. (1964) concluded, however, primarily by mineralogical and structural arguments, that shock could not have caused the differences, and instead suggest that a particle irradiation, like the solar wind, may be the cause.

A second group of gas-rich meteorites consists primarily of carbonaceous and enstatite chondrites. Here the concentrations of gas are lower but still appreciable, and there is no light-dark structure or recognizable physical distinction from other meteorites (Reynolds, 1960; Stauffer, 1961). Signer and Suess (1963) have discussed these two types of excess rare gases, and have explained them without requiring the large diffusive losses as suggested by Stauffer (1961). They call the first type the solar primordial gas. It is unfractionated, with the atomic and isotopic composition of the sun. A possible mechanism for introduction of this component is the solar wind acting upon grains before accumulation into a larger or more compact body, or possibly direct absorption from the unfractionated primordial solar nebula. The second type, the planetary component, is the result of some fractionation process such as gravitational, wherein the lighter gases

were lost preferentially. Diffusive losses are probably more important in explaining this fractionation. When observing a typical distribution, it is seen that the planetary anomalies tend to follow the terrestrial abundances from He through Kr. However, for the primordial component, the Kr and Xe concentrations tend to be greater than the solar abundance pattern (Pepin and Signer, 1965).

Eberhardt et al. (1965), when studying separated minerals and grain sizes in Khor Temiki, discovered that upon etching away the surface with dilute HF the primordial gas concentration was radically decreased. In this way they were able to show that more than 75% of the trapped He^4, for instance, in a pyroxene grain with $r \leqslant 43\mu$, was in the outer 0.5μ. Furthermore, gas contents were measured in a series of samples graded into six grain sizes varying from about 5 to about 100μ. There was a definite correlation of increasing gas content with decreasing grain size for those gases expected to be primordial, but with He^3 (cosmogenic) they found only a slight change. They suggest that a low energy ($\leqslant 100$ keV) particle irradiation, like solar wind, was the cause. Further work by this group has shown that separated feldspars show significant diffusive losses of radiogenic, cosmogenic, and primordial rare gases while the separated pyroxenes show no diffusive loss of at least the cosmogenic nuclides (Eberhardt et al., 1966). Also it is observed that the primordial gas is present primarily only in the relatively fine-grained matrix material, i.e. pyroxene and feldspar.

Zähringer (1966) has carried out a unique experiment wherein polished samples of Fayetteville and also Kapoeta are scanned with an electron microprobe (25 keV electrons), with a mass spectrometer behind

the diffusion pump to measure any gas given off by this heating of the grains. He found that the He was released in spikes and that about 60% of these, for each meteorite, occurred as the beam passed over a grain boundary. The boundary location was determined by following the iron concentration. However the other 40% occurred either in the middle of crystals (possibly as much as 100μ from an edge), or at the interface of two chemically similar crystals. He ascribes this to interior grain features, as defect structures, etc., and thus argues that solar wind is not the cause.

The location of these gases needs to be studied further to help settle this question. When the concentration of gas in the lattice is high, standard diffusion is replaced by bubble formation (Barnes, 1964; Ruedl and Kelly, 1965). In that case the bubbles migrate to a grain boundary or defect before the gas is released. Thus the release of gas at the boundary is not evidence that the gas was sitting there all a-long. On the other hand gas released from the interior of a grain does not rule out solar wind as one does not know the location of the other two edges when looking at a polished section.

Merrihue (1964) detected primordial He, Ne, and Ar in the magnetic concentrate of a modern red clay from the Pacific Ocean. Tilles (1966) has confirmed these results and also detected primordial Ar in a high density ($\rho > 3.2$) concentrate of dust collected from Greenland ice. This is not necessarily solar wind injected gas, but further studies of the release pattern, host material, and depth of the layer containing the gas should help to decide.

Experimental

A variety of silicates, comprising the primary condensates determined in Part I of this work, were irradiated with a simulated solar wind. These samples are then analyzed for gas retention, determining simultaneously the temperature release pattern. From this, diffusion constants are calculated allowing comparisons to other studies of gas release from minerals. Then a saturation value for the incident ions in the lattice is calculated.

The physical effects of the irradiation are also of interest. Microprobe analysis of Mg, Si, Fe on the surfaces of both a standard and an irradiated sample was used to indicate the importance of preferential sputtering. X-ray analysis was used for similar determinations on powders, as well as for assessing the importance of phase changes and new compound formation. Finally, microscopic examination was used for the detection of gross surface changes.

Sample preparation: Large peridotite nodules (diameter ≥ 1 cm) from San Carlos, Arizona were obtained by John Sinkankas. Powder was not used, as (a) the early irradiations were carried out at Cornell, and it would be difficult to transport them undisturbed to La Jolla, (b) large areas are more useful for surface analysis by photomicrography and electron microprobe, and (c) the samples should be isolated from their surroundings, which was attempted by enclosing the sample in the same material.
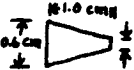
Typical size of the nodules is 2 cm^3 (largest is about 2x2x2 cm), and they appear to grade in color from light to dark green. They are fractured, but were easily cut into 1 cm x 1 cm x 1 mm slices using

a diamond saw.

Three irradiations were made by Dr. Bruce Hapke at Cornell University. (Details of the irradiation are given on page 74). For the first irradiation, four nodules were used as sample holders. They were squared up using a diamond saw, and then had wells drilled into them using an ultrasonic drill, SiC powder, and a stainless steel tool. Table 15 describes the physical properties of these wells. Well #1a

Table 15. Well description.

Well	Weight (gm.)	Surface Area*(cm^2)	Contents
1a	4.377	2.0	blank
1b	8.264	1.9	slab i - point up
1c	6.382	1.0	powder
1d	9.811	2.2	slab ii - point down
Slab			
i	0.2946	0.4	
ii	0.2682	0.4	*corrected for contents

was empty, and used as a control. Wells 1b and 1d each held a slab. These were to be used for photomicrography, and then electron micro-probe studies and gas measurements. The slabs were approximately this shape and size and 0.1 cm thick. In well 1b, the slab (i) was placed point down, while in well 1d, the slab (ii) was placed point up. Finally well 1c was partially filled with powder to be used for X-ray diffraction studies. A representative light and a represent-ative dark nodule were each ground up using first a "diamond" mortar, followed by an agate mortar and pestle. X-ray diffraction comparisons

of the two samples were made (for details of the procedure, see page 72),
and they could not be distinguished. Thus no further notice was taken
of the color of the nodules.

For the second irradiation the samples were prepared in a
different way. Two wells were formed as for the first bombardment, and
these (2a and 2c) were used as containers for powder for X-ray work.
The other two samples (2b and 2d) each were prepared by stacking four
1x1x0.1 cm slabs and surrounding these with four more slabs so as to
enclose the stack completely. Thus each of these sample configurations
consisted of eight slices.

A third irradiation was obtained to look at saturation effects
and also effects of varying the temperature of the substrate. It was
found in the second irradiation that enclosing the sample was not im-
portant, at least for the long bombardments used here. Thus the slabs
can be simply placed on a pyrex dish and irradiated. Furthermore,
this low profile reduces the area not directly exposed to the beam.
Because the beam from the irradiation source is three inches in diameter
(details are given on page 72) many samples could be irradiated at the
same time. For each bombardment, the following materials were used:

    (a)   peridotite nodules from San Carlos, Arizona

    (b)   dunite from Jackson County, North Carolina

    (c)   enstatite (pyroxenite) from Nye County, Montana

    (d)   fayalite from Rockport, Massachusetts

These three latter samples were obtained as bulk specimens from
Wards Natural Science Establishment, Inc. They were sliced with a
diamond saw into slabs with dimensions of 4.0x4.0x0.2 cm. The enstatite

rod. In this way a clean surface was obtained. A chromel-alumel thermocouple, which is quite sensitive to small temperature changes, was inserted into the C cylinder. This unit was positioned in the center of the flashlamp. The thermocouple wires above the C block were shielded with a standard ceramic sleeve. This was then wrapped in Al foil to reflect the incident radiation from the lamp. An ice junction was used for increased accuracy. The potential difference was read on a Leeds and Northrup, 10 mv full scale, recorder with a chart speed of 1 div/minute.

Each lamp was flashed at a number of different voltages without a choke in the system, both with and without a reflector. The recorder measures a temperature rise in the block and from the heat capacity of C and from the calculated surface area of the block, the radiant energy (j/cm^2) is calculated. For this work, the following formula for calculating the heat capacity was used (Kelley, 1949):

$$C_p = 4.10 + 1.02 \times 10^{-3} T - 2.10 \times 10^{5} T^{-2}$$

The reflectance of the C block was set equal to 27%, as derived by Kuebler and Nelson (1961). The results of these measurements are shown in Fig. 2. Note that above about 4 kjoules (which is about 6.5 kV) the G.E. lamp output levels off. The reason for this is not clearly understood, but it should be remembered that the tube is recommended for operating voltages only up to 4 kV. Next note the large radiant energies obtainable when a reflector is used with the Kemlite lamp.

For low operating voltages (< 1000 V) the typical Xe filled flashlamp has a bimodal spectral distribution, having one of the maxima about 4600 Å and the other in the near infra-red (G.E. Flashtube Data

and fayalite were polished on one face using 120, 220, 320, and 400 grit paper. Then the slices were further cut with a diamond saw into approximately 1x1 cm slabs.

In all of these irradiations the samples are simply lined up in a pyrex petrie dish and placed under the beam. For the second bombardment (He) a small drop of epoxy was placed at the foot of each of the vertical wall slabs to hold it in place. This in no way affected the He content, but may have caused some darkening of these samples.

Bombardment procedure: The samples were irradiated by Dr. Bruce Hapke in his laboratory at Cornell with his apparatus and experimental procedure used for the study of the photometric properties of the lunar surface (Hapke, 1962, 1965, 1966). Essentially the apparatus is one similar to that designed by Kaufman (1961) in which a plasma is generated by bombarding the appropriate gas with electrons. The ions are accelerated through a grid network, brought to the desired energy, 2 keV, and then allowed to strike the target. The target is kept electrically neutral by spraying with electrons from a W filament (see fig. 3). The pressure in the chamber, and the sample temperature are monitored. The irradiation details are listed in Table 16.

Hapke irradiated his own samples with about 100 coul/cm^2 (equivalent to about 2x10^5 years solar wind bombardment) as longer bombardments caused the powders to become darker than the moon. This integrated flux was used for the first two irradiations. The third set of irradiations was with lower integrated fluxes in order to see if saturation can be detected. At least one irradiation must be below saturation, but the sample must contain detectable amounts of gas. An
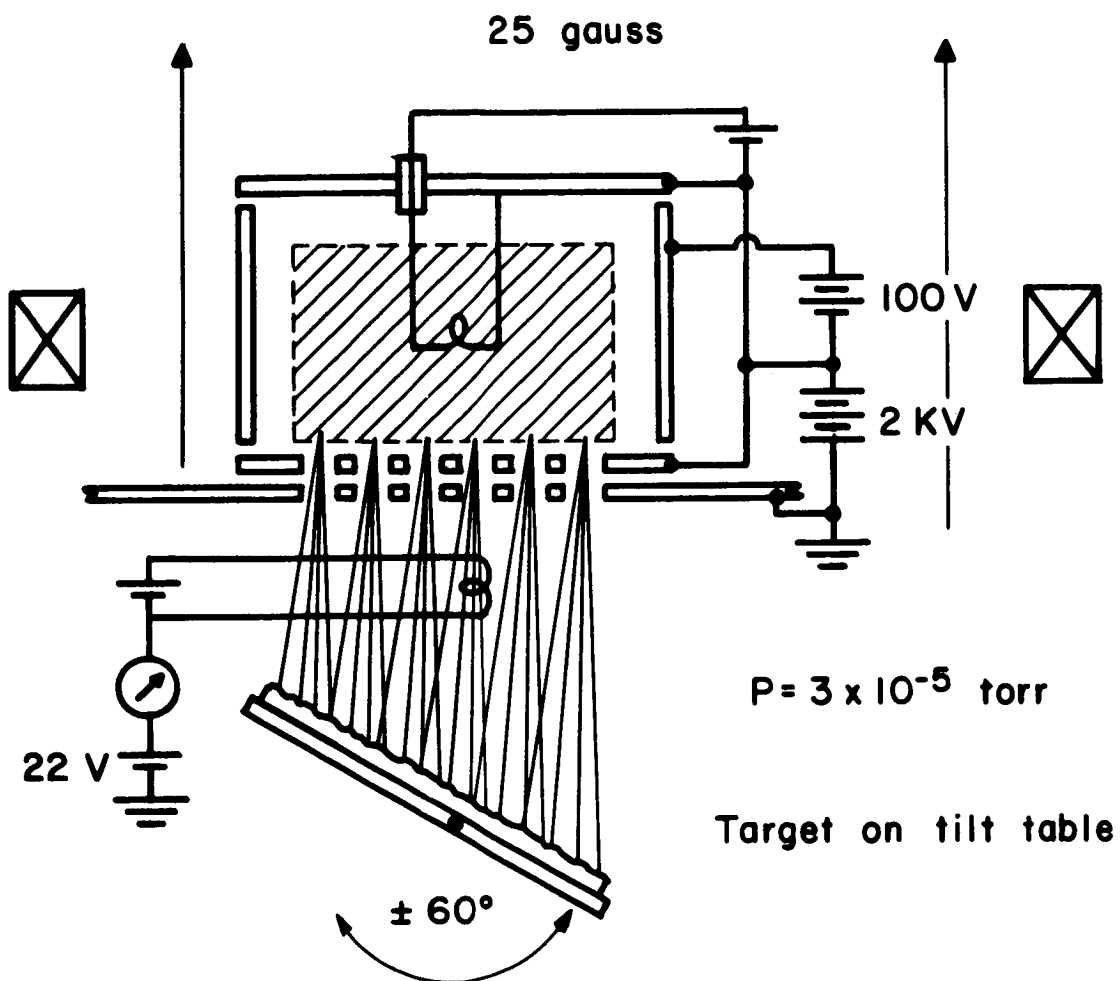
25 gauss

100 V

2 KV

$P = 3 \times 10^{-5}$ torr

Target on tilt table

22 V

± 60°

Fig. 4. Schematic of the Hapke irradiation apparatus
(after Hapke, 1965). Tilt table at 0°

Table 16. Details of the Hapke irradiations.

species	#1 H^+, H_2^+, H_3^+	#2 He^+, He^{2+}	#3 He^+, He^{2+}
energy (keV)	1.6	1.8	1.8
current density (ma/cm^2)	0.5	0.3	0.27 0.027
length of irradiation (hr.)	43.5	36.3	.1 - 10
integrated dose (coul/cm^2)	79	43.5	.01 - 10
approximate surface T ($^\circ$C)	350	300	100 - 300
$P_{ambient}$ during irradiation (torr)	1×10^{-4}	10^{-4}	10^{-5}

Breakdown of Irradiation #3

set	integrated dose (coul/cm^2)	current density (ma/cm^2)	time
A	0.01	0.027	6 min.
B	0.10	0.027	1 hr.
C	1.0	0.027	10 hr.
D	1.0	0.27	1 hr.
E	10	0.27	10 hr.

upper limit for the time required for saturation can be easily predicted from sputtering yields and penetration data. The results of Brown and Davies (1963) would predict a penetration of these ions of about $2 \mu g/cm^2$ and for olivine this corresponds to a depth of 57 Å. With a current density of 0.5 ma/cm^2 a layer of this depth will be completely eroded in six minutes.

Using a duoplasmatron as a bombardment source Wehner et al. (1965) have analyzed the composition of the ion beams. For He and Ar, greater than 99% of the beam is the singly charged ion, with impurity ions and multiply charged ions below their 1% detection limit. The composition of the hydrogen beam, however, was found to vary with pressure, with H_3^+ being the only detectable species above 10^{-1} torr. At lower pressures H_2^+ becomes predominant; for example, at 2×10^{-2} torr they find $H^+ : H_2^+ : H_3^+ = 1:10:6$. In Hapke's bombardments of my powder the ambient pressure was 1×10^{-4} torr H_2, implying that H_2^+ was probably the most important species in this work. Since only the number of incident charges/cm^2 is known, the ionic form of the incident species is required for the calculation of retention coefficients.

The ambient pressure of 10^{-5} torr, for the He bombardments, results in a mean free path of five meters. If the doubly ionized species are formed they should persist until they strike the target. The calculations have been made assuming the bombarding species is He^{2+}. A He^+ component would not change the estimated saturation values, but would reduce the retention coefficients up to a factor of two.

Electron probe micro analysis: The H_2 bombarded slab ii along with an unirradiated piece of olivine to be used as a standard were

mounted on their sides in a plastic disk, which was polished and then carbon coated. Using a modified ARL (Applied Research Laboratories) electron microprobe X-ray analyzer, with the power supply at 20 kV and 140 μamps, giving a sample surrent of 0.22 μamps, these samples were analyzed. This apparatus has three dispersive monochromators allowing three elements to be measured simultaneously. The scan rate was 8μ/min, and the beam width about 2μ with penetration of beam about 3μ. The Fe is observed to be completely homogeneous in the samples. A traverse was made across the slab, looking for concentration changes at the edges. As no changes were detected, any variations present must be in a layer less than 2μ thick. Fe, Mg, and Si were observed on both the sample and standard and found to be the same.

The actual chemical composition of this San Carlos olivine was determined by comparing to an internal olivine standard, the Marjalahti pallasite.

Results: 7.7% Fe   or   9.9% FeO

19.6% Si   41.9% SiO_2

30.2% Mg   50.1% MgO

giving a formula of $(Mg_{0.9}Fe_{0.1})_2SiO_4$.

X-ray powder diffraction analysis: The possibility of both chemical and physical changes due to the irradiation were investigated by running X-ray spectra of both standard (unirradiated) and irradiated olivine powder. The powder was sieved into various size fractions, and the fraction below 43μ was taken for this work. A General Electric Diffractometer was used. Cu $K\alpha$ (using Ni filter) irradiation was used as 40 kV and 20 ma. The slits were 1° MR entrance slit, HR Soller slit,

and a 0.05 ° MR receiving slit. The sample take-off angle for the goniometer was 4°. A General Electric Permaquartz Standard was run before and after samples. The sample was scanned at 0.2° or 0.4° per min, with a chart speed of 1 inch/min. The detector is a proportional counter operating at 1550 V. For these slow scans, the recorder (and ratemeter) was set to 100 c.p.s. linear, with time constant = 8.

The samples were prepared by marking with a template an area of about 22x14 mm on a glass slide 30x25 mm and covering this with vaseline and smoothing with a spatula. The powder was then lightly dusted onto the vaseline. In this way one hopes to obtain a random orientation of the grains. In practice this partially depends upon the grain size and it was found that in some cases as the samples were moved in the holder, relative intensities of peaks changed.

It was noticed that as these samples were being run, the results changed with time, (i.e. a second determination differed from the first) and then it was observed that the X-rays themselves were causing significant radiation damage, as there was a brown coloration to the area under X-ray bombardment. This result has not been explained and certainly was not expected. Thus later runs were made by sampling a different area of the powder preparation.

Willis (1958) has reviewed some of the more important changes occurring to a lattice during irradiation and also ways of detecting these by use of X-ray diffraction. These points are:

(1) Displacement of the Bragg reflections to lower a values, indicating an expansion of the lattice,

(2) Reduction of the integrated intensities of the Bragg

reflections,

(3) Broadening of the Bragg reflections,

(4) Appearance of "diffuse scattering" between the Bragg peaks,

(5) Appearance of low-angle scattering.

Nash (1964) obtained powders bombarded by Wehner and Rosenberg with 0.5 keV H ions (some mixture of H^+, H_2^+, H_3^+) for the "equivalent of up to 10^6 years of lunar surface exposure." In the more complex rock powders he found that differential sputtering occurred with the quartz being concentrated. In a powdered basalt sample no new phases were detected. A hematite sample however did show reduction to a mixture of magnetite and α-iron.

$$4 \ Fe_2O_3 + 8 \ H^+ + 8 \ e^- = 2 \ Fe_3O_4 + 2 \ Fe + 4 \ H_2O$$
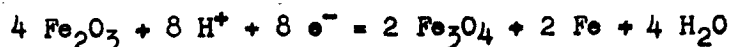
He was unable to detect any cause for the irradiation darkening of the silicate powders, such as free metal enrichment on their surfaces.

Rosenberg and Wehner (1964) report without giving any details that in irradiation crusts on oxides of iron and also copper, metal enrichment has been detected by X-ray diffraction analysis. At least at that time they had not detected metal enrichment in silicate powders, though.

No new phases were observed in any of the irradiated samples, but peak intensity, position, and breadth was observed to change. With further analysis these changes are ascribed primarily to the X-ray irradiation. Listed in Table 17 are the peaks observed between 35 and 40° 2 θ for standard and sample for various runs. It is seen that when the sample was offset so that the X-rays were sampling a new area of the powder, the peak heights have increased again but the position remains

Table 17. X-ray analysis of olivine: position of peaks between 35 and 40° 2θ.

	June 1966 standard	June 1966 sample	August 1966 standard	August 1966 sample
#1	35.68 (70)*	35.64 (100)	35.66 (40)	35.59 (50)
				35.64 (45)
#2	36.54 (90)	36.44 (90)	36.48 (55)	36.43 (50)
				36.46 (30)
#3	38.30 (20)		38.24 (15)	38.21 (30)
				38.27 (30)
#4			38.82 (10)	
#5	39.67 (30)	39.58 (25)	39.64 (20)	39.58 (30)
	39.76 (30)	39.66 (25)		39.67 (25)
#6	40.02 (25)	39.97 (20)	39.99 (55)	39.93 (50)
	40.08 (20)			40.02 (40)

*relative intensities

September 1966

	standard	sample 2θ	corresponding d	ASTM card #7-75
#1	35.62 (60)	35.56 (75)	2.522	2.52 (80) 131
	35.09 (95)	35.64 (50)	2.517	
#2	36.43 (35)	36.37 (80)	2.468	2.46 (60) 112
	36.51 (30)	36.46 (60)	2.462	
#3	38.16 (10)	38.16 (20)	2.356	2.35 (20) 041
	38.25 (10)	38.28 (0)	2.349	
#5	39.57 (25)	39.56 (70)	2.276	2.27 (30) 122
	39.62 (25)	39.65 (50)	2.271	
#6	39.97 (35)	39.93 (45)	2.256	2.25 (30) 140
	40.10 (20)	40.01 (30)	2.247	

the same, and is about 0.001 Å lower than for the standard. In those cases where differences in peak width occur it is always the unirradiated olivine having the wider peak.

Unfortunately the penetration depth of these X-rays is large. For Cu Kα radiation (λ =1.54 Å) in Mg_2SiO_4, the linear absorption coefficient, μ =93 cm^{-1}, giving a penetration depth (where the beam intensity reduced to 1/e of the incident beam) of 110μ. Similarly, for fayalite this depth is 12μ. These depths are more than three orders of magnitude greater than the penetration depths of the 2 keV ions.

Thus it is concluded that the density of defects and the chemical changes were not great enough to be detected by this method. A method of sampling only a fraction of a wave length of light is necessary for these physical studies. Furthermore chemical as well as physical analyses are desired for this layer. These were obtained, and are described on page 83.

Microscopic Examination: The olivine samples were observed to be darkened after bombardment. This turned out to be true only for the higher current density irradiations. It is particularly noticeable in the powders, and is an effect seen with some samples by Hapke (1965, 1966). When the grains are observed with a microscope they have a salt and pepper appearance, with possibly 10% of the grains considerably darkened and 1% opaque. This is in contrast to 1 or 2% dark and 1% opaque before bombardment. Also it was noticed that the darkening is not uniform over the grain, but is reminiscent of results on the sputtering darkening of an Al_2O_3 ball by Hapke (1966).

Carefully comparing Slab ii with a similar unbombarded sample,

using the microscope, it was noticed that the color was greatly en-
hanced. The sample was dark green after irradiation as compared to
light green before. Also large (2x2 mm) patches of brown are seen.
Secondly, striations from the original slicing of the slab are now much
more apparent. Finally the opaque inclusions are still readily seen,
but now they have brown haloes around them. Most likely these minerals
are chromite and augite.

The above discussion applies to the top side (irradiated side)
of this slab. The bottom side is not as dark as the top and there are
no brown patches. The only observable structure under the microscope
is a series of aligned, hollow (?) splashes. Their centers appear to
be the same as the surrounding material, but they have this dark out-
line:

Irradiation Darkening: Many investigators have noticed that
the irradiation darkens their samples (Wehner et al., 1965; Hapke, 1965,
1966; Glaser, 1964), and in most cases this was ignored or ascribed to
radiation damage. However evidence indicates that at least under cer-
tain conditions this darkening is due to contamination, called a
"burn-mark". Kelly and Brown (1965) treated their samples with a hot,
dilute detergent solution to remove organic films, and no burn-marks
were observed. An Al sample was deliberately given an organic coating,
and it was found to have both a burn-mark after irradiation, and an
"anomalous" gas release pattern. Kelly and Matzke (1965) report that
similarly a burn-marked Al_2O_3 sample showed a release pattern not con-
sistent with other experiments. Kelly and Ruedl (1966) have found that,
typically, Al releases 90% of its gas load over a small temperature

range, 630-680° C. However, in all of these studies there was an anomalous low-temperature gas release, which Kelly and Ruedl (1966) ascribed to gases "trapped in burn-marks, and freed when the burn-marks disappear at 150 to 500° C." Probably this is due to gas trapped in a disordered lattice, as it is also true for high dose irradiations.

Those samples bombarded for me by Dr. Hapke at the higher current density were surface darkened, but after the samples had been heated to at least 1000° C, the original color returned. This was first thought to be due to lattice disorder which was annealed out. Smoluchowski (1966) states that the radiation damage from the solar wind to a lunar dust layer would be significant. He suggests that each incident proton displaces 5 to 10 atoms. For the rather deep penetration of 500 Å for a material of $\rho = 3.5$ gm/cc and $\bar{M} = 20$ gm/mole, the number of lattice atoms is 5.3×10^{17}. Thus after some thirty years of solar wind bombardment (2×10^{17} ions/cm^2), remembering that the lattice now contains 2×10^{17} protons as well as the original lattice atoms, statistically, <u>every</u> <u>atom</u> will have been displaced. This mechanism is a possible explanation for the darkening of irradiated samples. After doses several orders of magnitude larger than this, the surface layer should be completely amorphous. However the above evidence indicated that the darkening was a problem which must be studied in more detail.

The release patterns for these complex silicates have, as far as I know, not been studied before, so the results can not be compared to samples without surface darkening. In the third Hapke irradiation, darkening was seen only on those samples bombarded at the higher current density. Furthermore, only the sample sides parallel to the ion beam

were seen to be darkened. This suggests that the faces perpendicular are kept clean, most likely by sputtering. Therefore it seemed necessary to study this darkened layer itself to determine its chemical composition. Since the mean penetration depth of the incident ions is only on the order of 100 $\mathring{A}$ (or possibly 300 $\mathring{A}$ - Young, 1956), the contamination layer need only be a few hundred Angstroms thick to stop the particles completely and mask the target. On the other hand, the layer is thinner than a few microns, as it could not be detected with electron microprobe (see page 75) or X-ray diffraction (see page 76) analyses. Thus a special technique is required to sample such a thin layer.

One such possible technique is that of Patterson et al. (1965) wherein α-particle scattering is used to study the chemical composition of surfaces. When Dr. Franzgrote was contacted about this, it was learned that darkened silicate samples had been run for Dr. Nash at J.P.L. in Pasadena, Calif., and that C had been detected (personal communication). Nash (1967) has found that "attempts to darken silicate rock powders by irradiation with 5-16 keV protons were unsuccessful until ion-beam power was increased sufficiently to produce sample surface temperatures in excess of 150° C. Darkening then was found to increase with input power density for a given ion dose." Using an infra-red radiometer, the surface temperature of a packed powdered basalt sample, grain size $<37\mu$, was monitored with increasing incident power. For the Hapke irradiation of my olivine samples at 0.5 ma/cm^2 and 1.6 keV, the surface temperature was probably on the order of 300°C. Therefore my release patterns for the first two Hapke irradiations are typical for a surface heated to 300° C during bombardment.

A check on these conclusions is obtained by irradiating samples under different conditions and this was set up. The following irradiations were obtained:

(a) 1.8 keV He ions at 270 μa/cm^2 by Dr. Hapke-Cornell $T_{surf}=250^{\circ}C$

(b) 1.8 keV He ions at 27 μa/cm^2 by Dr. Hapke $T_{surf}= 80^{\circ}C$

(c) 2 keV H ions at 10 μa/cm^2 by Dr. Nash-J.P.L. $T_{surf}= 60^{\circ}C$

(d) 2 keV H ions at 160 μa/cm^2 by Mr. Lebduska- $T_{surf}=200^{\circ}C$
Physics Tech. Lab.

The detailed results of these experiments will be described later. For now, it is sufficient to see that a variety of sample surface temperatures are represented. It was found that irradiations (a) and (d) showed darkening while (b) and (c) did not. The onset of gas release occurs at higher temperatures for those samples irradiated at a higher equilibrium temperature. As there was an overlap in the length of bombardment and also total dose for (a) and (b), it is seen that the principal cause of the darkening is neither of these effects, which helps to substantiate Nash's results.

Khan et al. (1966, 1965) and Christensen et al. (1966) determine the elemental composition of surfaces by detecting the characteristic X-rays emitted from a thick target when it is bombarded by protons. They are able to detect a long list of elements using typically a proton energy of 50 to 100 keV and a current of 10 μa. The incident power of 0.5 watts/cm^2 indicates a sample surface temperature near 250° C, suggesting that C may build up here. To prevent sample charging or overheating, non-conducters are first given a thin Al coat.

An olivine standard and an olivine sample which had been irradiated by Hapke with 2 keV He ions at 270 μa/cm^2 for about 47 coulombs

were analyzed by this technique. They were first coated with about 300 $\overset{o}{A}$ of Al by vacuum deposition. The 50 keV protons penetrate on the order of 1000 $\overset{o}{A}$ so the Al was no hindrance. When first seeing the samples Dr. Worley thought that the darkening was due to some C compound contamination. All samples inspected by them show something like $8x10^{16}$ C atoms/cm^2 initially on the sample, and this value increases linearly with their bombardment time.

Because of the visual judgment the samples were first analyzed for C, using 50 keV protons. The results were:

standard - $8x10^{17}$ C atoms/cm^2

sample - $9x10^{16}$ C atoms/cm^2

indicating most conclusively that the darkening was not due to a C compound formation. There appeared to be more C than expected on the standard and this is best ascribed to the Freon used as a coolant in the diamond saw which sliced the olivine nodules. The sample was sputter-cleaned of any of this absorbed material.

Next a more general survey was obtained, looking in particular for Mg, Al, Si, W, Fe. Neither Mg nor Fe were seen, but on the irradi-ated sample there was a broad asymmetric peak rising from Al to W, suggesting that all three were there, or at least Al and W. This was a qualitative measurement, but sufficient for our purposes. The Al is explained by the conductive coating given the sample. The Si might be explained by the substrate, Mg_2SiO_4, but no Mg was seen, and is more likely explained by sputtering glass, as the sample during the Hapke irradiation sat on a pyrex dish. In the Hapke apparatus a W filament sprays electrons onto the sample surface to keep it neutral. It is

certainly probable that W atoms or ions are also sprayed. A rough estimate of the number of W atoms detected gives a few times 10^{16}.

It appears safe to say from these observations that contamination darkening is a fairly ubiquitous phenomenon, and that no single explanation will serve to explain all cases.

Gas analysis: For most of the experiments, a Carle Micro Detector, Model 100 (Carle Instruments, Inc., Anaheim, Calif.) gas chromatograph was used. This is a minimum volume thermal conductivity detector using a pair of matched thermistors as the sensing elements. The detector is operated normally at room temperatures. The 2" diameter by 2" high detector housing is mounted in a 4.5" diameter by 4.5" high Al block as a heat sink. A Millaflow Dual Back Reference controller (part #42400220) is used as the flow regulator (wrapped with 1" foam rubber and completely covered with Al foil, again as thermal insulation). This flow controller has a working pressure of 200 psig regulated, and a flow range from 1 cc/min to 25 l/min with a flow accuracy of ± 2%.

A Beckman Laboratory Potentiometric Recorder (#93500) was initially used with the thermistor detector. This has a 5 inch wide chart, with a full scale deflection of 10 mv. This was later replaced with a Sargent recorder from a Sargent Polarograph, Model XV. This has a 10 inch wide chart, and a full scale deflection of 2.5 mv. Periodically a known potential from a Minneapolis-Honeywell potentiometer, model #2732, is applied to the recorder as a calibration of the full scale deflection.

For the sample heating a resistance furnace was used. This has a Kanthal REH 4-30 element, capable of prolonged operation at 1300°C.

The element and the ceramic sleeve were surrounded with about a 3" thickness of firebrick, with MgO powder between. The furnace operates at 60a, 15V,850 watts maximum, and is controlled with a 20 amp variable voltage Powerstat and a transformer. A Chromel-Alumel thermocouple was used for some runs, but its temperature limit of 1200° C is too restrictive. Later a 10 mil Pt/Pt (13% Rh) thermocouple was used.

The released gas was handled with a simple vacuum line (fig. 5). A Hg manometer and an RCA 1946 thermocouple tube are used as vacuum gauges in this line. The sample is loaded into the side-arm on the well, with a piece of steel behind it. The well is outgased by heating to 1000° C with continuous pumping with a Hg diffusion pump and Welch fore-pump. Once the well has cooled again, the sample is dropped into the well using a magnet to move the steel. Before each heating run the well and the gas sampling reservoir (GSR) are evacuated to $\leqslant 10^{-3}$ torr.

A Toepler pump (1 l. capacity), manually operated, was used to move the evolved gas into the GSR. A cold trap was added to the vacuum line between the furnace and the Toepler pump, primarily to keep Hg from the pump out of the heating well, but also to prevent the passage of evolved water into the column. Water is held on the column (until baked out at temperatures above 300° C), and causes tailing of the peaks. To reduce the peak widths as much as possible, the volumes of the various lines were kept as small as possible. This means that the flow line into the column is 1/6" O.D. Cu tubing, and the GSR is made completely of 0.2 cm capillary tubing.

Stopcocks #4, 5, 6, 7, and 9 are all 120° high vacuum capillary stopcocks. For these, plus #15, Apiezon H grease is used. Apiezon N
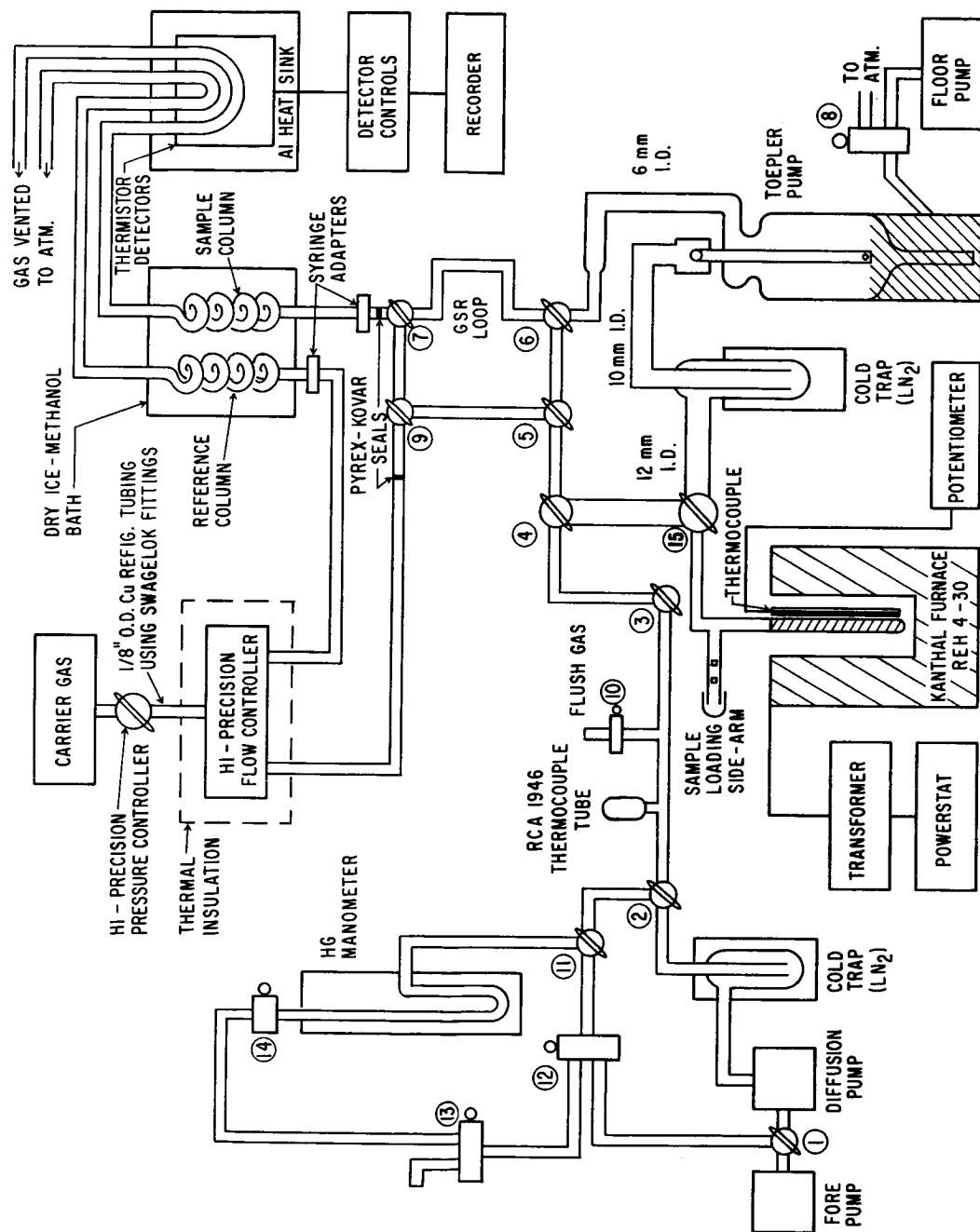
Fig. 5. Schematic of the vacuum line and apparatus.

is used for all the other stopcocks. The copper tubing of the gas line is connected with brass Swagelock connectors to 1/8" Kovar to pyrex seals.

Argon at 30 psi is used as the carrier gas for both the H_2 and He determinations. Various columns of 13x and 5A molecular sieves, ranging from 5 feet to 25 feet using 1/8" Cu tubing were tried. For separation of H_2 and He an 18' 13x column gives a reasonable compromise between retention times and separation. However the column must be cooled in a dry ice-methanol bath for this optimum separation. The column at $-78°$ C is only useful for measuring He, Ne, and H_2 as the other gases have very long retention times. Furthermore, N_2 is held by the column at $-78°$ C, and is only released when the column is again brought to room temperature. See Table 18 for typical retention times.

Table 18. Retention times.

	#1	#2	#3 a	b
He	t=1.9 min.		t=4.5 min.	7.1 min.
H_2	2.3 min.	t= 5.6 min.	5.1 min.	8.7 min.
O_2	3.3 min.	7.8 min.		
N_2	4.8 min.	11.6 min.		
CH_4	8.3 min.	18.2 min.		
CO	9.8 min.			

#1: room T, 5' 13x column, 40 psi Ar@ 5 ml/min.

#2: room T, 18' 13x column, 30 psi Ar @ 5 ml/min.

#3: $-78°$ C, 18' 13x column, 30 psi Ar; a) 8.1 ml/min. b) 3.8 ml/min.

Furthermore, using He as the carrier it was determined that the Ar has a retention time just slightly less than O_2 on a 13x column.

The detector is calibrated periodically by syringing a known volume of gas through the syringe adaptor (fig. 6) which is connected into the carrier gas line ahead of the column. A Hamilton 50 μl gas-tight syringe is used for most of these studies. The most sensitive calibration is obtained by tracing the peak, cutting it out, and weighing it. All sample peaks are then weighed and compared with the weight of this known volume. As the area under the peak varies with the flow rate, this requires that the flow rate be carefully controlled and monitored. On the other hand the peak height is almost completely independent of the flow rate and thus this calibration method can be used for cases where the flow rate is unknown or suspected to have varied. A typical set of calibration results are given in Table 19, and the variation of sensitivity with flow rate is shown in fig. 7. So as to minimize the retention times but still effect complete separation of He and H_2, a sample flow rate of about 8 ml/min was used for most of this work. The reference flow rate has no direct effect on the sample peak shape, but the slower the flow rate, the better the thermal equilibration in the cold bath. This resulted in increased base-line stability for the recorder and consequently the reference flow rate was maintained at about 2 ml/min.

In a similar way the optimum current for the thermistors is determined (fig. 8). For the H_2 measurements 15 ma was used, while for any studies involving He, 9 ma was used.

The calculation of the column plate count was made following

RUBBER
SEPTUM

SYRINGE
ENTRANCE

OUTGOING
CARRIER GAS
(to column)

SWAGELOK FITTING

INCOMING
CARRIER GAS
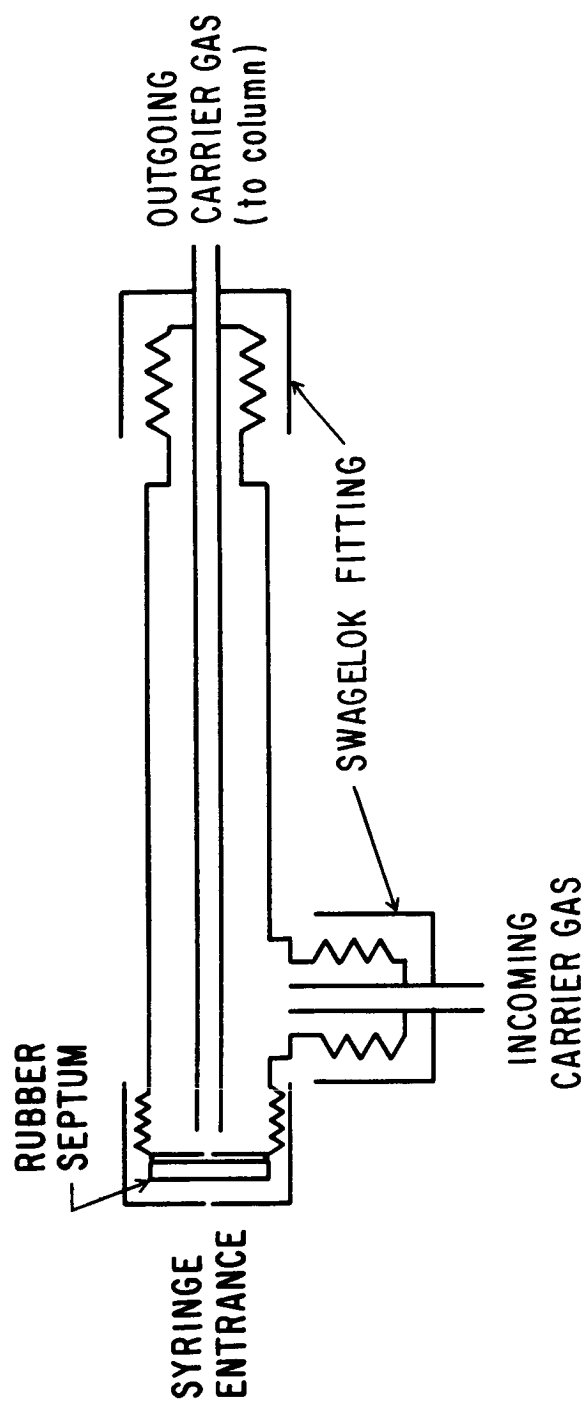
Fig. 6. Detail of the syringe adaptor.

Table 19. Typical calibration results.

H_2 Calibration Run   20 ma, 40 psi, 5 ml Ar/min., 5' 13x column

Volume	Detector Attenuation	Peak Weight (pk ht)
5 μl	5x	0.0343 gm (63 units)
		0.0335 gm (59 units)
		0.0363 gm (62 units)
10 μl	10x	0.0329 gm (56 units)
		0.0349 gm (60 units)
20 μl	20x	0.0318 gm (58 units)
		0.0322 gm (59 units)
50 μl	50x	0.0325 gm (55 units)
		0.0350 gm (59 units)
		0.0335 gm (59 units)
1 cc	1000x	0.0317 gm (21 units)
		0.0336 gm (21 units)

He Calibration

Volume	Detector Attenuation	Peak Weight
5 μl	2x	not traceable
10 μl	5x	not traceable
20 μl	10x	0.0301 gm
40 μl	20x	0.0323 gm
0.2 cc	100x	0.0331 gm
0.4 cc	200x	0.0344 gm
1 cc	500x	0.0425 gm

Thus: 1×10^{-3} cc H_2 = 0.034 gm @ 1x; 1×10^{-3} cc He = 0.017 gm @ 1x.
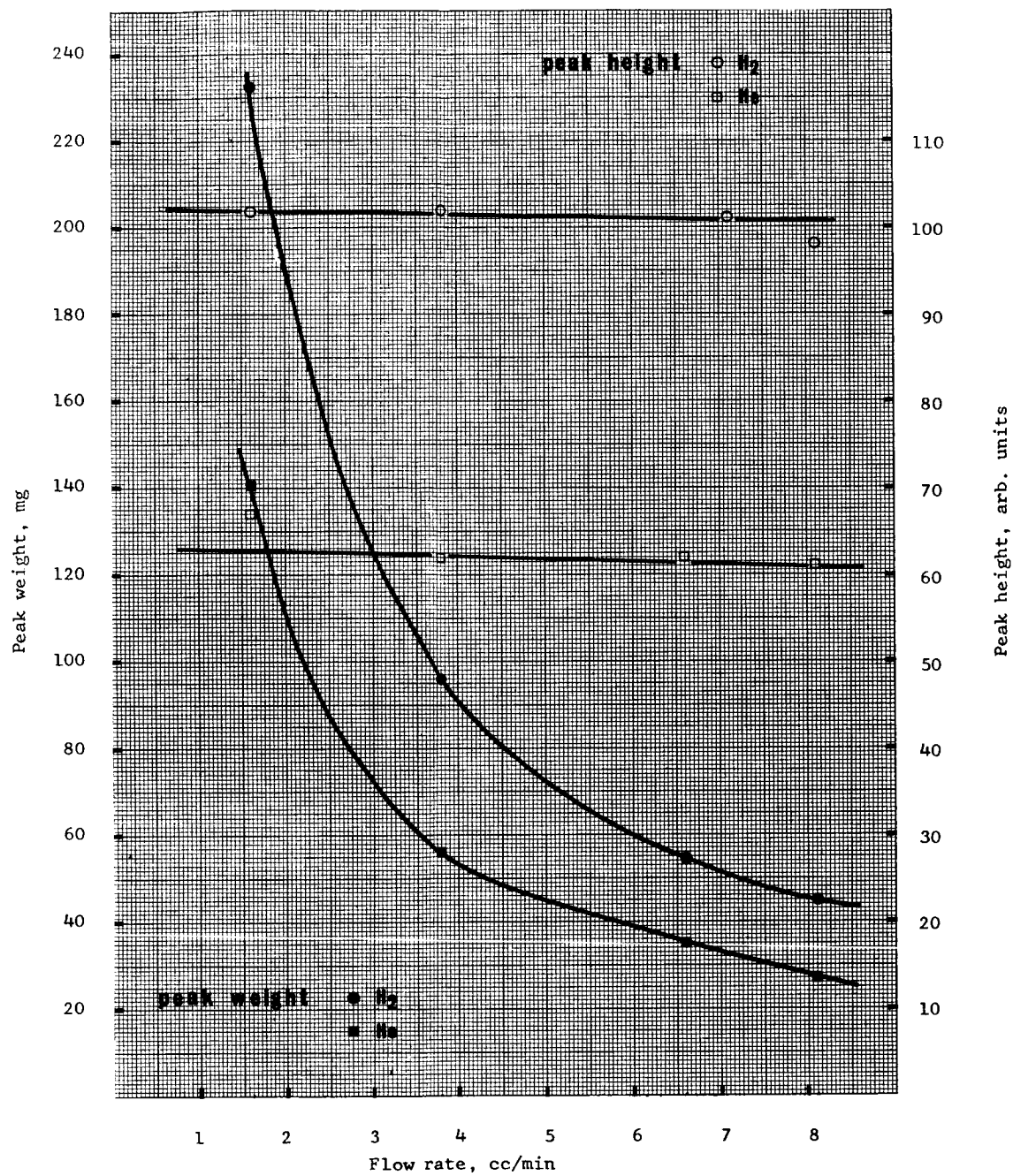
Fig. 7. Variation of detector sensitivity with flow rate.

Peak height, arb. units
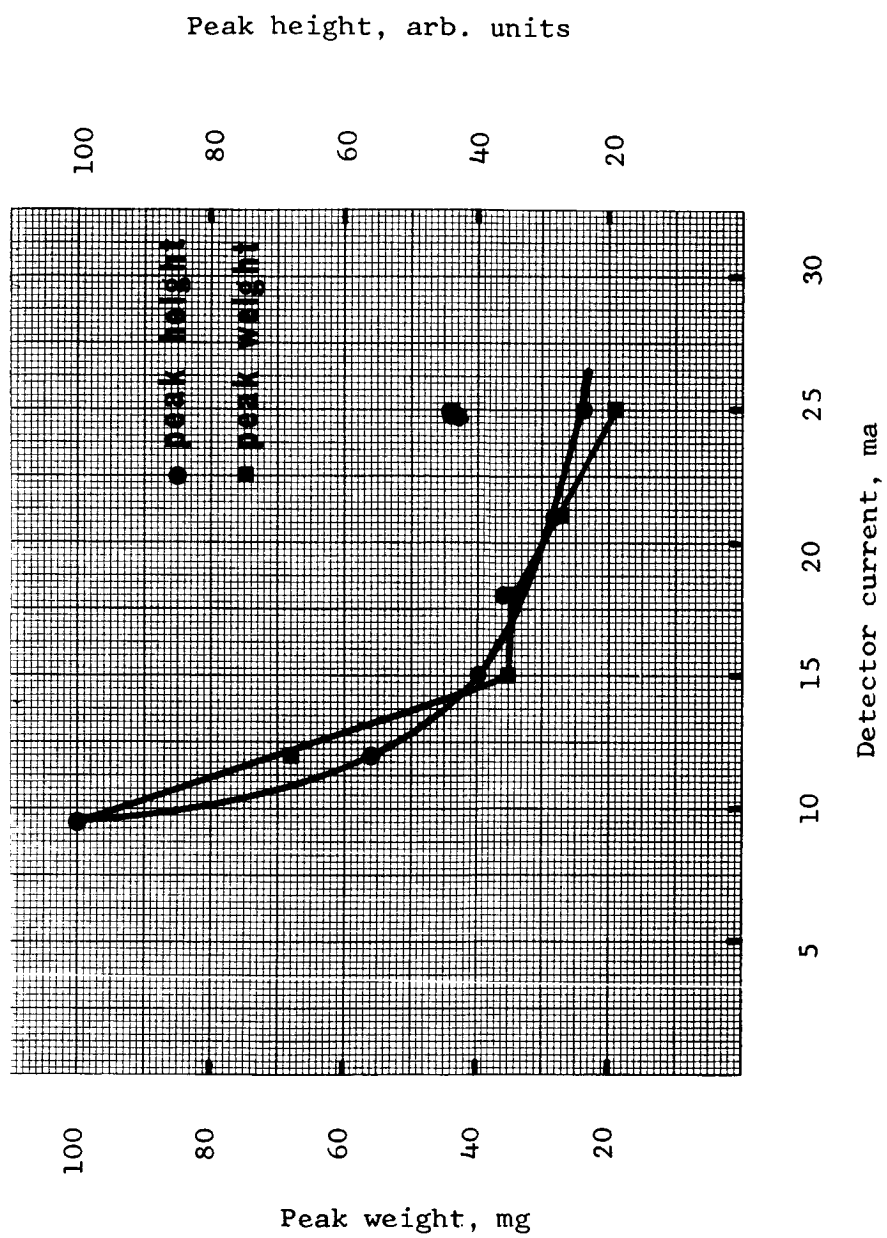
Fig. 8. Variation of detector sensitivity
with detector current.
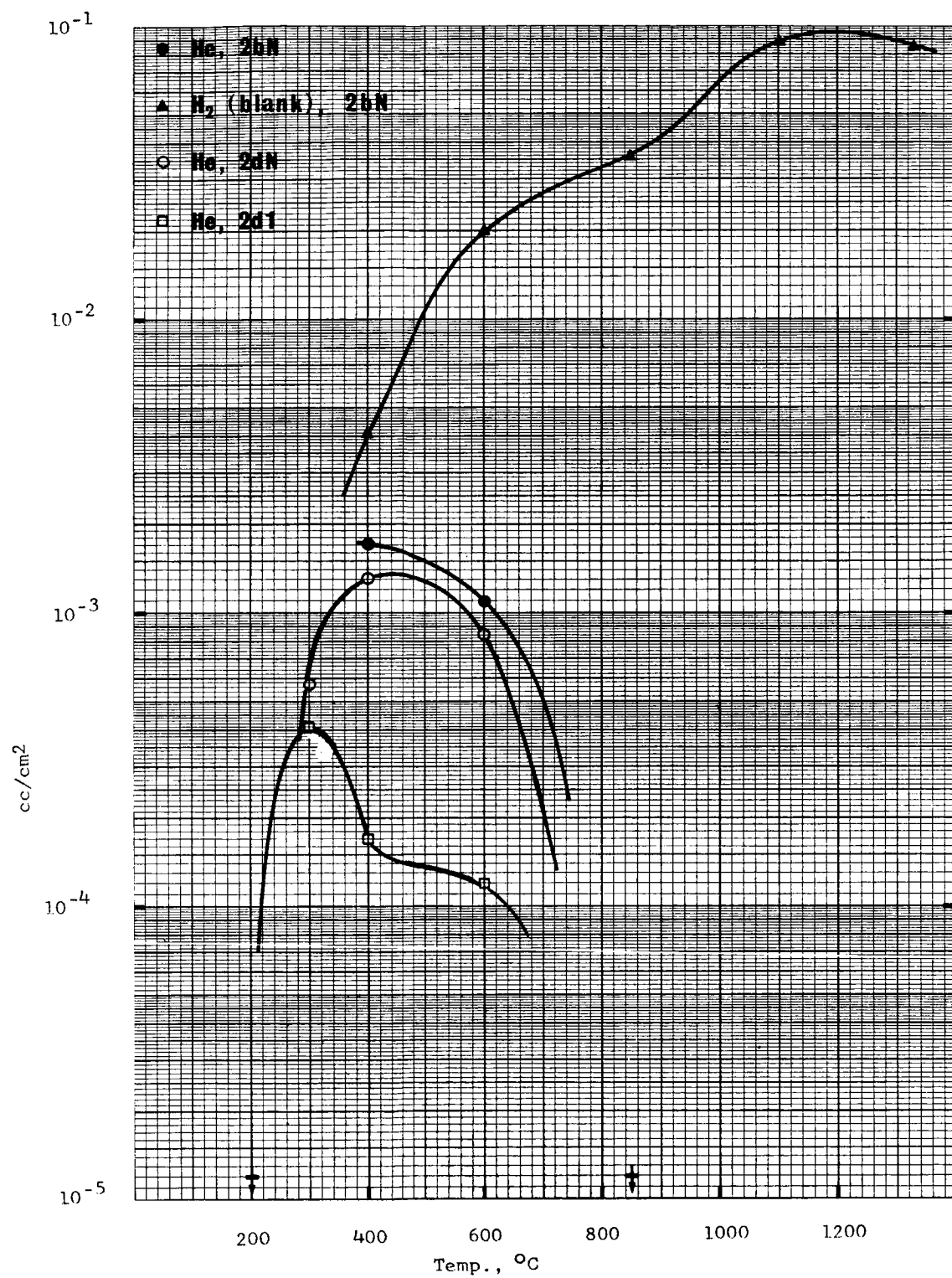
Fig. 9. Results for samples 2bN, 2dN, 2d1.

Cazes (1966).

where: P=plates/foot

f=# ft. of column

$$P = \frac{16}{f}\left(\frac{x}{d}\right)^2$$

x=elution volume from injection to peak

apex (ml)

d=peak base width (ml)

A typical result on the 13x column at -78° C was P=12 plates/foot, or a total of 216 plates.

At this point it is instructive to consider one analysis in detail. First a blank was run on the heating well. Normally the well is used for many runs before being replaced. However between runs the well is heated to at least 1000° (or more, depending upon the temperatures to be studied in the run) with continuous pumping. This blank run, resulting from a half hour hold at each temperature, showed no He or H_2 detected at 400, 600, or 800° C. (However, later work showed that there is an appreciable H_2 blank at temperatures as low as 600° for new wells. After about 2 weeks the blank is reduced so that no H_2 is detected below 1000° C.)

Sample 2bN was one of the first samples run from Hapke's second irradiation (1.8 keV He ions). Although this sample was bombarded only with He, H_2 was also detected. This H_2 is a contaminant, and the release pattern indicates that the contamination is not from the well but rather must be from the sample. The results are listed here in Table 20 and shown in fig. 9. The detection limit in this analysis was 1×10^{-5} cc He and 5×10^{-6} cc H_2. Following this, a standard (a sample prepared in the same way but not irradiated) was run and found to have

Table 20. H_2, He results for sample 2bN.

400° C	2×10^{-3} cc He	4×10^{-3} cc H_2
600	1×10^{-3} cc He	2×10^{-2} cc H_2
850	none detected	4×10^{-2} cc H_2
1100	none detected	9×10^{-2} cc H_2
1350	none detected	8×10^{-2} cc H_2
Total	3×10^{-3} cc He	2.3×10^{-1} cc H_2

no detectable He, but a H_2 release pattern essentially the same as above. Subsequent experiments proved what this suggests—all of these samples were contaminated with H_2. These results validate, I believe, the dismissal of the earlier H_2 results (first Hapke bombardment). Also it shows that the He is released at low temperatures, and thus later runs included 100, 200, and 300° C points.

It became standard operating procedure to check the flow rate at least once a day. The whole system was gone over several times each week checking for leaks, and if a flow rate decrease was detected, a leak-check was performed immediately. Also the calibration of full-scale recorder deflection was performed several times a week, if not daily. Detector calibration runs were made approximately once a week, and always after any procedural change. Finally, as part of a preventive maintenance procedure, the cells were replaced in the detector control unit, in the recorder, and also in the potentiometer every three months. Aging of these increases the noise level of the system significantly and in some cases causes random drift.

Occasionally other noise is seen in the recorder trace. In

particular a periodic pip in the base-line turned out to be due to condensate inside the detector chamber. The detector unit was removed from the flow line and cleaned with acetone and compressed air. This always removed the noise.

Errors: One of the hardest problems in this work is the determination of the experimental errors. Among the factors which must be considered are:

Calibration errors:

incomplete syringing

syringe leak

rubber septum leak

flow line leak

flow rate change

detector temperature change

recorder calibration drift

error in the tracing and weighing of peaks

Sampling errors:

incomplete emptying of Toepler Pump

GSR stopcock leak

flow line leak

closed Toepler valve

errors in the calculation of the sample area irradiated

sample near or less than detection limit

In principle, the calibration errors are easily assessed by repetition of the calibration procedure. For any given day this calibration gives 2σ errors of about 1%, as shown in Table 21. When this is

Table 21. Error limits for typical calibration.

50 μl H_2/200x   3-24-07

0.0552 gm.

0.0530   d'=0.00004

0.0529   0.00006

0.0520   0.00096

0.0532   0.00024

0.0537   0.00074

and omitting the first value 0.0552:

mean=0.05296

$$ s = \left(\frac{15320 \times 10^{-10}}{4}\right)^{\frac{1}{2}} = \left(3830 \times 10^{-10}\right)^{\frac{1}{2}} = 0.00062 $$

$$ S = \frac{s}{\sqrt{n}} = \frac{0.00062}{\sqrt{5}} = 0.00028 $$

giving   0.05296 $\pm$ 0.00056 gm.

for our use   0.0530 $\pm$ 0.0006 gm.

not true, it has been found that there is a leak either in the syringe or in the line. However, because of changes made in the apparatus to increase the sensitivity or to simplify the procedure, day-to-day comparisons of the calibrations are not possible. For a "mature" system wherein all conditions are optimized these comparisons would be of great value.

The recorder calibration was checked often and usually found to be off by less than 1 unit in 200, but never more than 1%. Furthermore the errors associated with the data reduction are normally small. As an exercise, several peaks were retraced and weighed five times. The 2σ deviations were found to be about 0.5%.

The magnitudes of the possible sampling errors are hard to estimate. However certain results are signs indicating problems. Since the volume of the Toepler pump is only 80% of the total volume containing sample gas, a second introduction of gas into the GSR is always made. Incomplete sampling is suspected when this second introduction gives no gas, much less than 20% of the first sampling, or more than the initial sampling. This has happened several times, and in at least one instance was due to Hg caught in the float valve at the top of the Toepler pump. Since the well is not pumped out between runs the gas not collected at one temperature is stored and run at the next step. Therefore the total gas evolved will not be in error, but the release pattern will be skewed.

The absolute detection limit varies with operating conditions but is on the order of 5×10^{-6} cc H_2 and 1×10^{-5} cc He. Thus for very small samples $\leqslant 10^{-4}$ cc, this detection limit introduces fairly large

errors.

The above discussion indicates that if no irregularities are observed, samples greater than 10^{-3} cc have 2σ experimental errors of only a few percent. For smaller samples, the errors increase depending upon the ratio of the detection limit to sample detected.

Finally, there are errors introduced in the irradiation which at this point are impossible to assess. These include a non-uniformity of the flux in the ion beam in time and in space. Hapke reports (personal communication) that the ion beam is unstable for about the first hour of operation, and he suggests that the reported integrated dosage may be in error by $\pm$ 10%. These factors limit the reproducibility.

Results

Hydrogen Bombardments: As discussed earlier, the first hydrogen irradiation by Hapke is not reported because of the problems involved. However two other sets of H-ion irradiations, representing two different sample surface temperatures during irradiation, were obtained (see page 84).

As H_2 had been detected in the blanks for earlier samples, care was taken to keep all hydrogen-containing compounds away from these samples. Chips of the uncut olivine nodules were run as a standard. They were free of any detectable gases except at 100° C where O_2 and N_2 (presumably adsorbed) were detected. The nodules were cut with a diamond saw, using the highly volatile coolant CCl_2CF_2. This was purified by distillation. After cutting, the samples were placed in a vacuum desiccator. All handling was performed with tweezers.

Eight samples were sent to Dr. Nash, to obtain three irradiations (of two samples each) for total doses of about 5×10^{16}, 5×10^{17}, and 5×10^{18} H$^+$/cm^2. An ion current of 10 μa/cm^2 was used so that the samples would not be heated above 100° C. Two samples were being irradiated when his ion pump broke down. These samples were sent to me, with irradiation data listed in Table 22.

Table 22. Details of a hydrogen irradiation by Dr. Nash.

ionic species	90% H$^+$, remainder H$_2$$^+$, H$_3$$^+$
ion energy	2.0 keV
current density	10 μa/cm^2
total dose	3.2×10^{17} H$^+$/cm^2
sample surface temperature	55° C
chamber pressure—beam off	5×10^{-7} torr
—beam on	2×10^{-6} torr

The sample surface temperature during irradiation is measured with an infra-red radiometer. Other details of the apparatus are given in Nash (1966).

In preparation for these samples, a well blank was run, measuring the evolved gas in 200° steps to 1000° C. At each temperature two gas collections were made and consecutively measured. Thus the total heating time at a given temperature is about 38 minutes. The results of the run are shown in Fig. 10.

Next, a standard was run. This was a piece of olivine cut and handled in the same manner as the samples, but not irradiated. As
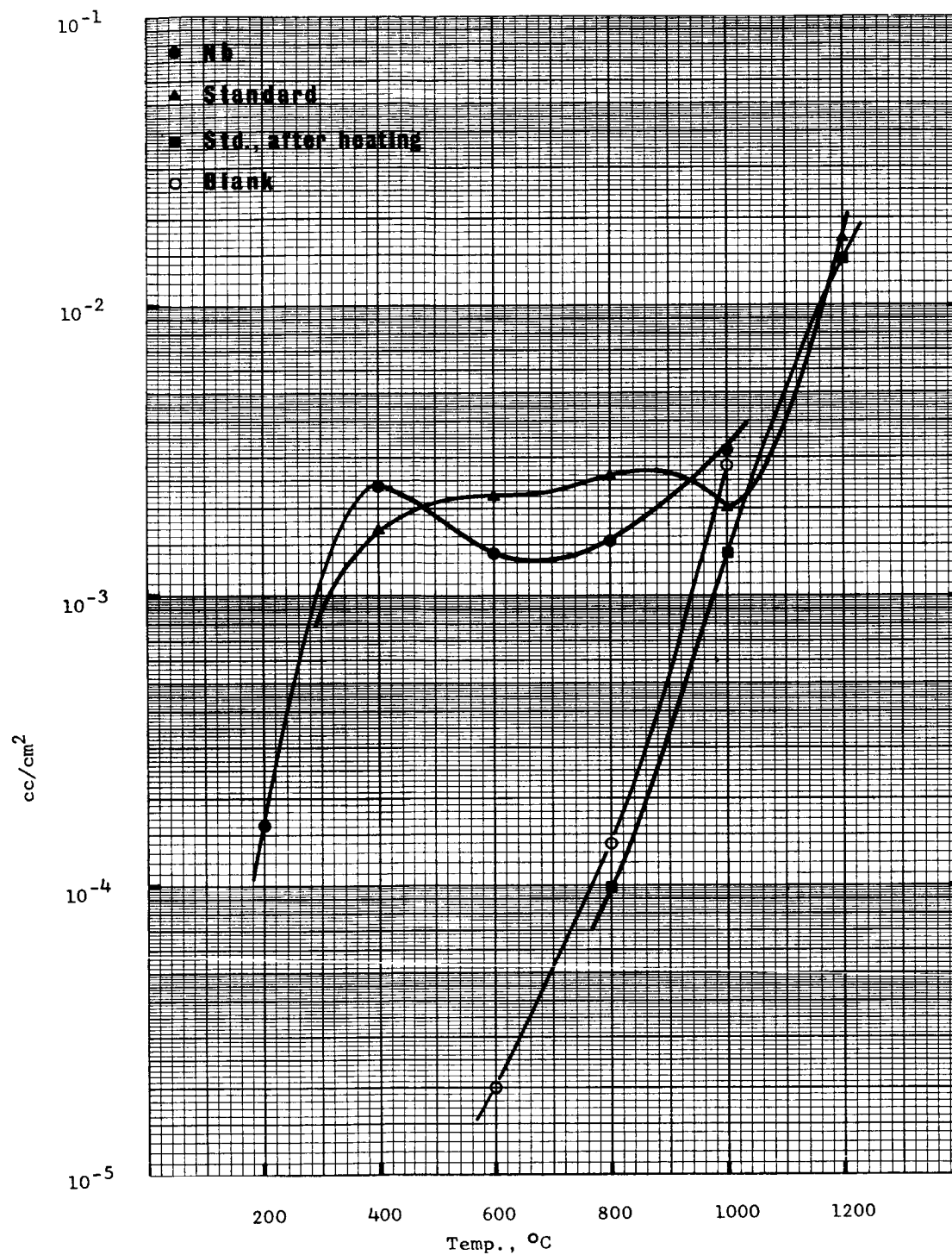
Fig. 10. Preliminary results for the Nash irradiations.

shown in Fig. 10, significant H_2 was detected at all temperatures from 200° to the highest run, but only the 1000° and 1200° C points match the well blank. Thus, although the sample was carefully handled, it was somehow contaminated. One of the Nash-irradiated samples (Nb) was run, followed by a well blank. The results are also plotted in Fig. 10.

To insure that no low-temperature releasable gas remained in the samples, all subsequent samples were heated in a vacuum to above 800° C with continuous evacuation. The standard used above was run through the heating cycle again collecting evolved gas and measuring with the VPC. The results are shown in Fig. 10. The release was the same as the previously run well blank (except displaced to lower gas evolution, slightly, as the blank decreases with time). The samples were now considered clean, and were sent to Dr. Nash again.

The following irradiations were obtained:

Samples 1Al, 1Ad 5.4×10^{16} H^+/cm^2

1Bl, 1Bd 5.4×10^{17} H^+/cm^2

2Al, 2Ad   loaded, but not irradiated

2Bl, 2Bd 5.4×10^{18} H^+/cm^2

All other conditions during the irradiation were the same as listed in Table 22. As before, well blanks and standards were run, intermixed with samples. The results are shown in Figs. 11, 12, 13, and 14. It is seen that the maximum gas release for 2 keV protons injected into olivine occurs around 300-400° C. Both the temperature where gas is first detected and the temperature where the release is a maximum decrease with increasing integrated flux. This suggests that the presence of some hydrogen in the lattice forces the subsequent ions
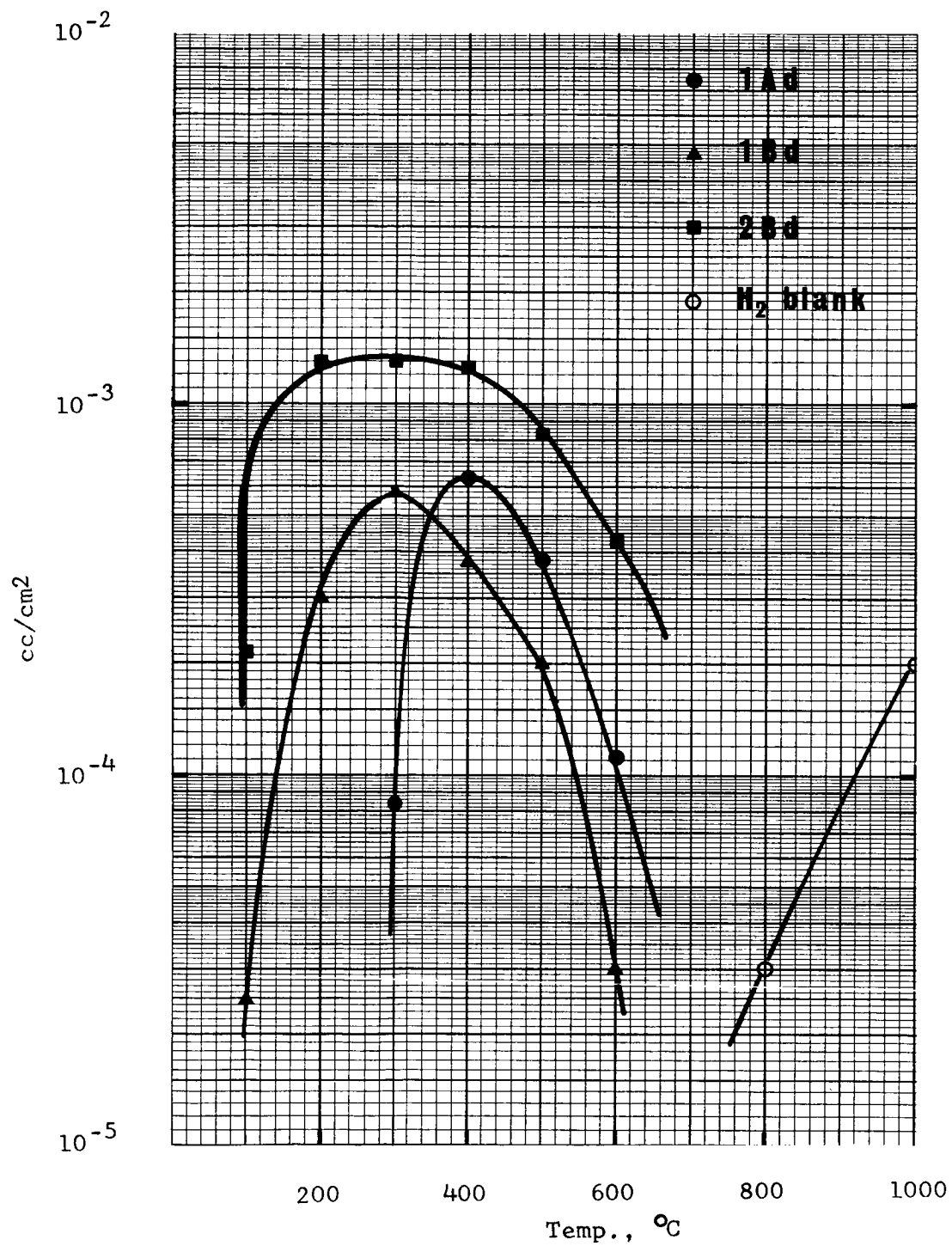
Fig. 11. Differential gas release curves
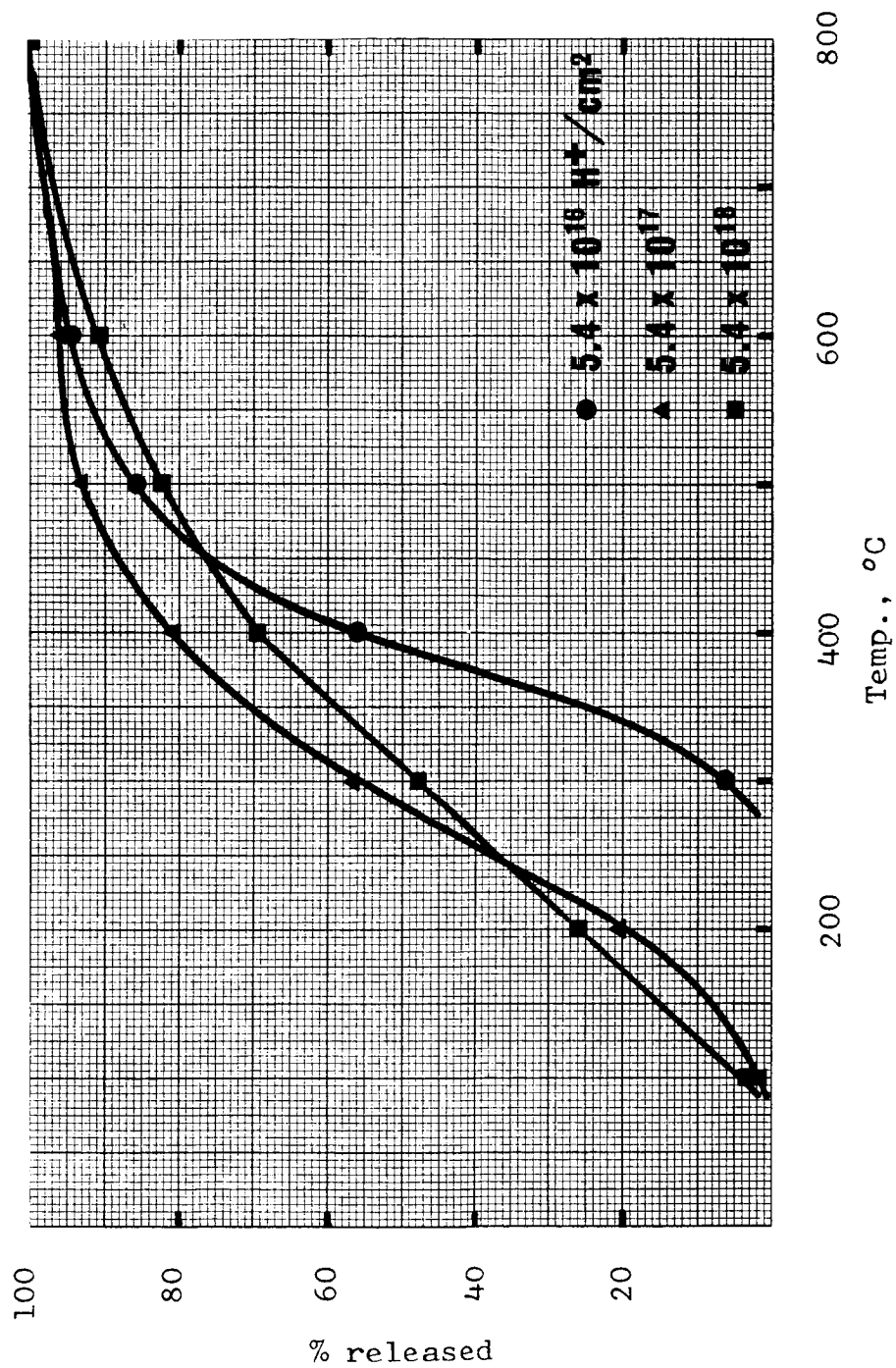for the Nash irradiations.

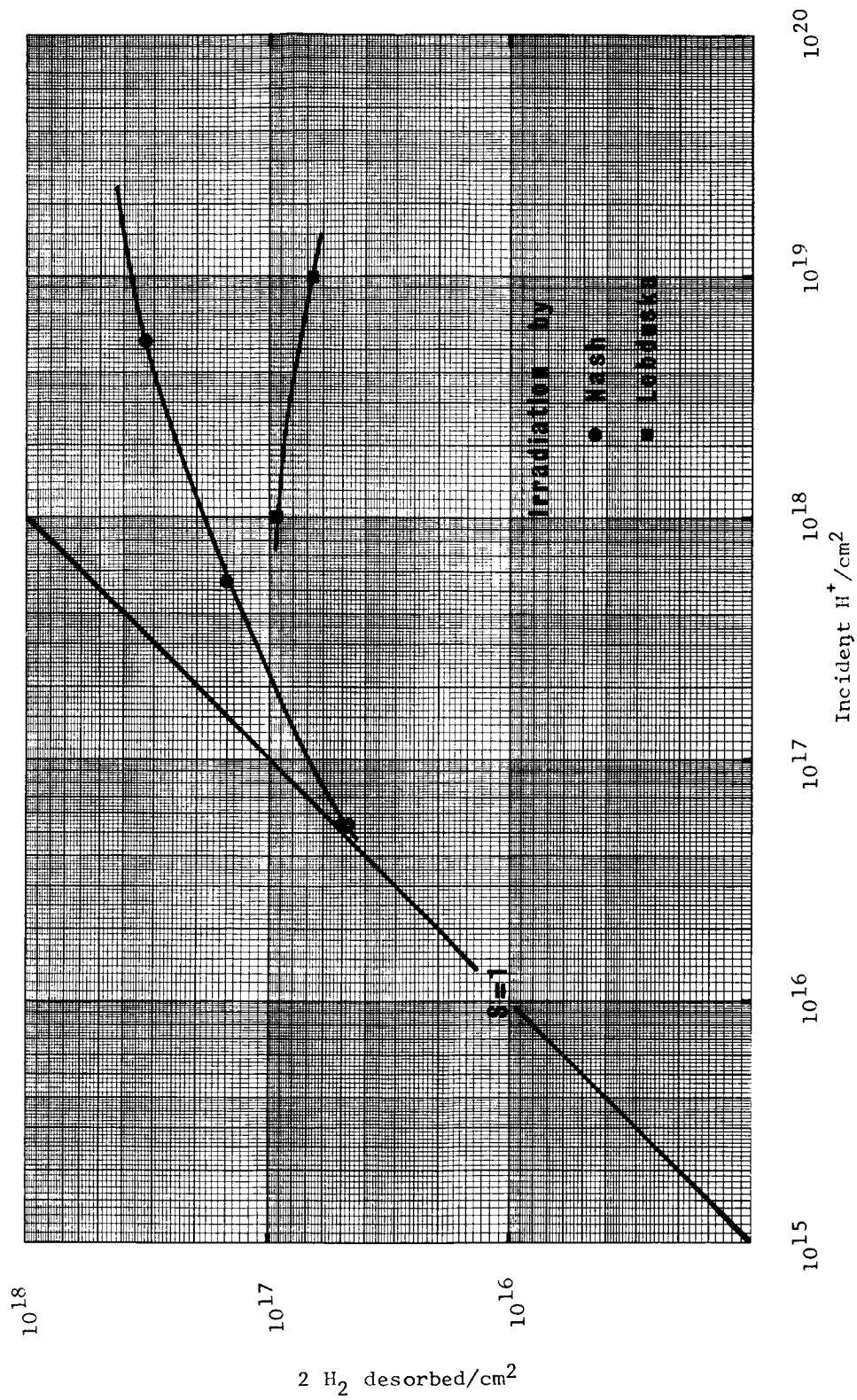Fig. 12. Integral gas release curves for the Nash irradiations.

Fig. 13. Desorbed hydrogen as a function of the
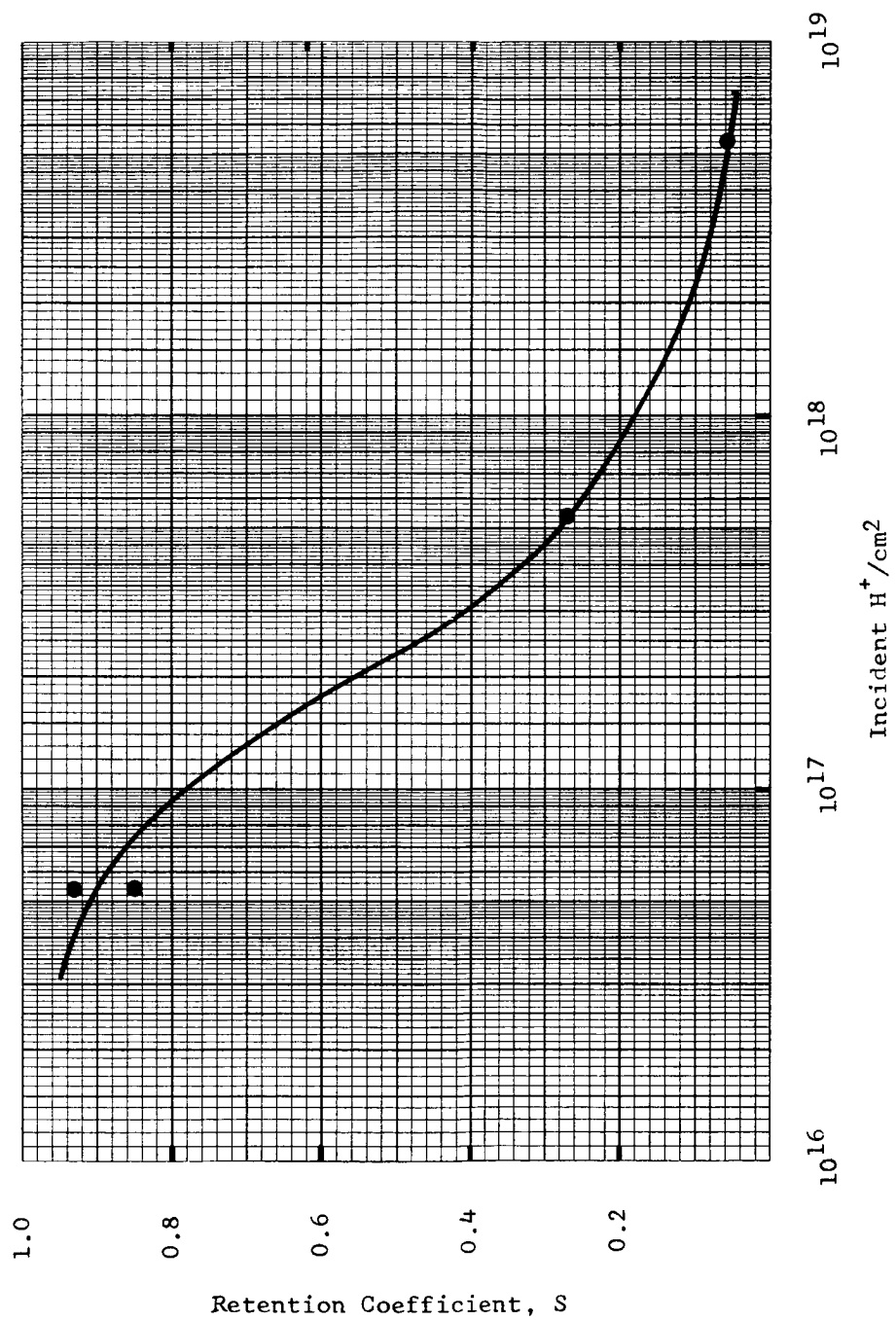integrated incident flux.

Fig. 14. Hydrogen trapping as a function of the integrated incident flux.

to occupy lower energy sites until eventually a steady state is established where one atom leaves for every incoming atom (saturation). Fig. 13 allows an estimate to be made of the saturation value for 2 keV protons in olivine at a temperature of 60° C. This number is on the order of 5×10^{17} protons/cm^2.

To supplement this data a proton irradiation of olivine at a higher current density (and therefore higher sample temperature) was obtained from Mr. Lebduska. Two olivine slabs (prepared as above) were irradiated, as described in Table 23.

Table 23. Details of the hydrogen irradiations by Mr. Lebduska.

ionic species	unknown, some mixture of H$^+$, H$_2$$^+$, H$_3$$^+$
ion energy	2 keV
current density	160 μa/cm^2
total dose #1	10^{18} ions/cm^2
#2	10^{19} ions/cm^2
sample surface temperature	100° C (a)
	200° C (b)
chamber pressure—beam off	10^{-7} torr
—beam on	10^{-4} torr

(a) reported by Mr. Lebduska from another measurement with a thermocouple embedded in a powder

(b) estimated from Dr. Nash's results, when P = 0.32 watts/cm^2

The samples were held in position for irradiation by a small drop of epoxy cement, so there is a possibility of contamination. When

received here, the epoxy was carefully removed with a scalpel. Then this face was polished (dry) with #320 emery paper until a fresh smooth surface was obtained. It was thought that all the epoxy had been removed. Each sample was run by dropping it into the well at 800° C and measuring the total evolved gas. Besides H_2, another gas was detected, having a retention time of 29 minutes. This was observed in both samples, and is present in considerable amounts. It is thought to be CO, and to be present in volumes of a few times 10^{-3} cc. This is most likely contamination from the irradiation apparatus.

The results are shown in Fig. 12 superimposed upon Dr. Nash's results. Most striking is the fact that increasing integrated flux caused decreased retention. This is observed with the He bombardments, also (see page 117). The simplest explanation is a temperature effect. These materials are all refractories, and the fifteen minute irradiation time for the 10^{18} ion/cm^2 irradiation may not have heated the sample as much as the longer, 150 minute irradiation. This is consistent with both points being below the line established from Dr. Nash's irradiations.

He Bombardments: The samples used for the initial He irradiation (second Hapke irradiation) were first tested and found to have no detectable H_2 or He at any temperature. No special care was taken during their preparation in the selection of solvents, etc. As a result there was a large H_2 blank, typically on the order of a few times 10^{-1} cc H_2/cm^2. The H_2 release pattern is shown along with two of the He release patterns in Fig. 9. Thus there exists the possibility that the H_2 filled sites, not allowing He retention. One would then expect

these values to only be a lower limit. As seen in the figure, the He release decreases rapidly above 400° C, while the H_2 blank is still increasing. Is there a cause and effect relationship? Later He release studies as well as H_2 release work indicate that the release curve is not substantially affected by the presence of large amounts of H_2, although nothing can be said about the absolute retention.

In this irradiation, only slabs 2b1 and 2d1 are both exposed and perpendicular to the incident beam. Slabs 2b2, 2b3, 2b4, and also 2d2, 2d3, 2d4, are parallel to, but underneath the #1 slabs, and thus shielded from the beam. All the other slabs are parallel to the beam and form the vertical walls of a box around the horizontal slabs. The results of the irradiation are given in Table 24. Note that the vertical wall slabs (2bW, 2bN, 2bS, 2dW, 2dN, 2dE, 2dS) all retained more gas than the slabs perpendicular to the beam, 2b1 and 2d1. This can possibly be explained as gas occluded in an amorphous layer built up on these slabs by the retention of sputtered atoms from the pyrex petrie dish. Samples 2bS and 2dW are only lower limits, as sample was lost during the analysis.

For the later He irradiation (third Hapke irradiation), 1 cm^2 slabs perpendicular to the beam were irradiated. See page 74 for irradiation details. Four materials as described on page 71 were used for each irradiation. This study looked for chemical as well as physical properties which are important for the process of retention. In particular, comparison between dunite samples (which are fine-grained olivine) and single crystal olivine slices gave an estimate of the importance of grain size. Also, comparison of the results for enstatite

Table 24.   Results of the 43.5 coul/cm^2 helium irradiation.

	area	total area exposed	evolved gas	$\frac{\text{atoms}}{\text{cm}^2}$	S (if He$^+$)
2b1	1.0 cm^2	1.0 cm^2	5.9x10^{-4} cc	1.5x10^{16}	2.2x10^{-4}
2d1	1.0 cm^2	1.0 cm^2	7.0x10^{-4} cc	1.8x10^{16}	2.6x10^{-4}
2b2					
2b3	N		N		
2d2	O		O		
2d3	N		N		
2d4	E		E		
2bN	0.14 cm^2	1.0 cm^2	2.8x10^{-3} cc	7.2x10^{16}	
2bS	0.14 cm^2	2.1 cm^2	1.2x10^{-3} cc	1.5x10^{16}	
2bW	0.10 cm^2	1.5 cm^2	4.2x10^{-3} cc	7.2x10^{16}	
2dN	0.14 cm^2	2.2 cm^2	2.7x10^{-3} cc	3.1x10^{16}	
2dE	0.10 cm^2	1.6 cm^2	3.9x10^{-3} cc	6.1x10^{16}	
2dS	0.14 cm^2	2.2 cm^2	1.5x10^{-3} cc	1.7x10^{16}	
2dW	0.10 cm^2	1.3 cm^2	8.3x10^{-4} cc	1.6x10^{16}	

and olivine provided an estimate of the significance of mineralogical differences. Thirdly, since both olivine and fayalite were irradiated, comparisons were made with the Fe content. Finally two different current dinsities were used giving two different sample surface temperatures.

After the bombardment, the polished surfaces of both low and high current density irradiations were examined with a microscope at 100x, and no changes were detected. However when the single crystal olivine samples were inspected with the unaided eye, there were noticeable silver patches on the side which had been irradiated. These were random in shape and position, and were not seen on any other material (possibly the contrast with the transparent pale green made this the most favorable case for observation).

A code was derived for labelling these samples, consisting of three letters and a number, XYZA: where

    X = H for Hapke bombardment

    Y = A, B, C, D, or E as a code for a particular integrated
        dosage and current density (see page

    Z = O, E, D, F for material irradiated

    A = 1, 2, 3, or 4 for individual sample number

Thus HDE2 refers to a Hapke irradiation of the higher current density with an integrated flux = 3.0×10^{18} He^{2+} on enstatite slice #2.

These samples were analyzed and the results are given in Table 25 and Fig. 15. The lowest integrated flux bombardment, A, shows the greatest variability between samples. Partially this is due to small samples being measured, and partially it may be due to the instability

Table 25. Results of the final set of helium irradiations (cont.).

integrated flux	surface T	sample	He desorbed	S
3.05×10^{18} He^{2+}/cm^2	$\sim 250^\circ$ C	HDE7	1.69×10^{16} atoms/cm^2	5.54×10^{-3}
		HDE3	1.14×10^{16}	3.72×10^{-3}
		HDD1	3.66×10^{16}	1.20×10^{-2}
		HDD2	3.68×10^{16}	1.21×10^{-2}
		HDO3	1.62×10^{16}	5.31×10^{-3}
		HDO4	1.89×10^{16}	6.20×10^{-3}
		HDF1	1.12×10^{16}	3.67×10^{-3}
3.05×10^{19} He^{2+}/cm^2	$\sim 250^\circ$ C	HEE3	1.38×10^{16}	4.51×10^{-4}
		HED1	2.74×10^{16}	8.98×10^{-4}
		HED2	2.56×10^{16}	8.40×10^{-4}
		HEO1	1.23×10^{16}	4.04×10^{-4}
		HEO4	1.29×10^{16}	4.24×10^{-4}
		HEF1	8.22×10^{15}	2.70×10^{-4}

Table 25. Results of the final set of helium irradiations.

integrated flux	surface T	sample	He desorbed	S
3.05×10^{16} He^{2+}/cm^2	~80° C	HAE1	1.07×10^{16} atoms/cm^2	0.340
		HAE2	9.82×10^{15}	0.322
		HAD1	2.42×10^{16}	0.792
		HAD2	2.87×10^{16}	0.936
		HAD3	1.71×10^{16}	0.562
		HAO1	7.12×10^{15}	0.233
		HAO2	1.63×10^{16}	0.533
		HAO3	2.05×10^{16}	0.672
		HAO4	8.45×10^{15}	0.277
3.05×10^{17} He^{2+}/cm^2	~80° C	HBE1	$>1.70 \times 10^{16}$	$> 5.56 \times 10^{-2}$
		HBE3	2.56×10^{16}	8.40×10^{-2}
		HBD1	3.82×10^{16}	1.25×10^{-1}
		HBD3	3.79×10^{16}	1.24×10^{-1}
		HBO3	3.12×10^{16}	1.02×10^{-1}
		HBO4	3.25×10^{16}	1.06×10^{-1}
3.65×10^{18} He^{2+}/cm^2	~80° C	HCE1	3.87×10^{16}	1.27×10^{-2}
		HCE3	3.93×10^{16}	1.29×10^{-2}
		HCD1	9.18×10^{16}	3.06×10^{-2}
		HCD2	7.27×10^{16}	2.38×10^{-2}
		HCO1	4.66×10^{16}	1.52×10^{-2}
		HCO2	4.40×10^{16}	1.46×10^{-2}
		HCO3	4.40×10^{16}	1.46×10^{-2}
		HCF1	3.18×10^{16}	1.04×10^{-2}
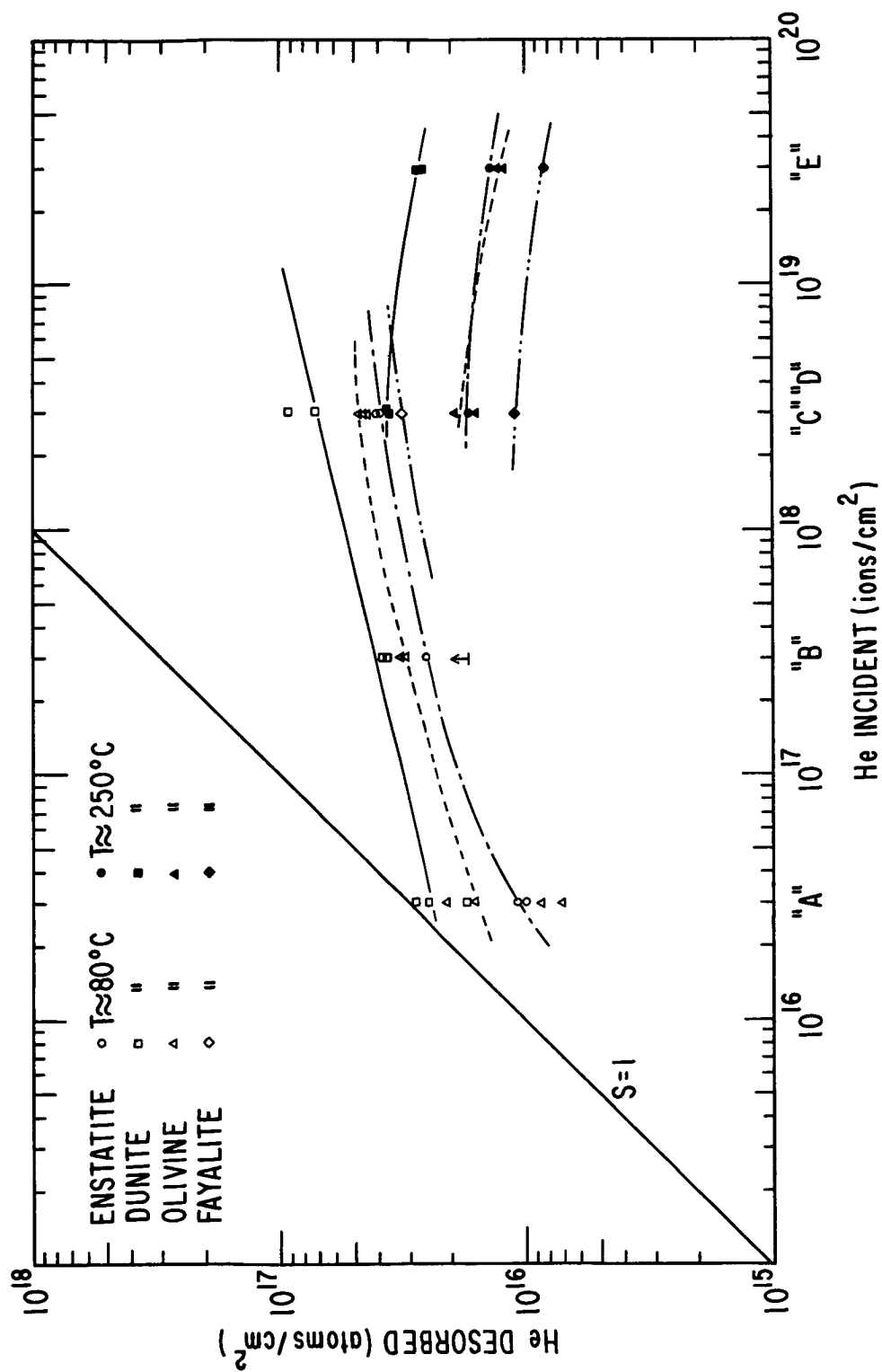
Fig. 15. Desorbed helium as a function of the integrated incident flux.

of the bombardment source before it warms up (about an hour is required, while this is a six minute irradiation). Furthermore, both the dunite and the enstatite are composed of grains that easily chip off and have irregular surface areas. This is another possible cause of variability observed between samples. The analyses are straight-forward except that a leak developed in a Swagelok fitting and this gave erroneous, low results for some samples. These are not included here. After the leak was detected and eliminated, repeat samples were run where possible. This affects only the enstatite and fayalite samples, and only with two fayalite irradiations (A and B) was it impossible to run repeat analyses.

It is seen from Fig. 15 that for all materials except the dunite, the curves suggest that saturation values are less than 10^{17} He/cm^2, while the value for the dunite is on the order of 3×10^{17} He/cm^2. These retained atoms are in a layer less than 500 Å (and possibly less than 100 Å). With a density of 3.5 gm/cc and a mean atomic weight of 20 for these silicates, this layer contains 5×10^{17} atoms/cm^2. Surface roughness would increase this value by a factor of a few, but the conclusions are obvious. The trapped atoms are present in approximately 1 to 1 correlation with the lattice atoms.

As noticed with the hydrogen bombardments, increasing the time for bombardment at the higher current density decreases the amount of desorbed He. One would like a longer bombardment plus better temperature control. The earlier Hapke He irradiation (page 112), although most likely not exactly at the same conditions, gives some clue as to what happens. The average of 2b1 and 2d1 is 1.65×10^{16} He atoms/cm^2. This is between the values shown in Fig. 15 for the equivalent

irradiation with lower integrated dose. Apparently saturation is a real effect, and these experiments do detect its onset.

As is evident in Fig. 16 the dunite sample had the largest retention coefficient under all conditions studied. For this fine-grained, loosely packed material, the true surface area is larger than the geometrical area.

In Figs. 17, 18, 19, and 20 are plotted the percent of total desorbed gas released at each temperature interval. The points used for the enstatite and fayalite curves are from those samples where gas loss occurred, but as the flow rate, etc., was constant for any one day, the release curve is probably not affected. The various samples release He approximately in the same manner. There are no gross differences between the various mineralogical samples studied. However, there is a substantial difference in the temperature for the onset of release between the low and high current density bombardments. This certainly would be expected, if some higher equilibrium surface temperature were achieved during the "D" and "E" irradiations.

It is interesting to compare the hydrogen release from olivine (Fig. 12) with the He release. Considering only the low surface temperature irradiations we see for the He release that increasing the integrated flux moves the release pattern to higher temperatures, although essentially maintaining the same shape. However, for the hydrogen release, increasing the length of bombardment and thus the integrated flux, flattens the release curves, and moves the onset of release to lower temperatures. Note, though, that for any integrated flux the release for hydrogen occurs at a higher temperature than for
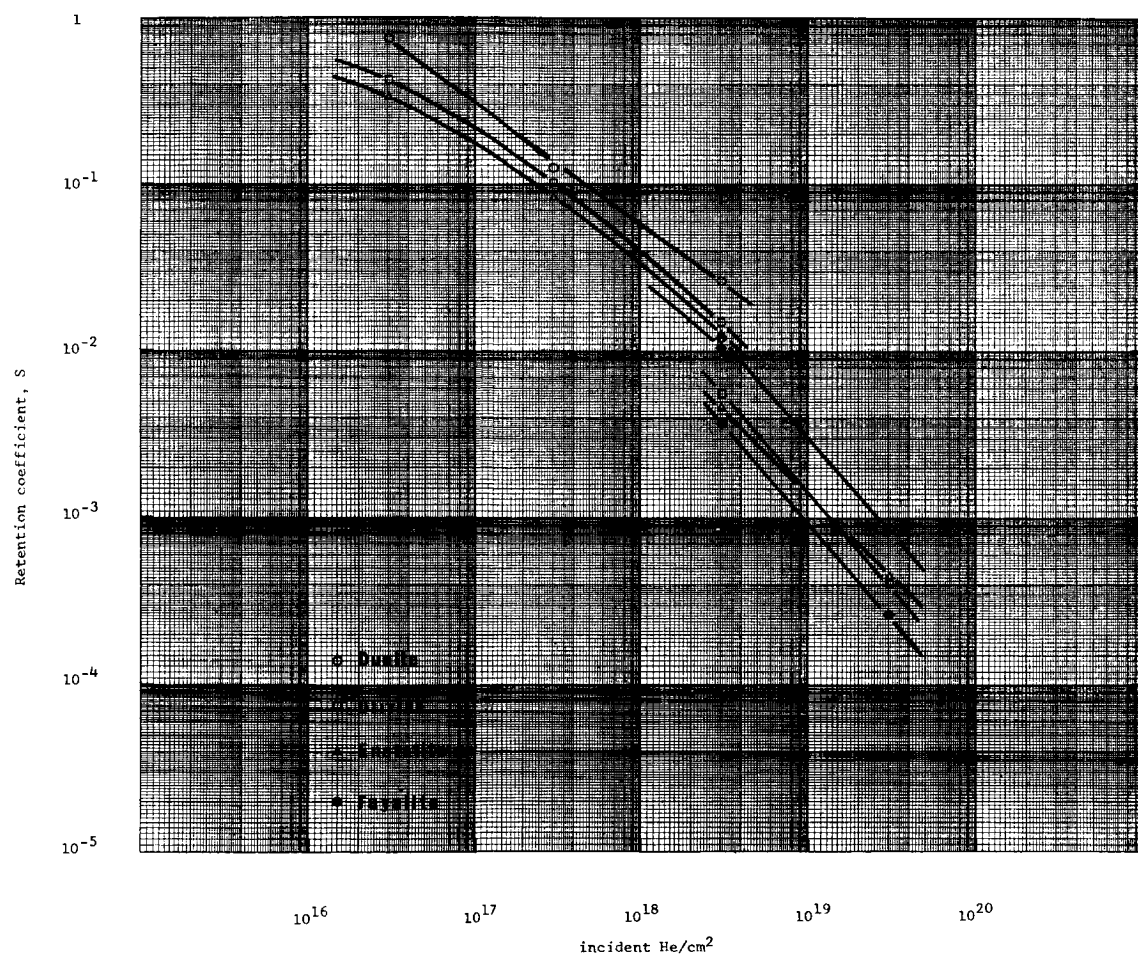
Fig. 16. Helium trapping efficiency as a function
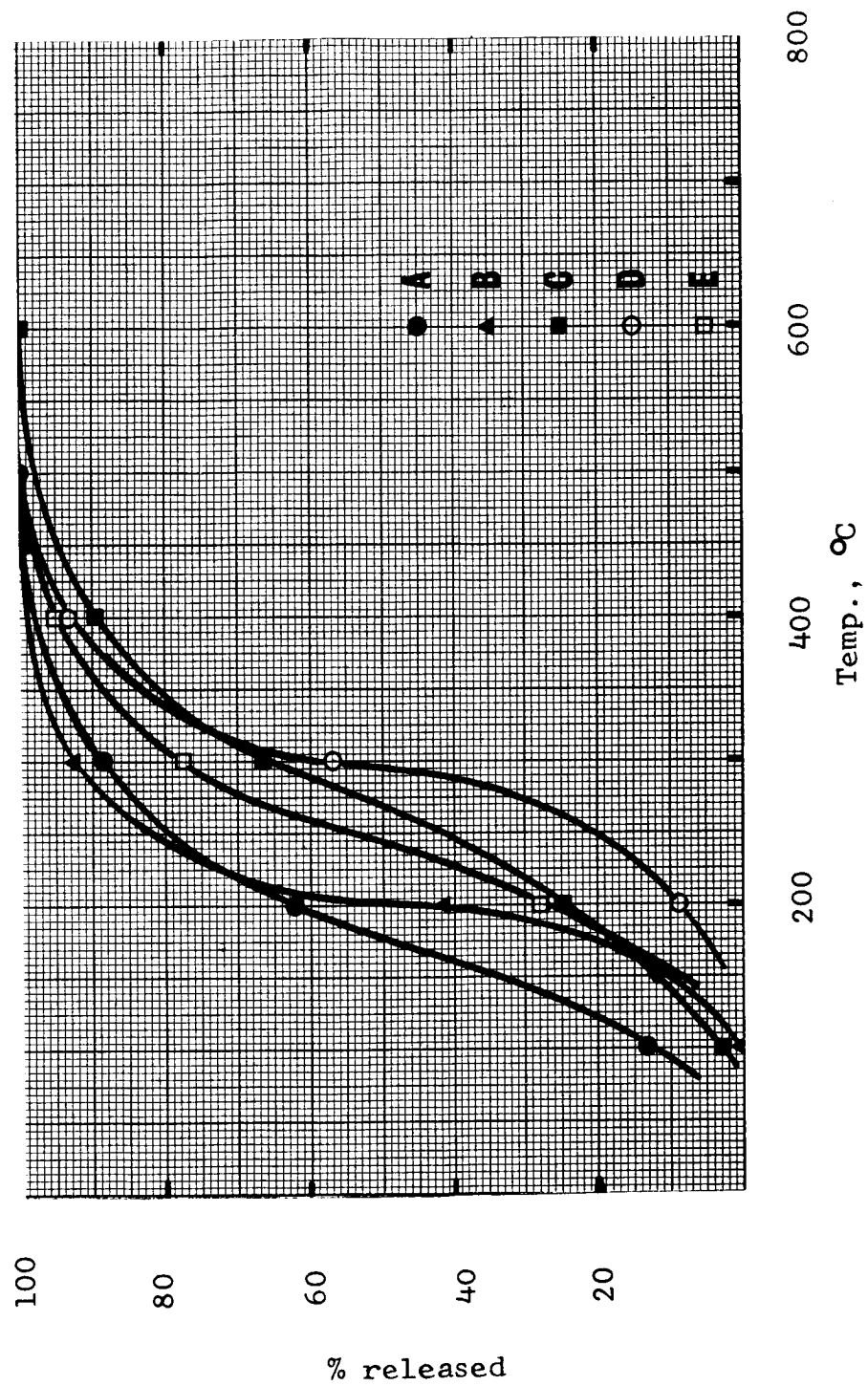of the integrated incident flux.

Fig. 17. Integral helium release curves for enstatite.
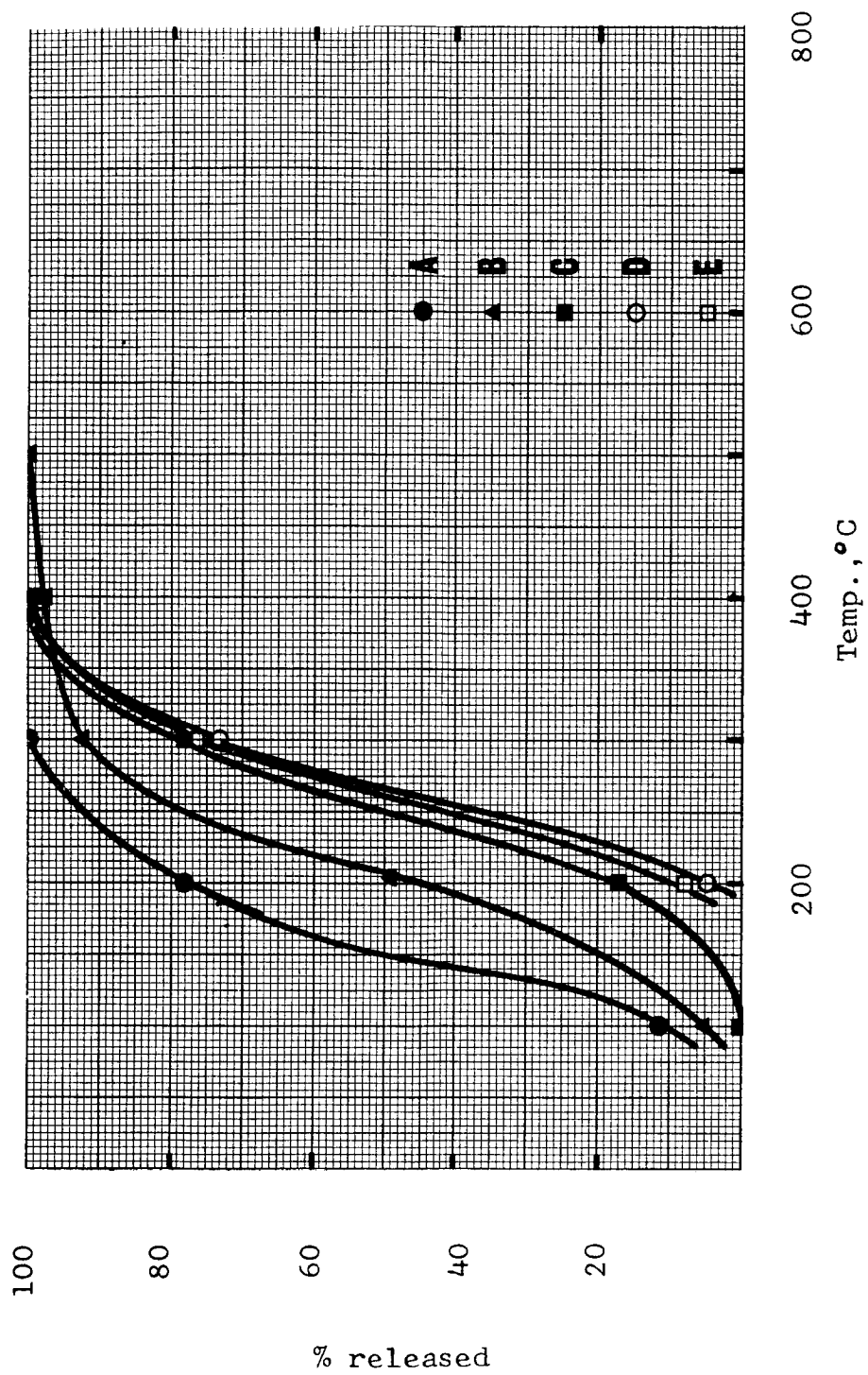
Temp., °C

% released
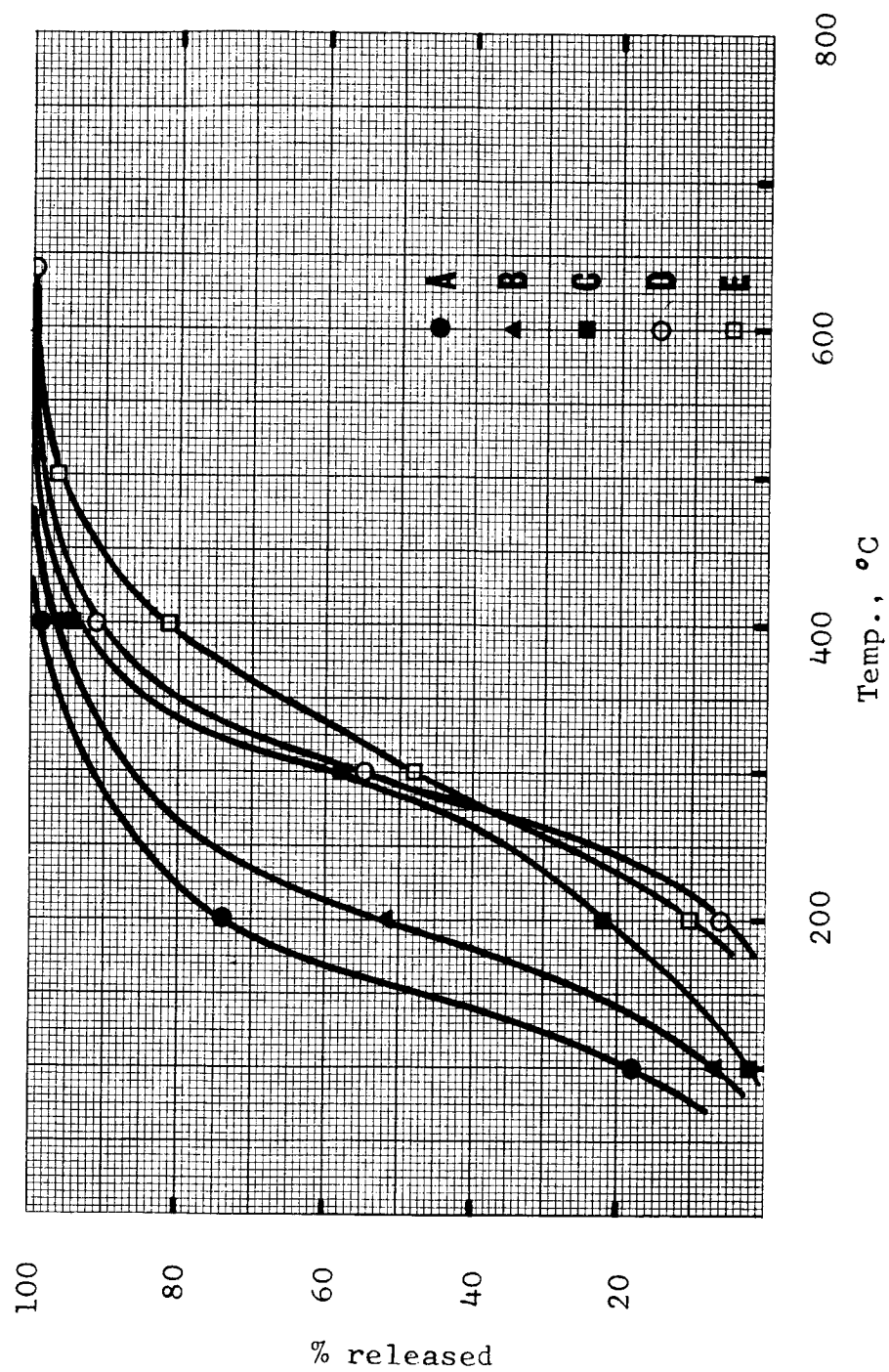
Fig. 18. Integral helium release curves for olivine.

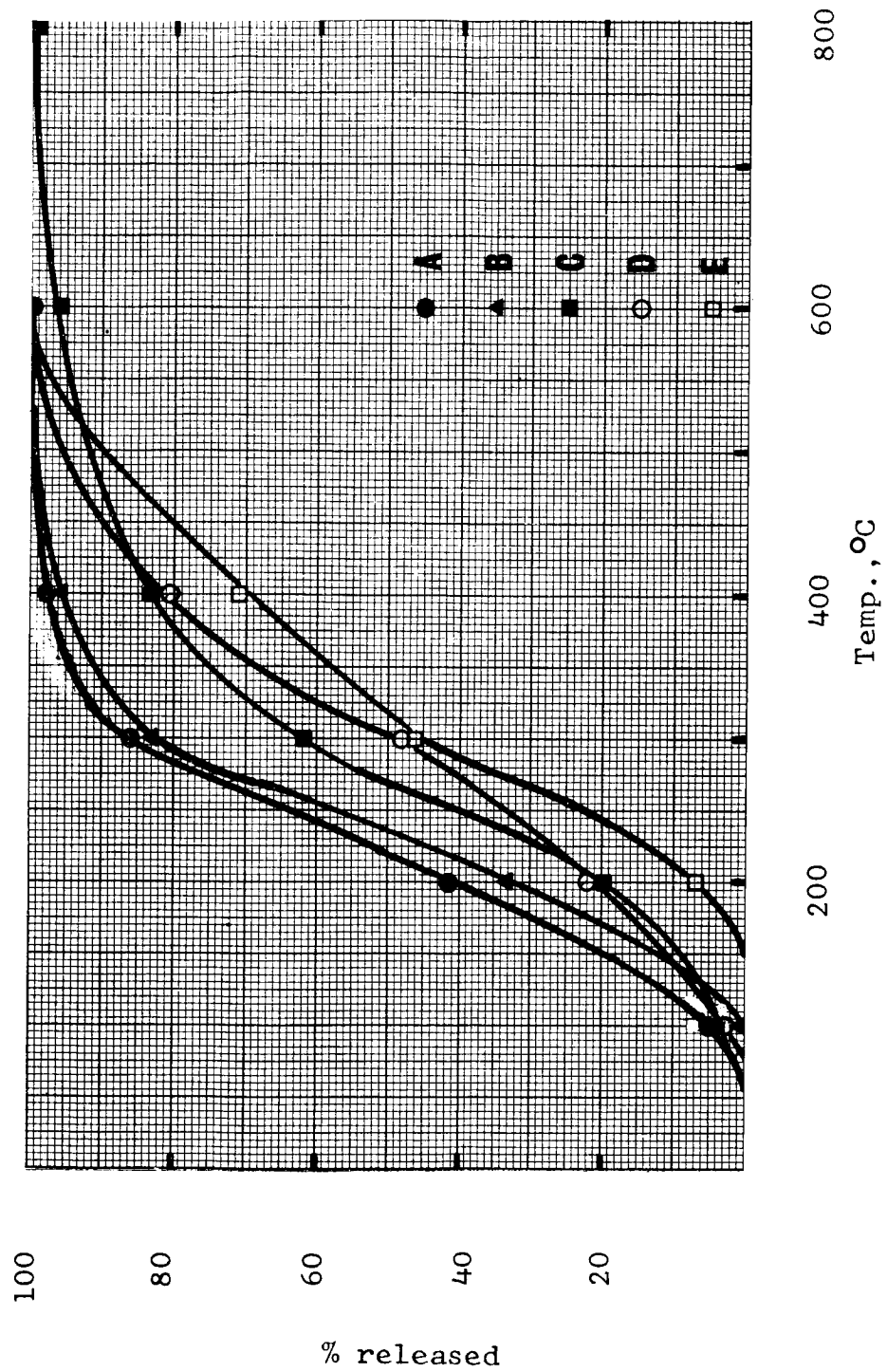Fig. 19. Integral helium release curves for dunite.

Fig. 20. Integral helium release curves for fayalite.

He. This is an argument for a difference in the method of retention of these species. More energy is required to release the H_2, indicating the possibility of some weak chemical bonding of this hydrogen.

This difference is also seen by looking at the diffusion constants. Following Fechtig et al. (1963), the following equation has been used:

$$D/a^2 = \frac{\pi}{36t} \left(\frac{C_o-C}{C_o}\right)^2$$

where t is the diffusion time, a is the single crystal radius, C_o is the initial gas concentration, and C is the gas concentration after diffusion. The diffusion time used here is 40 minutes for He, and 30 minutes for H_2 as gas is collected at each temperature for that length of time. However the gas release may all occur in the first minute, so this calculation gives only a lower limit. Figs. 21, 22, and 23 give the results for the hydrogen experiments, He in olivine, and He in enstatite respectively. Differences between the various He experiments are slight but H_2 and He results for olivine are significantly different.

These experiments confirm that substantial gas is retained by minerals when irradiated with low energy (2 keV) ions. Furthermore the onset of the release of the inert gases is at least an upper limit to the temperature to which the sample has been heated (during or since irradiation). More work is required before deciding how characteristic a fingerprint the various release parameters are in describing the original irradiation.

Because of the higher release temperature of hydrogen and because of the preponderance of hydrogen in the solar wind, one would expect to be able to detect solar wind hydrogen when solar wind helium
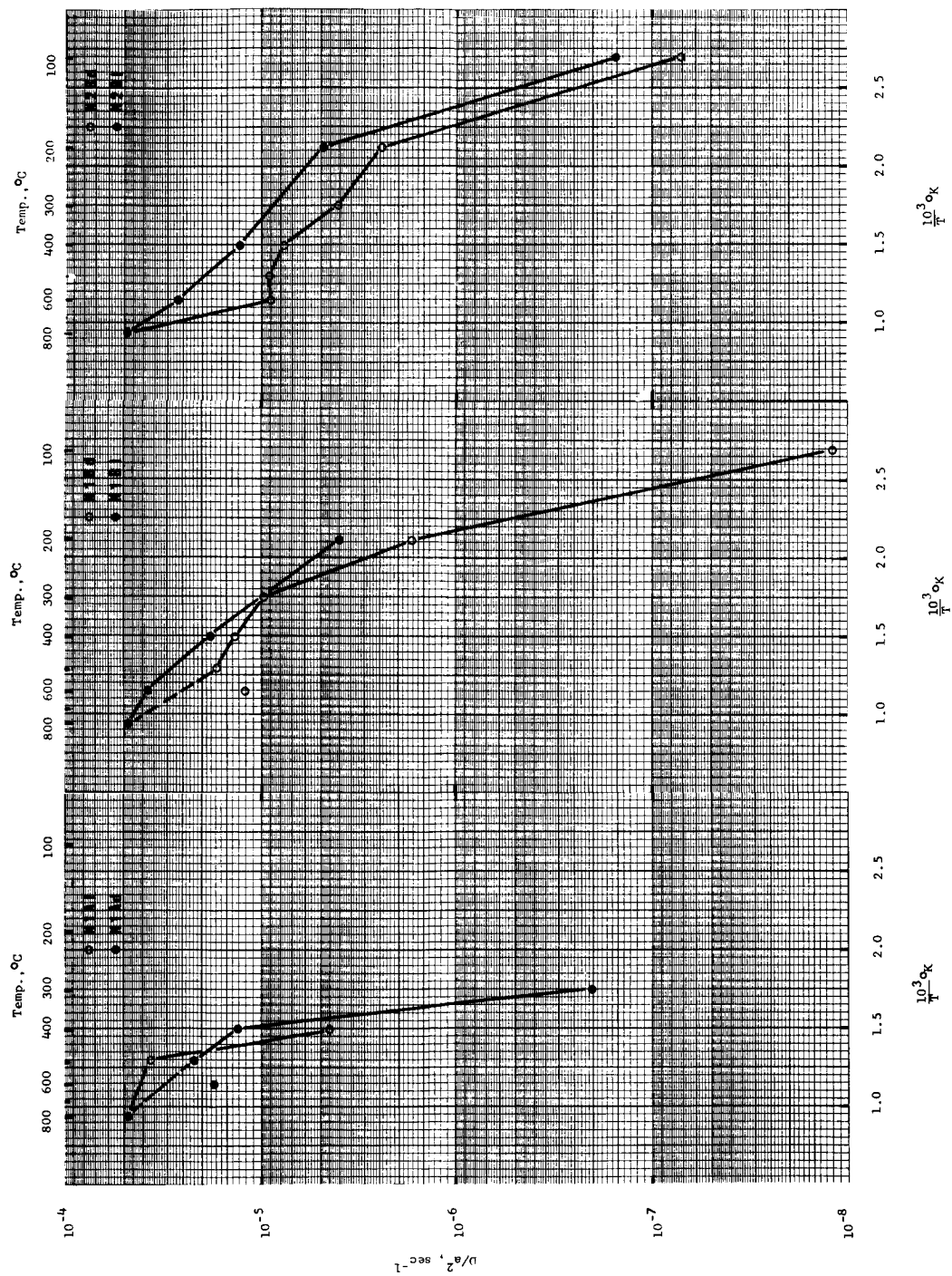
Fig. 21. Hydrogen diffusion in olivine.

Temp., °C

800   600   400 300   200   100

10^{-4}

○ H A 0 2

□ H B 0 3

▲ H C 0 1

● H D 0 4

10^{-5}

D/a^2, sec^{-1}

10^{-6}

10^{-7}

10^{-8}

0.5   1.0   1.5   2.0   2.5   3.0
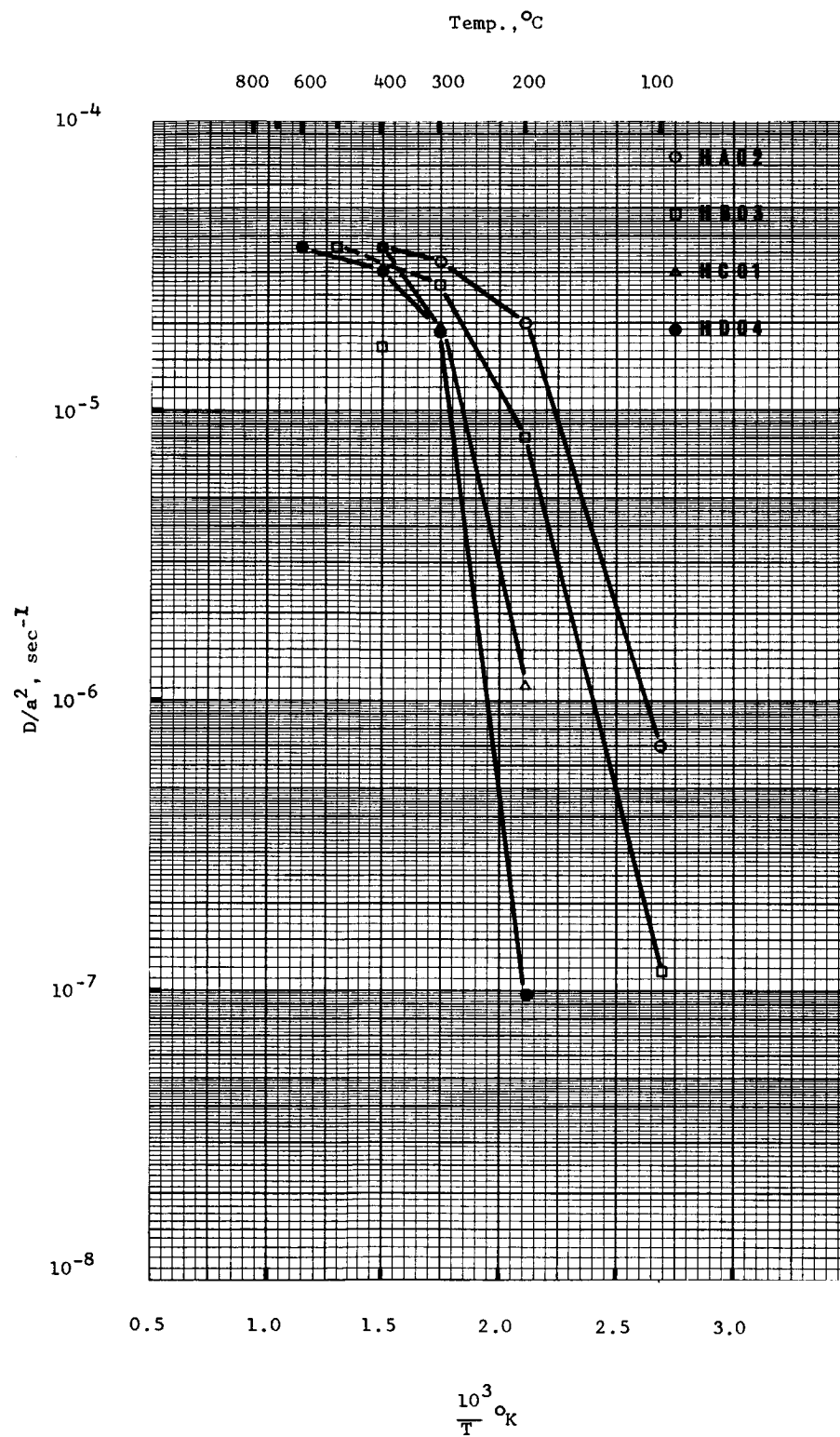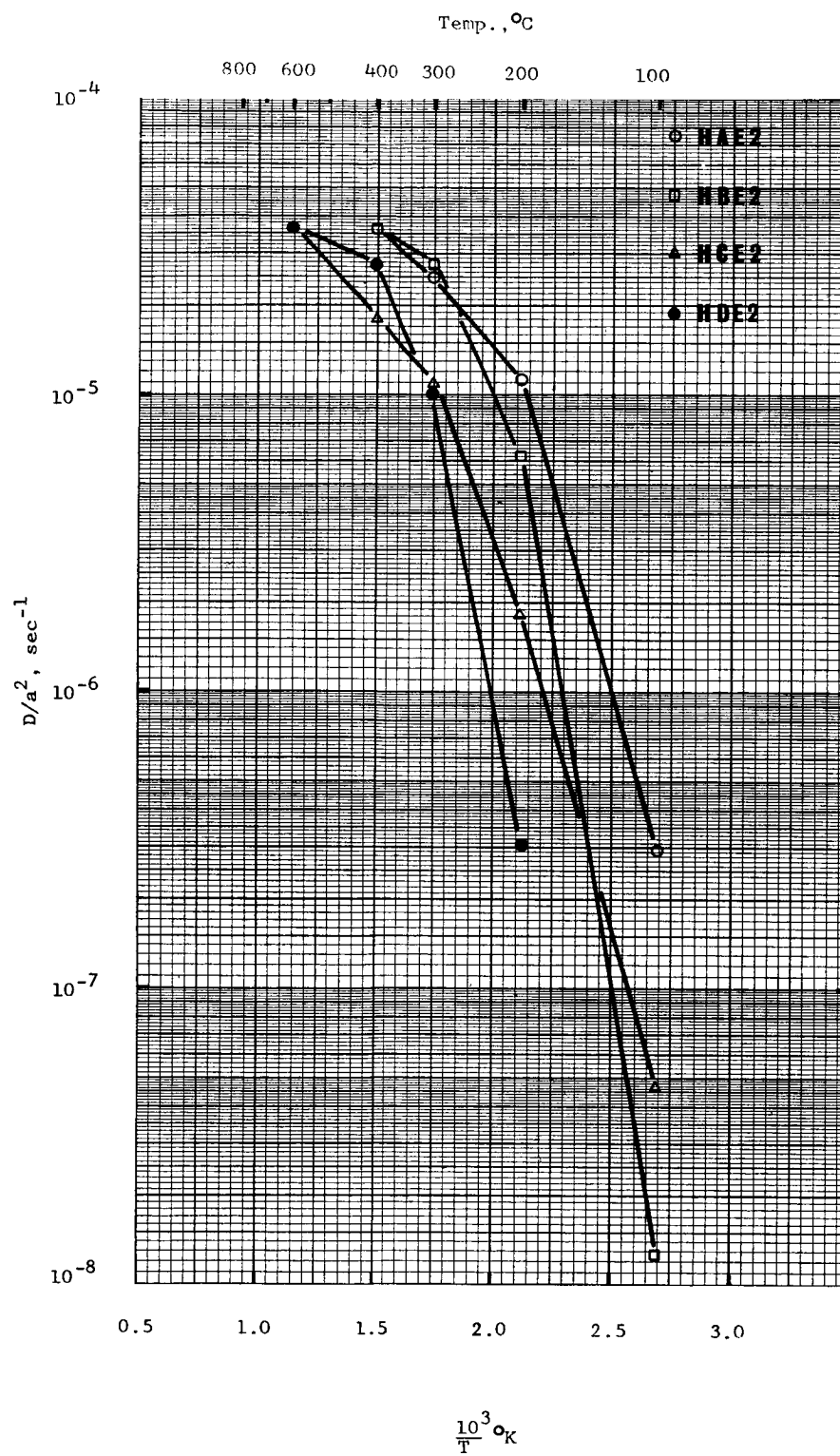
$$\frac{10^3}{T} \, °K$$

Fig. 22. Helium diffusion in olivine.

Fig. 23. Helium diffusion in enstatite.

is detected.

As discussed earlier in the paper, the primordial rare gases observed in meteorites are thought by most workers to be due to solar wind injection into the grains. As 87.2 mg sample of Pesyanoe was obtained from Dr. Kurt Marti. This is an aubrite (a calcium-poor enstatite achondrite) seen to fall in Russia in 1933. Large amounts of primordial gases have been detected in it (Zahringer, 1962). A blank was run on the well and then the sample was run. The gas-release results are shown in Figs. 24 and 25. As indicated there, both He and H_2 were detected. The ratio He/H = 0.061 is less than half the solar value (Goldberg et al., 1960) but when compared to the rough estimates for the solar wind it does not appear to be an unreasonable value. These numbers are given in Table 26, while Table 27 reports the total evolved gas.

Table 26. Extraterrestrial He/H values.

Solar	0.16	Goldberg et al., 1960
Solar Wind	0.042 (mean)	Hundhausen et al., 1967
	0.095 (mean)	Wolfe et al., 1966
	0.046±0.038	Neugebauer and Snyder, 1966
Solar Photosphere	0.09	Neugebauer and Snyder, 1966
Pesyanoe	0.061	this work

From Figs. 13 and 15 we see that for olivine at saturation there are about seven times as many hydrogen as helium atoms in the lattice. Assuming this to be true for enstatite also, the He/H
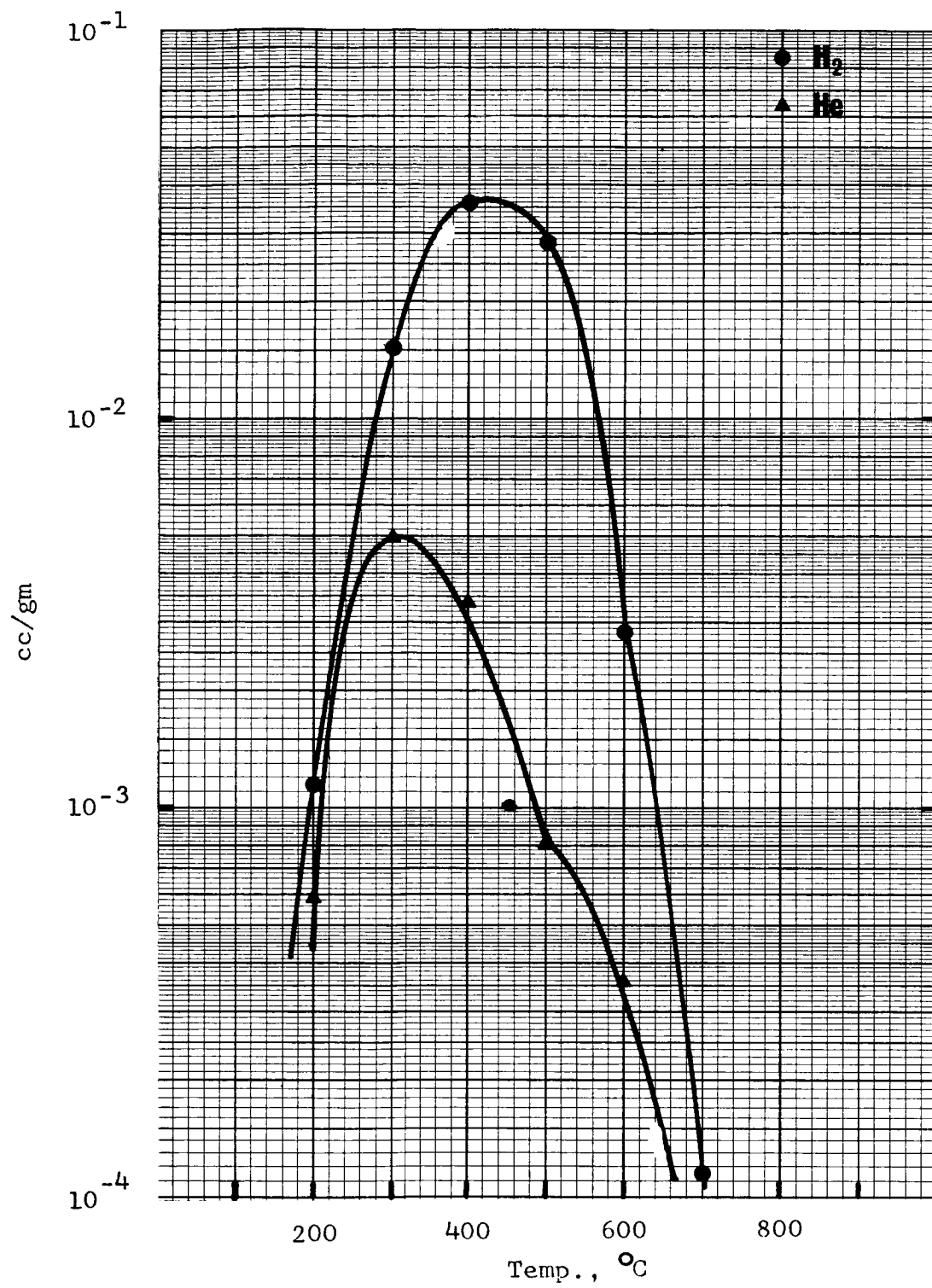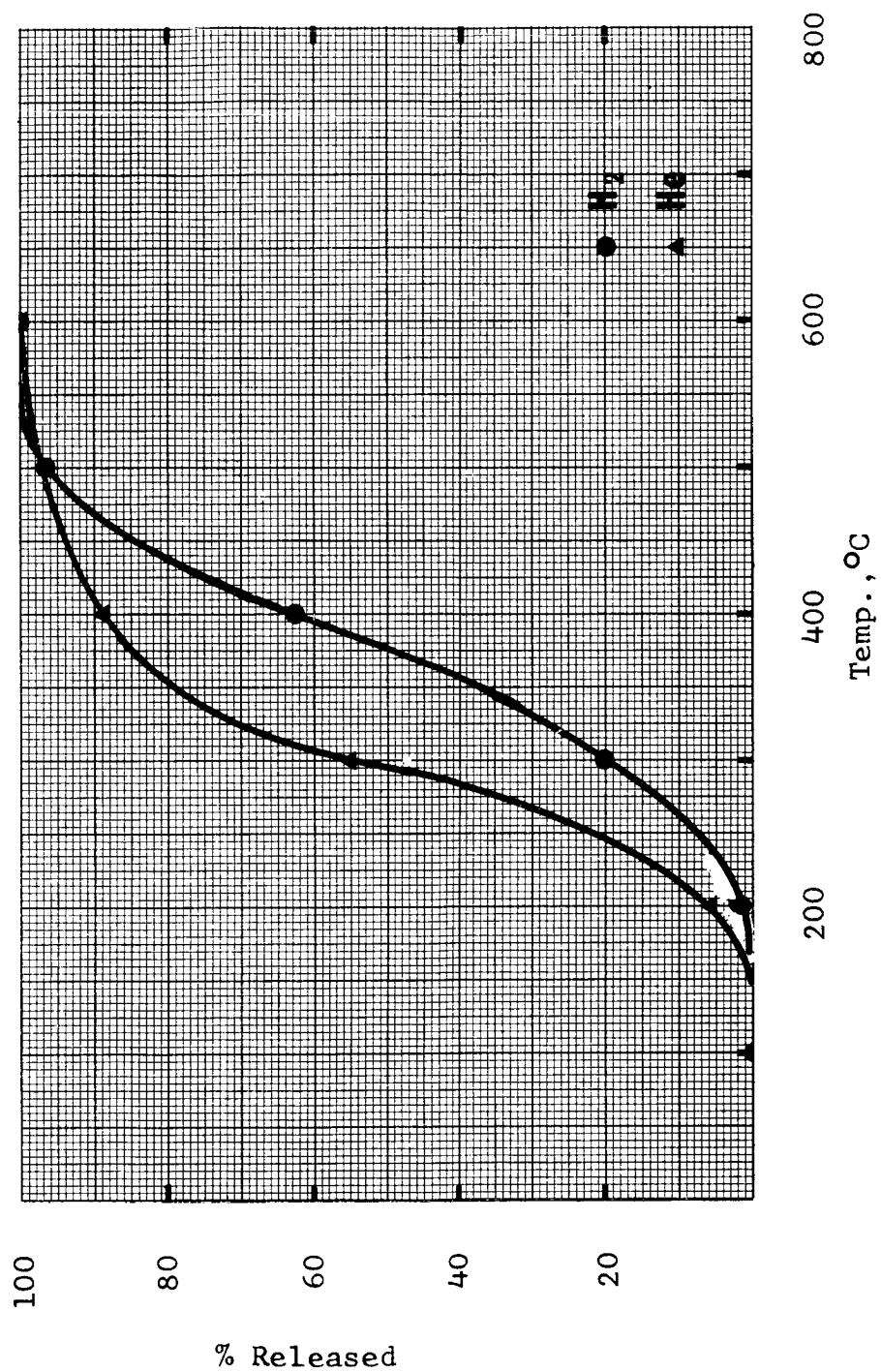
Fig. 24. Differential gas release from Pesyanoe.

Fig. 25. Integral gas release from Pesyanoe.

Table 27. Total evolved H_2 and He from natural samples.

	H_2	He
Pesyanoe	8.4×10^{-2} cc/gm	1.0×10^{-2} cc/gm
Norton County	2.8×10^{-2} cc/gm	not detected
Plainview	7.8×10^{-2} cc/gm	not detected
Biotite	3.0 cc/gm	not detected

saturation ratio derived is 0.14. This is more than double the observed value. However, as no combined hydrogen and helium irradiations have been performed, it is impossible at this time to decide whether these atoms sit in different sites in the lattice or in similar sites. In the latter case, the atoms in greater abundance (hydrogen) will fill the majority of sites.

From Fig. 15, we see that saturation of helium in enstatite occurs at about 6×10^{16} atoms/cm^2, giving a value for the saturation of hydrogen in enstatite of about 4×10^{17} atoms/cm^2. From these numbers, and using the total evolved He and H_2 per gram (Table 27) from Pesyanoe, one can calculate the surface area of the constituent grains required for saturation. For helium this is 4.3 cm^2/gm and for hydrogen the required area is 10.8 cm^2/gm. Using 10 cm^2/gm, a density of 3.5 gm/cc, and assuming spherical particles, one calculates the particle radius required to give this surface area per gram to be equal to 1.7 mm. This is much larger than the average grain size of Pesyanoe $r \approx 30 \mu$.

Comparing the diffusion constants (D/a^2) for the gas release from Pesyanoe, Fig. 26, with the experimental work, it is seen that the He values are comparable only to the higher current density bombardment

results (see values for HDE2). This is an irradiation close to saturation. However the saturation level was found to decrease with increasing temperature. For He, this reduces the amount of trapped gas, depending upon the temperature, up to as much as a factor of five in these experiments.

Thus it appears that Pesyanoe is saturated with He. Assuming that, one should be able to derive the sample temperature during the irradiation. For $r = 30\mu$, and a saturation value of He of 1×10^{16} atoms/cm^2, it turns out that at least 10% of the saturation value of the gas is retained. (Increasing r, or decreasing the saturation value, would bring the amount retained closer to 100%). Using this number, one calculates a D/a^2 of 2.5×10^{-11} sec^{-1} giving a temperature of 100° C from the HDE2 results, and a temperature of 120° C from the Pesyanoe He results. This compares very favorably with the maximum temperature of the moon, $\sim 120°$ C.

Furthermore, in comparing these D/a^2 results, we see that the H_2 values are not similar to any of the experimental curves. It is not likely that this is solely due to the fact that the experimental work only includes H_2 release from olivine, as the He release from the various minerals is quite similar. More likely, the lack of agreement is due to the absence of H_2 release studies for irradiations at higher sample surface temperatures (i.e. $\sim 200°$ C). The deviations between Pesyanoe and the experimental irradiations are such that an increased surface temperature could cause the curves to overlap.

An alternate explanation for this lack of agreement is that low temperature diffusion has occurred for long periods of time. This seems
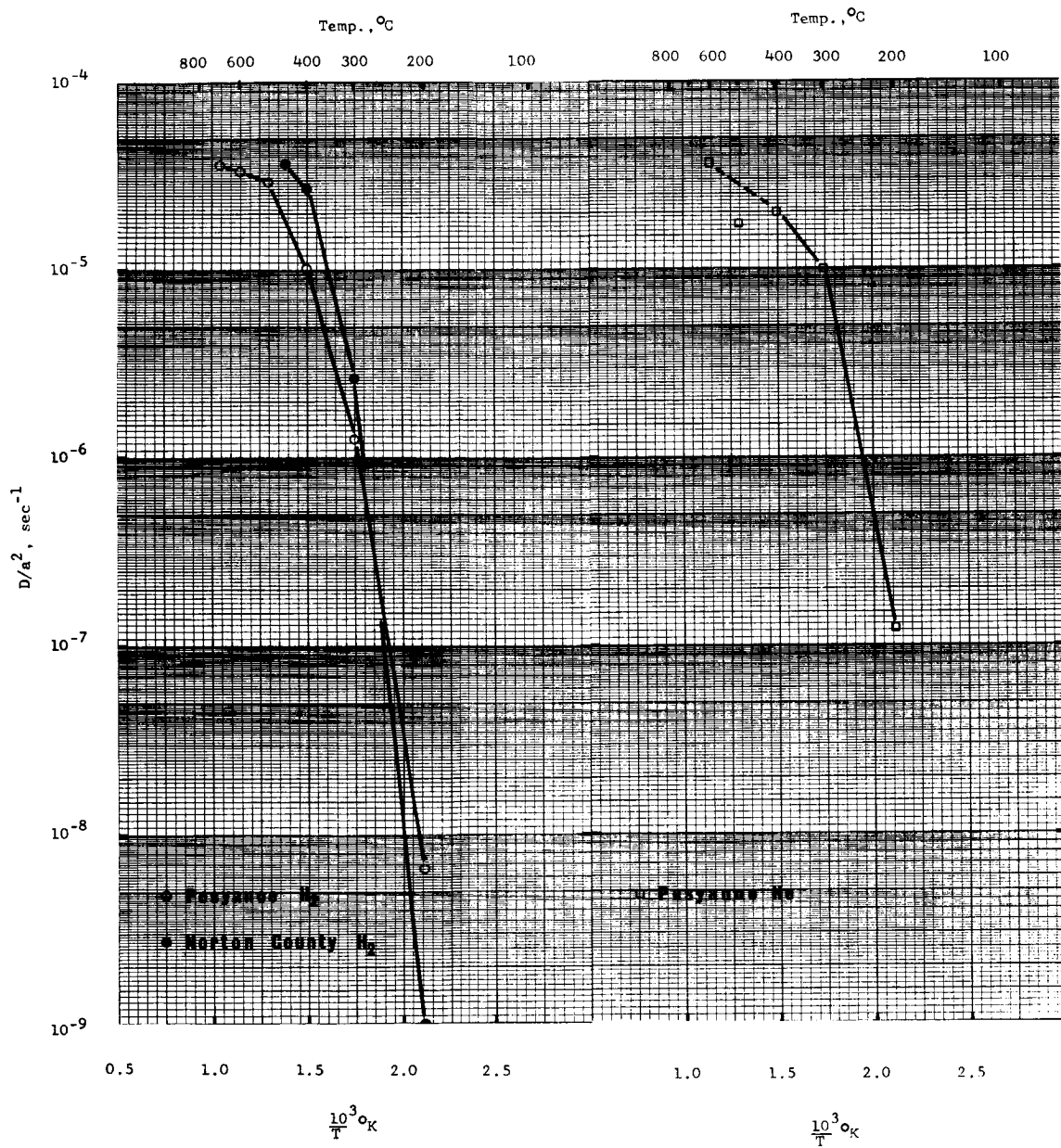
Temp., °C

800 600 400 300 200 100

Temp., °C

800 600 400 300 200 100

10^{-4}

10^{-5}

10^{-6}

D/a^2, sec^{-1}

10^{-7}

10^{-8}

10^{-9}

○ Pesyanoe H$_2$

● Norton County H$_2$

0.5   1.0   1.5   2.0   2.5

1.0   1.5   2.0   2.5

$\frac{10^3}{T}$ °K

$\frac{10^3}{T}$ °K

Fig. 26. Diffusion in Pesyanoe and Norton County.

unreasonable, since for all comparable irradiations, the diffusion constants for H_2 are lower or a maximum of twice the value for He. Thus with any major H_2 loss, no matter at what temperature, simultaneous He loss must have occurred.

These results imply that under favorable circumstances trapped solar wind should be detectable in cosmic dust. However, heating to 200° C for a few hours is sufficient to remove a large fraction of the helium, and with longer times, major hydrogen loss also occurs. The time required for a large fractional loss at 100° C can be estimated from the D/a^2 curves. It is assumed that the curve for the Pesyanoe results makes another small break at 200° C, as seen at all the higher temperatures, and as seen at 200° C for all the He studies in olivine and enstatite. Using $D/a^2 = 10^{-14}$ sec^{-1}, a 50% loss of trapped gases would occur in 7×10^4 years. This time is comparable to the predicted lifetimes for the lower end of the size range for cosmic dust.

The blackbody temperature of a particle at 1 A. U. is only 17° C. Furthermore, a saturation bombardment at 1 A. U. occurs in the order of 10^2 years. One would then not expect gas loss. For a collection of cosmic enstatite dust with a particle radius of 10μ, one would expect to see on the order of 7 cc/gm H_2 and 2 cc/gm He. An order of magnitude reduction in the particle radius increases the gas content per gram by a factor of ten.

Alternately, we can ask what the conditions are for gas loss by diffusion to occur on the same time scale as the saturation bombardment. Assuming total gas loss, surface temperature of 75° C, and a time of 10^2 years, the resulting D/a^2 is 2.9×10^{11} sec^{-1}. We see from the work

here on Pesyanoe, Fig. 26, that for He this D/a^2 occurs at about 150° C. This further says that if the sample has not been heated much above 100° C, a saturation amount of gas should be obtained in 10^2 years.

As a blank for the Pesyanoe results, an aubrite without detectable primordial rare gases was also run. 140.8 mg. of Norton County were analyzed in the same manner as the Pesyanoe sample. There was no He detected at any temperature; however significant amounts of H_2 were detected (see Table 27), with a release curve very similar to that obtained for Pesyanoe (see Fig. 27). The diffusion constants for that release are plotted with the values for Pesyanoe. The similarity here appears to be an important discovery. Either Norton County has primordial H_2 and has somehow lost or not received the other primordial gases, or the similarity of release does not imply a similarity for the origin of the gas.

It does not seem reasonable that this detected hydrogen is contamination as hydrogen, but it may be the result of the reduction of contamination or indigenous water by the Fe present in the sample. As a check on this, the Pesyanoe sample was recovered from the well, shaken vigorously several times while completely submerged in water for $4\frac{1}{2}$ hours, and then re-run. No H_2 was unambiguously detected in this analysis. At 600° C there was a slight rise in the base line where H_2 would be expected. If this were H_2, the maximum evolution would be 1×10^{-5} cc H_2.

This is a very difficult problem to solve by these techniques. A more definitive experiment would be the examination of the H/D ratio. If it is found to be substantially different from the terrestrial value,
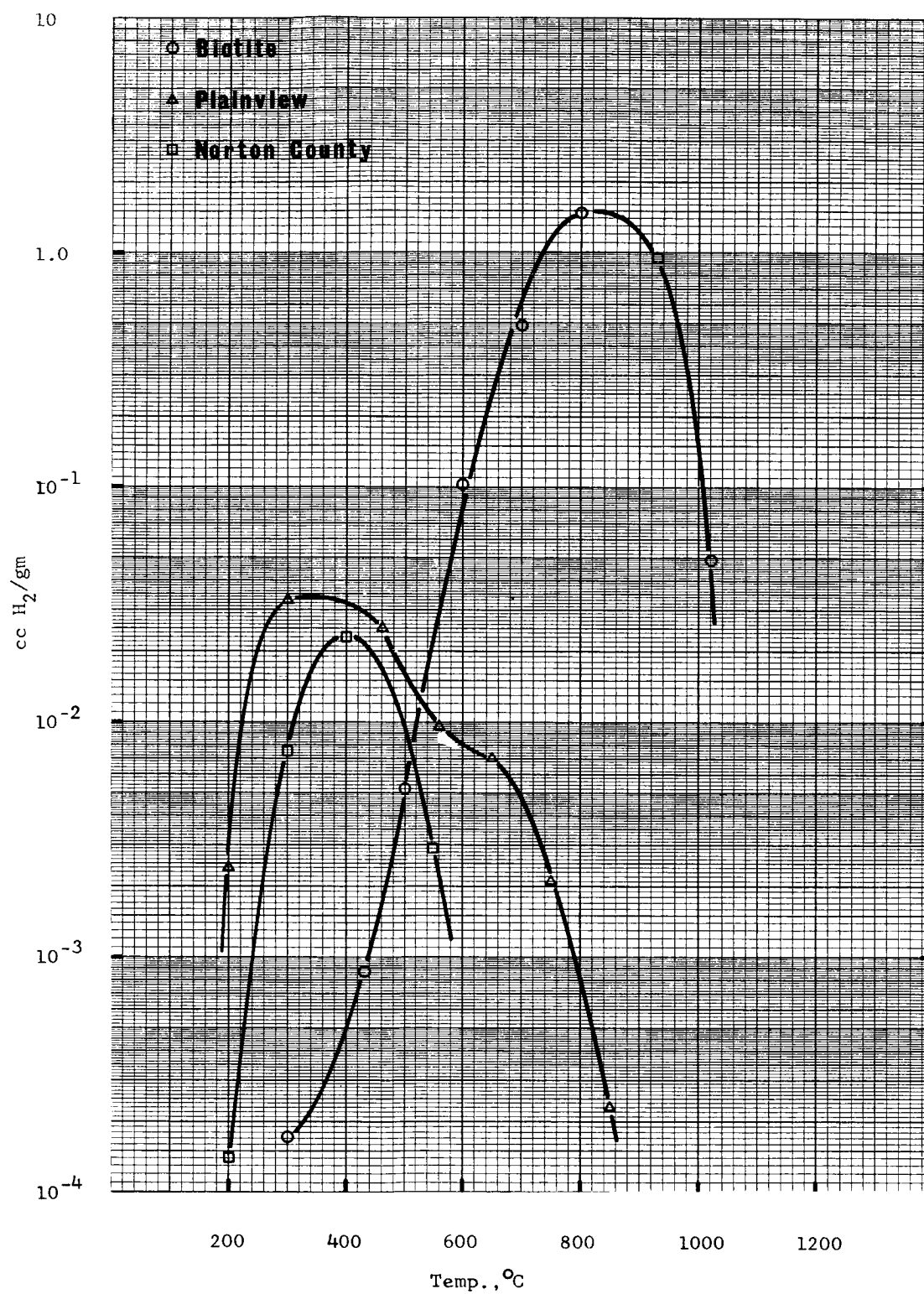
10

○ **Biotite**

△ **Plainview**

▣ **Norton County**

1.0

10^{-1}

10^{-2}

cc H_2/gm

10^{-3}

10^{-4}

200   400   600   800   1000   1200

Temp., °C

Fig. 27. Differential gas release from Norton County,
Plainview, and biotite.

an extraterrestrial origin for the H_2 would be indicated.

In the meantime, several other analyses were run so as to be able to compare the results. First, a known weathered find, the bronzite chondrite Plainview, with a piece of the fusion crust, was analyzed. It is hoped that this sample has contamination water in it. Again H_2 was detected (see Table 27). The release curve is different from any seen so far in this work (Fig. 27) and shows the suggestion of a double peak. The first peak occurs at $300-400^\circ$ C as has been found in the earlier samples, but the curve is skewed, indicating another peak at 600° C. One is tempted to attribute the higher peak to water contamination, but this is certainly speculation at this time.

Finally, sample containing known bound water and oxidizable iron, biotite, was analyzed. Fig. 27 and Table 27 show the results. Much higher temperatures are required for the H_2 release. This result is consistent with the studies of Roy and Weber (1964) for the stability of hydrous minerals, including muscovite. This suggests then that the process is the release of the water and subsequent reduction. In that case absorbed or interstitial water should be released at a lower temperature.This may be at room temperature or slightly above when in an evacuated volume. Also the kinetics of the reduction are less favorable at low temperatures allowing the water to be quickly retained at the liquid N_2 traps.

Dehydration studies of minerals have been extensively carried out by Weber and Roy (1965a, 1965b), Weber et al. (1964, 1965), and Roy and Weber (1964). In particular, they find that the older literature reporting dehydration at fairly high water pressures (P_{H_2O} from

10^2 to 10^4 bars) can not be extrapolated down to lower water pressures, of the order of 1 bar (Roy and Weber, 1964). At these lower pressures, higher than expected temperatures are necessary for the dehydroxylation. They suggest that this is due to metastable retention. Data at water pressures greater than 10^3 psi suggest that for low water pressures the hydration should occur between 475 and 575° C. (Roy and Weber, 1964)

Because of their interest in recovering water from the moon, Weber et al. (1965) irradiated both kaolinite and rutile with high energy (2 to 5.5 MeV) protons. By using infra-red absorption spectroscopy, several new peaks were detected in the rutile and attributed to O-H bonds formed by the retention of the bombarding protons. The kaolinite was studied by differential thermal analysis (DTA) and both the irradiated and non-irradiated samples showed the same release pattern, with a very sharp release occurring between 500 and 600° C. However the irradiated samples exhibited a larger weight loss than the non-irradiated, and this weight loss was several orders of magnitude larger than the weight of the incident hydrogen. Thus they ascribe this weight loss to release of water chemisorbed in the radiation damaged mineral surface. 2 MeV protons penetrate on the order of 30 microns in silicates and thus major radiation damage is to be expected. If this can be substantiated it might explain part of the observed H_2 contamination evolved in the experiments described in this work.

References

Aller L. H. (1963) Astrophysics: the Atmospheres of the Sun and Stars, second edition. Ronald Press, New York.

Almen O. and Bruce G. (1961) Collection and sputtering experiments with noble gas ions. Nucl. Instr. Meth. 11, 257-278.

Antal J. J., Weiss R. J., and Dienes G. J. (1955) Long-wavelength neutron transmission as an absolute method for determining the concentration of lattice defects in crystals. Phys. Rev. 99, 1081-1085.

Barnes R. S. (1964) A theory of swelling and gas release for reactor materials. J. Nucl. Mater. 11, 135-148.

Belton M. J. S., Brandt J. C. and Hodge P. W. (1963) On the characteristics of distant comets. Ann. D'Astrophys. 26, 250-252.

Biermann L. and Lüst R (1963) Comets: structure and dynamics of tails. The Solar System IV, Chpt. 18, Kuiper G. P. and Middlehurst B., editors, Univ. of Chicago.

Bohr N. (1948) The penetration of atomic particles through matter. Kgl. Danske Videnskab. Selskab, Mat.-fys Medd. 18, #8, 144 pages.

Bonetti A., Bridge H. S., Lazarus A. J., Rossi B., and Scherb F. (1963) Explorer 10 plasma measurements. J. Geophys. Res. 68, 4017-4063.

Brown F. and Davies J. A. (1963) The effect of energy and integrated flux on the retention and range of inert gas ions injected at KeV energies in metals. Can. J. Phys. 41, 844-857.

Bühler F., Geiss J., Meister J., Eberhardt P., Huneke J., and Signer P. (1966) Trapping of the solar wind in solids, part I. Trapping probability of low energy He, Ne, and Ar ions. Earth Planet. Sci. Letts. 1, 249-255.

Cazes J. (1966) Gel permeation chromatography - Part I. J. Chem. Ed. 43, A567-A582.

Christensen L. J., Khan J. M., and Brunner W. F. (1966) Measurement of microgram surface densities by observation of proton-produced X-rays. UCRL-70006. Preprint.

Davies J. A., Brown F. and McCargo M. (1963) Range of Xe^{133} and Ar^{41} ions of kiloelectron volt energies in aluminum. Can. J. Phys. 41, 829-843.

References (cont.)

Dessler A. J. (1967) Solar wind and interplanetary magnetic field. Rev. Geophys. 5, 1-41.

Eberhardt P. (1964) Rare gas measurements in meteorites and possible applications to the lunar surface. "Venia Docendi" thesis.

Eberhardt P., Geiss J., and Grögler N. (1965) Further evidence on the origin of trapped gases in the meteorite Khor Temiki. J. Geophys. Res. 70, 4375-4378.

Eberhardt P., Geiss J., and Grögler N. (1966) Distribution of gases in the pyroxene and feldspar of the Khor Temiki meteorite. Earth Planet. Sci. Lett. 1, 7-12.

Fredriksson K. and Keil K. (1963) The light-dark structure in the Pantar and Kapoeta stone meteorites. Geochim. Cosmochim. Acta 27, 717-739.

Gerling E. K. and Levskii L. K. (1956) On the origin of the rare gases in stony meteorites. Dokl. Akad. Nauk. SSSR 110, 750-755.

Glaser P. E. editor (1964) Studies of the physical characteristics of probable lunar surface materials: Part II. Arthur D. Little, Inc., for Air Force Cambridge Research Laboratories, report # AFCRL-64-970(11).

Gringauz K. I., Bezrukikh V. V., Ozerov V. D., and Rybchinskii R. E. (1960) A study of interplanetary ionized gas, energetic electrons, and solar corpuscular radiation by means of three electrode traps for charged particles on the second soviet cosmic rocket. Sov. Phys. Dokl. Eng. Transl. 5, 361-364.

Grønlund F. and Moore W. J. (1960) Sputtering of silver by light ions with energies from 2 to 12 keV. J. Chem. Phys. 32, 1540-1545.

Hapke B. (1962) Second preliminary report on experiments relating to the lunar surface. Cornell Univ. Rept. CRSR 127.

Hapke B. (1965) Effects of a simulated solar wind on the photometric properties of rocks and powders. Ann. N. Y. Acad. Sci. 123, art. 2, 711-721.

Hapke B. (1966) Optical properties of the moon's surface. The Nature of the Lunar Surface. Hess W. N., Menzel D. H., and O'Keefe J. A., editors, John Hopkins Press, Baltimore.

Heymann D. and Fluit J. M. (1962) Sputtering by 20-keV Ar$^+$ ions at normal incidence on meteorites. J. Geophys. Res. 67, 2921-2924.

References (cont.)

Heymann D. and Mazor E. (1966) St. Mesmin, a gas-rich amphoteric chondrite. J. Geophys. Res. 71, 4695-4697.

Hintenberger H., Konig H., Schultz L., and Wanke H. (1964) Radiogene, Spallogene, und primordiale Edelgase in Steinmeteoriten. Z. Naturforschg. 19a, 327-341.

Hundhausen A. J., Ashbridge J. R., Barne S. J., Gilbert H. E., and Strong I. B. (1967) Vela 3 satellite observations of solar wind ions: a preliminary report. J. Geophys. Res. 72, 87-100.

Ingham M. F. (1961) Observations of the zodiacal light from a very high altitude station. IV. The nature and distribution of the interplanetary dust. Monthly Not. Roy. Astr. Soc. 122, 157-176.

Ingham M. F. (1963) Interplanetary matter. Space Sci. Rev. 1, 576-588.

Jeffrey P. M. and Reynolds J. H. (1961) Origin of excess Xe^{129} in stone meteorites. J. Geophys. Res. 66, 3582-3583.

Kaufman H. R. (1961) An ion rocket with an electron-bombardment ion source. NASA-TND - 585.

Kelly R. and Brown F. (1965) Release processes in metal and oxide targets following bombardments with Xe at energies up to 40 keV. Acta Metall. 13, 169-180.

Kelly R. and Matzke H. (1965) A study of inert-gas diffusion in ionic crystals and sinters with emphasis on the ion-bombardment technique. J. Nucl. Mat. 17, 179-191.

Kelly R. and Ruedl E. (1966) Diffusion in inert-gas bombarded Pt and Al. Phys. Stat. Sol. 13, 55-69.

Khan J. M., Potter K. L., and Worley R. D. (1965a) Studies in X-ray production by proton bombardment of C, Mg, Al, Nd, Sm, Gd, Tb, Dy, and Ho. Phys. Rev. 139, A1735-1746.

Khan J. M., Potter D. L., and Worley R. D. (1965b) Proposed method for microgram surface density measurements by observation of proton-produced X-rays. J. Appl. Phys. 37, 564-567.

Kornelson E. V. (1964) The ionic entrapment and thermal desorption of inert gases in tungsten for kinetic energies of 40 eV to 5 keV. Can. J. Phys. 42, 364-381.

References (cont.)

Lindhard J., Nielson V., Scharff M., and Thompsen P. V. (1963) Integral equations governing radiation effects (Notes on atomic collisions, III). Kg. Danske Videnskab. Selskab, Mat.-fys Medd. 33 #10, 42 pages.

Lindhard J. and Scharff M. (1961) Energy disspiation by ions in the keV region. Phys. Rev. 124, 128-130.

Mackin R. J., Jr. and Neugebauer M., editors (1966) The Solar Wind. Pergamon Press, Oxford, England.

Manuel O. K. and Kuroda P. K. (1964) Isotopic composition of the rare gases in the Fayetteville meteorite. J. Geophys. Res. 69, 1413-1419.

McCracken G. M. and Maple J. H. C. (1966) The trapping of hydrogen ions in molybdenum, titanium, tantalum, and zirconium. U. K. At. En. Auth. Culham Laboratory, preprint, CLM-P118.

McCracken G. M., Maple J. H. C., and Watson H. H. H. (1966) 30 keV ion bombardment apparatus for study of interaction of light ions with surfaces. Rev. Sci. Instr. 37, 860-866.

Merrihue C. (1964) Rare gas evidence for cosmic dust in modern Pacific red clay. Cosmic Dust, Cassidy W. editor, Ann. N. Y. Acad. Sci. 119, 351-367.

Müller O. and Zähringer J. (1966) Chemishce Unterscheide bei uredelgashaltigen Steinmeteoriten. Earth Planet. Sci. Lett. 1, 25-29.

Nash D. B. (1964) Results of X-ray diffraction analysis of proton-irradiated rock powders. J. P. L. Space Programs Summary #37-30, IV, 178-183.

Nash D. B. (1966) Proton-excited luminescence of silicates: Experimental results and lunar implications. J. Geophys. Res. 71, 2517-2534.

Nash D. B. (1967) Proton-irradiation darkening of rock powders and solar-wind darkening of the moon. J. P. L. Preprint.

Neugebauer M. and Snyder C. W. (1962) The mission of Mariner II: preliminary observations. Science 138, 1095-1097.

Neugebauer M. and Snyder C. W. (1966) Mariner II observations of the solar wind: 1. Average properties. J. Geophys. Res. 71, 4469-4484.

Öpik E. J. (1951) Astronomy and the bottom of the sea. *Irish Astron. J.* 1, 145-158.

Öpik E. J. (1956) Interplanetary dust and terrestrial accretion of meteoric matter. *Irish Astron. J.* 4, 84-135.

Ormrod J. H., MacDonald J. R., and Duckworth H. E. (1965) Some low-energy atomic stopping cross sections. *Can. J. Phys.* 43, 275-284.

Parker E. N. (1964) The solar wind. *Sci. Am.* April. pp. 66-76.

Parker E. N. (1965) Dynamical theory of the solar wind. *Space Sci. Rev.* 4, 666-708.

Parkin D. W. and Tilles D. (1967) The influx of extraterrestrial material, preprint.

Patterson J. H., Turkevich A. L., and Franzgrote E. (1965) Chemical analysis of surfaces using alpha particles. *J. Geophys. Res.* 70, 1311-1327.

Pepin R. O. and Signer P. (1965) Primordial rare gases in meteorites. *Science* 149, 253-265.

Purcell J. E. and Ettre L. S. (1965) Analysis of hydrogen with thermal conductivity detectors. *J. of Gas Chrom.* 3, 69-71.

Reynolds J. H. (1960) Isotopic composition of primordial xenon. *Phys. Rev. Lett.* 4, 351-354.

Reynolds J. H. (1963) Xenology. *J. Geophys. Res.* 68, 2939-2956.

Robertson H. P. (1937) Dynamical effects of radiation in the solar system. *Astrophys. J.* 97, 423-438.

Robinson M. T. and Oen O. S. (1963) Computer studies of the slowing down of energetic atoms in crystals. *Phys. Rev.* 132, 2385-2398.

Rosenberg D. L. and Wehner G. K. (1964) Darkening of powdered basalt by simulated solar-wind bombardment. *J. Geophys. Res.* 69, 3307-3308.

Roy R. and Weber J. N. (1964) Stability - metastability relationships of hydrous minerals and their importance in designing facilities for the extraction of water from lunar rocks and minerals. *Proc. Ann. Meet. Working Group on Extraterrestrial Resources*, pp. 117-130.

References (cont.)

Ruedl E. and Kelly R. (1965) High-temperature gas release in krypton-bombarded platinum due to the formation and motion of bubbles. J. Nucl. Mater. 16, 89-102.

Signer P. and Suess H. E. (1963) Rare gases in the sun, in the atmosphere, and in meteorites. Earth Sciences and Meteoritics. Geiss J. and Goldberg E. D., editors. Chpt. 13. North-Holland.

Smallman R. E. and Willis B. T. M. (1957) An X-ray study of neutron irradiated lithium fluoride. Phil. Mag. 2, 8th series, 1018-1026.

Smoluchowski R. (1965) Radiation sintering of lunar dust. Science 150, 1025.

Smoluchowski R. (1966) Structure and coherence of the lunar dust layer. J. Geophys. Res. 71, 1569-1574.

Stauffer H. (1961) Primordial argon and neon in carbonaceous chondrites and ureilites. Geochim. Cosmochim. Acta 24, 70-82.

Suess H. E., Wanke H., and Wlotzka F. (1964) On the origin of gas-rich meteorites. Geochim. Cosmochim. Acta 28, 595-607.

Tilles D. (1965) Solar wind in extraterrestrial dust: A new source mechanism for the noble gases in the Earth's atmosphere. Science 148, 1085-1088.

Tilles D. (1966) Implantation in interplanetary dust of rare-gas ions from solar flares. Science 153, 981-984.

Van de Hulst H. C. (1947) Zodiacal light in the solar corona. Astrophys. J. 105, 471-488.

Watson F. (1937) Distribution of meteoric masses in interstellar space. Harvard Annals 105, 623-632.

Weber J. N. and Roy R. (1965a) Dehydroxylation of Kaolinite, Dickite, and Halloysite: Heats of reaction and kinetics of dehydration at P_{H_2O} = 15 psi. Am. Min. 50, 1038-1045.

Weber J. N. and Roy R. (1965b) Complex stable $\rightleftharpoons$ metastable solid reactions illustrated with the $Mg(OH)_2 \rightleftharpoons MgO$ reaction. Am. J. Sci. 263, 668-677.

Weber J. N., Roy R. and Greer R. T. (1964) Serpentine as a source of water on the moon: Thermodynamics and kinetics of dehydration and the effects of particle size and chemical composition. Proc. Ann. Meet. Working Group in Extraterr. Resources, 83-109.

References (cont.)

Weber J. N., Roy R. and Greer R. T. (1965) Water resources on the moon: Experimental studies concerned with predicting the nature of possible water deposits and determining optimum processing conditions for their exploitation. Sym. Post Apollo Space Expl.

Wehner G. K., Kenknight C., and Rosenberg D. L. (1963a) Sputtering rates under solar-wind bombardment. Planet. Space Sci. 11, 885-895.

Wehner G. K., Kenknight C., and Rosenberg D. L. (1963b) Modification of the lunar surface by the solar-wind bombardment. Planet. Space Sci. 11, 1257-1261.

Wehner G. K., Rosenberg D. L., and Kenknight C. E. (1965) Investigation of sputtering effects on the moon's surface. Litton Industries, Applied Science Division. Report 2845.

Whipple F. H. (1950) The theory of micrometeorites. Part I. In an isothermal atmosphere. Proc. Nat. Acad. Sci. 36, 687-695.

Willis B. T. M. (1958) "The Application of X-ray diffraction techniques to irradiation damage problems." Gr. Brit. At. Res. Establ., M+C/R 2751, 3.1-4.0.

Wolfe J. H., Silva R. W., McKibbin D. D., and Matson R. H. (1966) The compositional, anisotropic, and nonradial flow characteristics of the solar wind. J. Geophys. Res. 71, 3329-3335.

Wolfe J. H., Silva R. W., and Myers M. A. (1966) Observations of the solar wind during the flight of Imp. I. J. Geophys. Res. 71, 1319-1340.

Young J. R. (1956) Penetration of electrons and ions in Al. J. Appl. Phys. 27, 1-4.

Zähringer J. (1962) Uber die Uredelgase in den Achondriten Kapoeta und Staroe Pesjanoe. Geochim. Cosmochim. Acta 26, 665-680.

Zähringer J. (1966) Primordial helium detection by microprobe technique. Earth Planet. Sci. Lett. 1, 20-22.

Corrections

Pg 71, line 18, details are given on page 72

Pg 140

Fechtig H., Gentner W. and Lämmerzahl P (1963)
Argonbestimmungen an kaliumineralien - XII. Edelgas-
diffusionsmessungen an Stein- und Eisenmeteoriten.
Geochim. et Cosmochim. Acta 27 1149-1169.